Engineering Journal

American Institute of Steel Construction

Third Quarter 2017 Volume 54, No. 3

www.aisc.org

Engineering Journal

American Institute of Steel Construction

Dedicated to the development and improvement of structural steel design, fabrication and erection through the interchange of ideas, experiences and data.

Engineering Journal (ISSN 0013-8029) is published quarterly. Subscriptions: Members: one subscription, $40 per year, included in dues; Additional Member Subscriptions: $40 per year. Non-Members U.S.: $160 per year. Foreign (Canada and Mexico): Members $80 per year. Non-Members $160 per year. Published by the American Institute of Steel Construction at 130 E. Randolph Street, Suite 2000, Chicago, IL 60601.

Periodicals postage paid at Chicago, IL and additional mailing offices. **Postmaster:** Send address changes to *Engineering Journal* in care of the American Institute of Steel Construction, 130 E. Randolph Street, Suite 2000, Chicago, IL 60601.

Submissions: Manuscripts are welcomed, but publication cannot be guaranteed. Authors do not receive remuneration. Guidelines for authors are printed on the inside back cover and available online at **www.aisc.org/ej**.

Subscriptions: subscriptions@aisc.org, 312.670.2400

Archives: Search at **www.aisc.org/ej**. Article downloads are free for current members and are available for a nominal fee for non-members.

Yield Line Approaches for Design of End Plate Tension Connections for Square and Rectangular HSS Members Using End Plate Tensile Strength

WILLIAM A. THORNTON

ABSTRACT

End plates, which are sometimes called flange plates, are a common way to treat HSS members loaded in tension. In this application, prying action must be considered in the design of the plate and bolts. This paper demonstrates that the prying action model can use the end plate minimum tensile strength rather than the yield strength to achieve satisfactory designs. Only connections with bolts on all four sides of the HSS are considered here.

Keywords: HSS connections, end plate, prying action, yield line pattern.

INTRODUCTION

Calculations for prying action have, for many years, used the material minimum yield strength F_y in the calculations of the Struik and deBack (1969) model. This model has been the basis of the AISC *Steel Construction Manual* prying action analysis since the 8th Edition (1980). As early as 1965, Douty and McGuire suggested that the material minimum tensile strength F_u gives a better fit to the experimental results for tee stubs. Thornton (1992, 1996) showed that the use of F_u in place of F_y in the Struik-deBack model gave excellent predictions of the failure loads obtained by Kato and McGuire (1973). Because the experimental data of these two papers (Douty and McGuire; Kato and McGuire) were based on steels available in the 1960s, the AISC *Manual* Committee was reluctant to replace F_y with F_u in the *Manual* prying calculations. In 2002, Swanson showed that the Struik-deBack model with F_u in place of F_y gave excellent correlation for tee stub connections using modern materials. This is the reason that the *Manual* Committee adopted F_u for the prying calculations in the 13th Edition *Manual* (2005), and this continues in the 14th Edition (2011) and the soon-to-be-available 15th Edition *Manual*. Because the mode of failure of the plate (T-stub) material in the Swanson tests was ductile yield, not rupture, the resistance factor ϕ of 0.90 is used with the tensile strength F_u.

A recent AISC publication, *Design Guide 24—Hollow Structural Section Connections* (Packer et al., 2010), uses F_y rather than F_u for the prying action analysis of end plated HSS tension connections with bolts on all four HSS faces. This is a variation in the prying action formulation of the current 14th Edition *Manual*, which uses F_u in these calculations. This may cause confusion in the industry. For instance, when is it correct to use F_u and when should F_y be used? Many engineers will opt for the more conservative approach if there seems to be disagreement in AISC publications as to the correct approach.

The author notes that the method of Design Guide 24 is completely viable. It uses yield line patterns that are different than those proposed here, coupled with the use of F_y rather than F_u. The purpose of this paper is to show that with appropriate yield line patterns it is possible to use F_u in lieu of F_y. This is verified by the comparison of the predicted results with the available test results.

Using a yield line approach to the end plated HSS tension connection, which is similar to the method validated by Swanson (2002) for tee stub tension connections, this paper shows that, using the experimental data for end plated hollow structural steel (HSS) tension connections produced by Willibald, Packer and Puthli (2002, 2003); Kato and Mukai (1985); and Caravaggio (1988), a valid design method based on the tensile strength F_u can be justified.

William A. Thornton, Ph.D., P.E., NAE, Cives Engineering Corporation, Alpharetta, GA. Email: bthornton@cives.com

Paper No. 2012-20R2

DISCUSSION

Use of the Tensile Strength, F_u, in the Plate Flexure Model

A stress block with F_u at all points above and below the neutral axis is not likely to be achieved. The fibers near the neutral axis will not achieve F_u, but because of their proximity to the neutral axis, they are relatively unimportant in the

overall capacity calculation. Because of this fact, the plastic stress block is currently used in many structural connection calculations even though it is theoretically impossible to achieve. It will be used in the method developed here.

Development of Yield Line Patterns and Bolt Tributary Length

There are many possible families of yield lines for the end plate HSS connections considered in this paper. Following the work of Willibald, Packer and Puthli (2002), three bolt arrangements are considered here. These are shown in Figures 1, 2 and 3 and are called patterns A, B and C, respectively. For these three bolt patterns, there are available a total of 55 physical tests; 26 for pattern A, 2 for pattern B, and 27 for pattern C. These are obtained from Willibald et al. (2002, 2003), Kato and Mukai (1985), and Caravaggio (1988).

Because of the availability of the physical test data for the A, B and C bolt arrangements, only these arrangements are considered here. As mentioned earlier, many possible yield line families are available for each of the three bolt patterns. For instance, circular yield lines at the HSS corners with radial fans are a possible family, as are straight line yield families. The author has reviewed a number of possibilities and determined by "trial and error" that the families chosen for this paper give the best correlation to the test data.

Note that the bolt holes are not explicitly removed in any of the three bolt patterns A, B and C. Bolt holes are removed through the use of the quantity δ in the prying action formulation presented in the "Proposed Analysis and Design Methods" section of the paper.

Yield Line Pattern A

This bolt pattern is applicable to both rectangular and square HSS members. Test data are available for both. The assumed yield line pattern is shown in Figure 1 for bolt pattern A. It is a combined curvilinear and straight line yield line pattern. It has an axial load capacity P_u given by

$$P_u = \frac{F_y t_p^2}{b}(w_i + h_i + \pi b) \tag{1}$$

where

F_y = end plate yield stress, ksi

t_p = end plate thickness, in.

and b, h_i and w_i are defined in Figure 1. Figure 1 also shows the end plate size as $w_p \times h_p$.

Equation 1 is derived by the usual upper-bound virtual work method of structural mechanics (see, e.g., Save and Massonnet, 1972), which satisfies equilibrium and compatibility but not necessarily the constitutive equations.

From Dowswell (2011), the strength of an equivalent pair of straight-line yield lines of length, l, is

$$P_u = \frac{F_y t_p^2}{2b} l \tag{2}$$

Setting Equation 1 equal to Equation 2, the effective straight-line yield line pattern that gives the same strength as the multiple yield line pattern will have a length, l, using a T-stub analogy, as given by Equation 3, as

$$l = 2(w_i + h_i + \pi b) \tag{3}$$

Thus, for yield line pattern A, the tributary yield line length per bolt, where n is the number of bolts, is

$$p_A = \frac{2(w_i + h_i + \pi b)}{n} \tag{4}$$

The tributary yield length per bolt is required for the prying action formulation that was mentioned earlier in this paper. This prying action formulation will be completely developed subsequently.

Yield Line Pattern B

This bolt pattern is applicable to square and rectangular HSS, but test data are available only for the square case. The

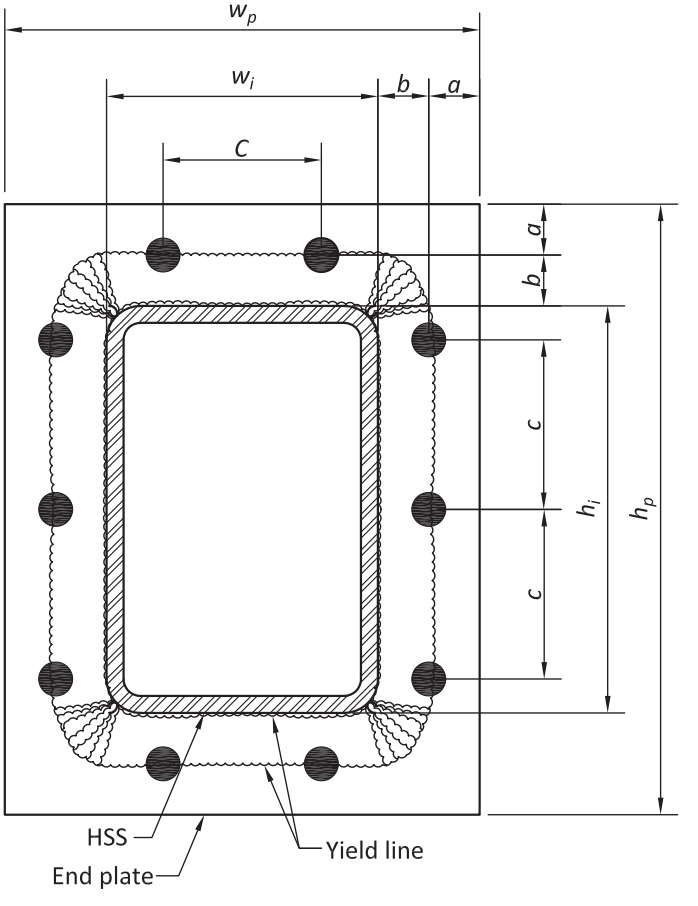

Fig. 1. Bolt pattern A and associated yield line.

bolt pattern and the assumed yield line pattern are shown in Figure 2. This yield line pattern was solved by Kapp (1974) to give the axial capacity P_u as

$$P_u = \frac{F_y t_p^2}{b}(w_i + h_i + 4b) \tag{5}$$

Using Dowswell's (2011) approach to determine the effective length of an equivalent straight-line yield line, using a T-stub analogy, gives

$$l_B = 2(w_i + h_i + 4b) \tag{6}$$

and the effective tributary length per bolt is

$$p_B = \frac{2(w_i + h_i + 4b)}{n} \tag{7}$$

Yield Line Pattern C

This yield line pattern has a single bolt on each HSS side. It could be applicable to both square and rectangular HSS, but test data are available in the referenced literature only for the square case. In order that the bolts on all sides be equally loaded, it is recommended that this pattern be used only for the square HSS case. Figure 3 shows the bolt pattern and the assumed yield line pattern. This yield line pattern is the same as that for bolt pattern A. Therefore

$$p_C = \frac{2(w_i + h_i + \pi b)}{n} \tag{8}$$

Limitation on Tributary Yield Line Length per Bolt Length

It is assumed that the yield line patterns of Figures 1, 2 and 3 will develop as shown. It is apparent that if the bolt spacing (tributary yield line length per bolt length) is too great, yield line patterns with less capacity than that calculated by Equation 1, 5 or 8, can develop. Dowswell (2011) has shown that if the tributary bolt length p is greater than

$$p = 4\sqrt{b'(a+b)} \tag{9}$$

where $b' = b - d/2$, a and b are defined in the figures, and d is the bolt diameter, independent yield line patterns can develop at each bolt, producing a capacity less than that determined by any of the patterns A, B or C. This is shown in Figure 4. The bolt spacing at which the localized pattern of Figure 4 can develop at each bolt is

$$p = 4\sqrt{b'(a+b)} \tag{10}$$

Therefore, to prevent this and to maintain the validity of the

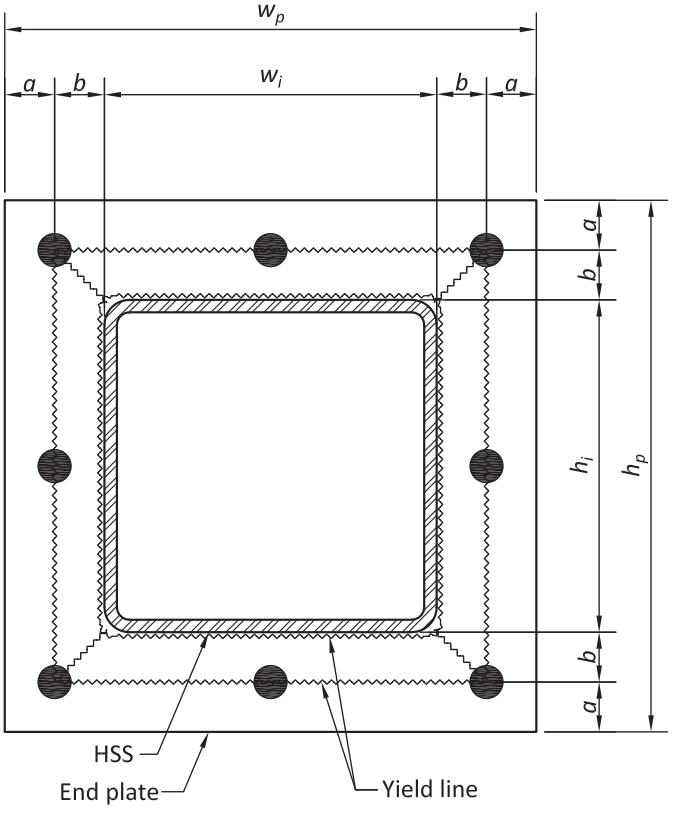

Fig. 2. Bolt pattern B and associated yield line.

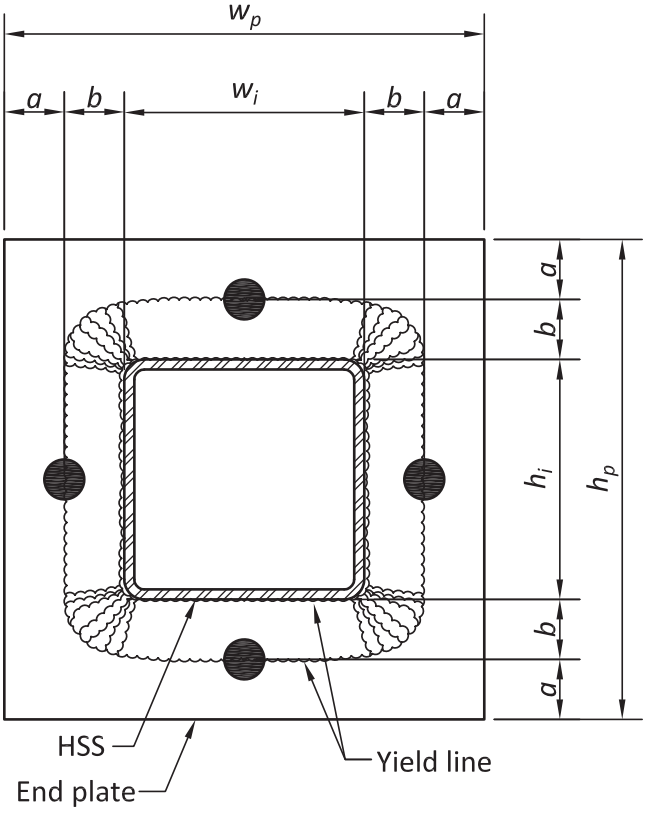

Fig. 3. Bolt pattern C and associated yield line.

assumed yield patterns of Figures 1, 2 and 3, the maximum tributary bolt lengths (p_A, p_B and p_C) are limited to

$$p_{i,max} = 4\sqrt{b'(a+b)} \tag{11}$$

Ultimately, whether or not the yield lines proposed for bolt patterns A, B and C are reasonable depends on how well they correlate to the physical test data. This is the subject of the "Physical Test Data" section of this paper. The next section of the paper will develop analysis and design methods proposed for the general analysis and design of this system. The analysis method was also used to develop the results given in Table 2. The design method is perhaps more convenient to use for routine design of this system. An example problem will show the use of both methods.

PROPOSED ANALYSIS AND DESIGN METHODS

Analysis Method

The proposed analysis method is that given in Part 9 of the AISC *Manual* (2011), with an additional requirement on the maximum value of α'. The method is as follows:

Given a, b, d, t_p, n, F_u, T and $B = \phi F_{nt} A_b$, find T_u and $N_u = nT_u$

A1. Check $a \le 1.25b$; if not, set $a = 1.25b$

A2. Calculate a', b', ρ, d':

$$a' = a + d/2 \tag{12}$$

$$b' = b - d/2 \tag{13}$$

$$\rho = b'/a \tag{14}$$

$$d' = d + 1/16 \text{ (for standard holes)} \tag{15}$$

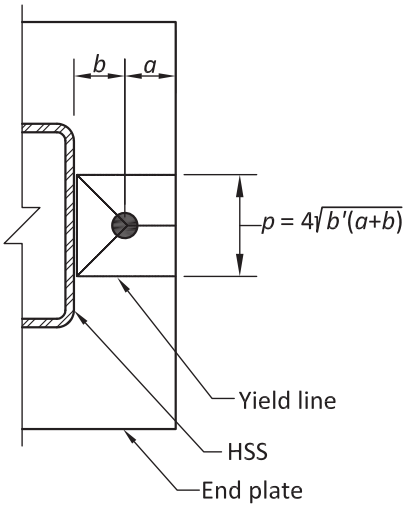

Fig. 4. Local yield line pattern when spacing is too large to allow patterns A, B or C to develop their associated p.

A3. Determine $p = p_i$, as appropriate for the bolt pattern; p_A, p_B or p_C:

$$p_A = \frac{2(w_i + h_i + \pi b)}{n} \tag{4}$$

$$p_B = \frac{2(w_i + h_i + 4b)}{n} \tag{7}$$

$$p_C = \frac{2(w_i + h_i + \pi b)}{n} \tag{8}$$

A4. Check that the determined p does not exceed $p_{i,max}$. If it does, use $p = p_{i,max}$.

$$p_{i,max} = 4\sqrt{b'(a+b)} \tag{11}$$

A5. Calculate δ:

$$\delta = 1 - d'/p \tag{16}$$

A6. Calculate t_c:

$$t_c = \sqrt{\frac{4Bb'}{\phi p F_u}} \tag{17}$$

Note that, as discussed in the "Introduction," $\phi = 0.90$ is used here.

A7. Calculate α':

$$\alpha' = \frac{1}{\delta(1+\rho)}\left[\left(\frac{t_c}{t_p}\right)^2 - 1\right] \tag{18}$$

$$T_u = B\left(\frac{t_p}{t_c}\right)^2 (1+\delta\alpha') \tag{19}$$

If $\alpha' \le 0$, set $\alpha' = 0$, $T_u = B \rightarrow$ bolts control

If $0 < \alpha' < 1$, $T_u = B\left(\frac{t_p}{t_c}\right)^2 (1+\delta\alpha')$

$\rightarrow$ bolts and plate control

If $\alpha' \ge 1$, set $\alpha' = 1$, $T_u = B\left(\frac{t_p}{t_c}\right)^2 (1+\delta)$

$\rightarrow$ plate controls

If $\alpha' > 1.5$, choose a larger t_p and repeat until $\alpha' \le 1.5$.

A8. Calculate N_u:

$$N_u = nT_u \tag{20}$$

A9. If $N_u \ge nT$, where T is the required strength per bolt, the design is satisfactory. In Table 2, N_u as calculated in Equation 20, is compared with the experimental value, N_{ux}.

Design Method

The proposed design method is also that given in Part 9 of the AISC *Manual* (2011), with an additional requirement on the maximum value of α', and is as follows:

Given T, a, b, p, F_u and $B = \phi F_{nt} A_b$, find t_p.

D1. Check $T \le B$. If true, proceed; otherwise increase the bolt number or bolt strength.

D2. Calculate β:

$$\beta = \frac{1}{\rho}\left(\frac{B}{T} - 1\right) \tag{21}$$

D3. If $\beta \ge 1$, set $\alpha^* = 1$

$$\text{If } 0 \le \beta < 1, \text{ set } \alpha^* = \min\left\{\frac{1}{\delta}\left(\frac{\beta}{1-\beta}\right), 1\right\} \tag{22}$$

D4. With the determined value of α^* and t_c from Equation 17, calculate t_p:

$$t_p = t_c \sqrt{\frac{T}{B}\left(\frac{1}{1+\delta\alpha^*}\right)} \tag{23}$$

D5. Calculate α':

$$\alpha' = \frac{1}{\delta(1+\rho)}\left[\left(\frac{t_c}{t_p}\right)^2 - 1\right] \tag{18}$$

D6. Check that $\alpha' \le 1.5$. If so, t_p is the required end plate thickness. If not, increase t_p until $\alpha' \le 1.5$. Note that α' and α^* are not the same physical quantity.

For the development of these methods, see Thornton (1985). Note that the methods are "reciprocal" to each other. That is, when the analysis method is run with a specified plate thickness t_p, a design strength T_u results. If the design method is then run with T_u as the required tension, the plate thickness t_p will result.

The additional requirement for the application of these methods to end plated HSS tension members is based on the results discussed in the section of the paper entitled, "Further Discussion and Observations." It is that α' should be less than or equal to 1.5.

Physical Test Data and Development of Tables 1, 2 and 3

Table 1 lists all of the physical properties of 55 specimens from four sources: (1) Willibald et al. (2002), (2) Kato and Mukai (1985), (3) Caravaggio (1988), and (4) Willibald et al. (2003). These test results are used to validate the yield line patterns proposed for the bolt patterns A, B and C. Except for some nominal HSS and plate dimensions, all of the data are measured rather than nominal.

Table 1 gives the physical specimen data, and Table 2 gives all of the calculations necessary to validate the proposed yield line patterns. The analysis method to provide these calculations is the same as the proposed analysis method given in the "Proposed Analysis and Design Methods" section of the paper, except that ϕ is taken to be 1.0 and actual measured values of B_u and F_u from Table 1 are used in the formula for t_c. Thus, the experimental value of t_c can be denoted as

$$t_{cx} = \sqrt{\frac{4B_u b'}{pF_u}} \tag{19}$$

Other than the t_{cx} value using $\phi = 1.0$ and the actual measured bolt and plate material tensile strengths, as shown in Equation 12, the method used to generate the connection capacities of Table 2 is exactly that of the "Proposed Analysis Method" section of this paper, without the $\alpha' \le 1.5$ requirement, which results from the physical data of Table 2.

The value of p, from Equation 4, 7 or 8, or from Equation 10, as appropriate, is included in Table 2. It is noted that Kato and Mukai (1985) include two specimens that exceeded the capacity of their testing system and, therefore, yielded no useful failure information. These are included in Tables 1 and 2 for completeness.

Discussion of Results

General

Table 2 shows excellent correlation between the experimental capacities N_{ux} and the predicted capacities N_u. The ratio N_{ux}/N_u shown in the last column of Table 2 should be approximately 1.0 or slightly bigger. Except for three outliers, this is the case, for types A and C. A discussion for types A and C follows. Type B will be discussed separately.

Types A and C

There are 26 type A specimens. Two of these exceeded the capacity of the testing apparatus and yielded no useful information, so there are 24 specimens to consider. Of these, two can be considered to be outliers. These are specimens 16 and 17. These had very thin end plates, approximately ¼ in. and 5⁄16 in., respectively. The prying ratios, β_{ux}, for these specimens were 233.4% and 77.5%, respectively. These very large prying ratios indicate that these connections are not acting as the theory assumes. The prying ratio is usually in the range of 0 to 30% for most connections in the author's experience. Willibald et al. (2003) reported that no visible separation of the plates occurred at a prying ratio of 41.7%. Ratios greater than about 50% indicate excessive deformation is occurring and that the load is very likely being carried by catenary action or membrane action, rather than flexure as assumed

Table 1. Specimen Physical Data														
				HSS	Plates	n								
		Specimen		$h_i \times w_i \times t$	$h_p \times w_p$	# of	a	b	c	t_p	d	d'	F_u	B_u
No.	Source	ID	Type	(in.)	(in.)	Bolts	(in.)	(in.)	(in.)	(in.)	(in.)	(in.)	(ksi)	(kips)
1	Willibald et al. (2002)	1-1	A	6.02×6.02×0.370	11.5×11.5	8	1.40	1.36	5.50	0.638	0.618	0.681	72.3	36.0
2	Willibald et al. (2002)	1-2	A	6.02×6.02×0.370	11.5×11.5	8	1.41	1.35	5.50	0.791	0.618	0.681	75.6	34.2
3	Willibald et al. (2002)	1-3	A	6.02×6.02×0.370	11.5×11.5	8	1.40	1.36	2.74	0.642	0.618	0.681	72.3	36.0
4	Willibald et al. (2002)	1-4	A	6.02×6.02×0.370	11.5×11.5	8	1.43	1.36	2.74	0.791	0.618	0.681	75.6	34.2
5	Willibald et al. (2002)	2-1	A	6.02×6.02×0.370	12.25×12.25	8	1.57	1.57	5.50	0.496	0.618	0.681	74.8	31.0
6	Willibald et al. (2002)	2-2	A	6.02×6.02×0.370	12.25×12.25	8	1.58	1.56	2.74	0.496	0.618	0.681	74.8	31.0
7	Willibald et al. (2002)	2-3	A	6.02×6.02×0.370	12.25×12.25	8	1.36	1.75	5.50	0.504	0.618	0.681	74.8	31.0
8	Willibald et al. (2002)	2-4	A	6.02×6.02×0.370	12.25×12.25	8	1.37	1.76	5.50	0.626	0.618	0.681	74.3	30.2
9	Willibald et al. (2002)	2-5	A	6.02×6.02×0.370	12.25×12.25	8	1.32	1.76	2.74	0.492	0.618	0.681	74.8	31.0
10	Willibald et al. (2002)	2-6	A	6.02×6.02×0.370	12.25×12.25	8	1.35	1.76	2.75	0.626	0.618	0.681	74.3	30.2
11	Kato and Mukai (1985)	26	A	7.87×7.87×0.303	12.6×12.6	8	1.18	1.18	3.94	0.449	0.630	0.692	63.5	37.1
12	Kato and Mukai (1985)	27	A	7.87×7.87×0.303	12.6×12.6	8	1.18	1.18	3.94	0.602	0.630	0.692	67.4	36.8
13	Kato and Mukai (1985)	28	A	7.87×7.87×0.303	12.6×12.6	8	1.18	1.18	3.94	0.728	0.630	0.692	66.3	38.4
14	Kato and Mukai (1985)	29	A	7.87×7.87×0.303	12.6×12.6	8	1.18	1.18	3.94	0.882	0.630	0.692	62.8	36.5
15	Kato and Mukai (1985)	30	A	7.87×7.87×0.303	12.6×12.6	8	1.18	1.18	3.94	0.992	0.630	0.692	62.9	37.7
16	Kato and Mukai (1985)	31	A	7.87×7.87×0.303	12.6×12.6	8	1.18	1.18	3.94	0.246	0.787	0.850	70.2	59.6
17	Kato and Mukai (1985)	32	A	7.87×7.87×0.303	12.6×12.6	8	1.18	1.18	3.94	0.350	0.787	0.850	71.2	59.6
18	Kato and Mukai (1985)	33	A	7.87×7.87×0.303	12.6×12.6	8	1.18	1.18	3.94	0.602	0.787	0.850	67.4	59.9
19	Kato and Mukai (1985)	34	A	7.87×7.87×0.303	12.6×12.6	8	1.18	1.18	3.94	0.728	0.787	0.850	66.3	59.9
20	Kato and Mukai (1985)	35	A	7.87×7.87×0.303	12.6×12.6	8	1.18	1.18	3.94	0.882	0.787	0.850	62.8	58.3
21	Kato and Mukai (1985)	36	A	7.87×7.87×0.303	12.6×12.6	8	1.18	1.18	3.94	0.992	0.787	0.850	62.9	58.9
22	Caravaggio (1988)	1	A	5×5×0.177	11.2×11.2	8	1.72	1.38	3.94	0.630	0.626	0.688	73.5	32.8
23	Willibald et al. (2003)	R1	A	9.98×5.98×.287	16.36×12.33	10	1.41	1.77	4.31	0.492	0.626	0.697	74.8	32.8
24	Willibald et al. (2003)	R2	A	9.98×5.98×.287	16.42×12.30	10	1.42	1.77	4.31	0.624	0.626	0.695	74.3	31.7
25	Willibald et al. (2003)	R3	A	9.98×5.98×.287	16.43×12.29	10	1.61	1.56	4.31	0.492	0.626	0.691	74.8	32.8
26	Willibald et al. (2003)	R4	A	9.98×5.98×.287	16.33×12.36	10	1.60	1.57	4.32	0.623	0.626	0.694	74.3	31.7
27	Willibald et al. (2002)	1-5	B	6.02×6.02×0.370	11.5×11.5	8	1.41	1.36	—	0.642	0.618	0.681	72.3	36.0
28	Willibald et al. (2002)	1-6	B	6.02×6.02×0.370	11.5×11.5	8	1.41	1.36	—	0.787	0.618	0.681	75.6	34.1
29	Kato and Mukai (1985)	1	C	5.91×5.91×0.236	10.63×10.63	4	1.18	1.18	—	0.355	0.630	0.693	59.0	37.5
30	Kato and Mukai (1985)	2	C	5.91×5.91×0.236	10.63×10.63	4	1.18	1.18	—	0.449	0.630	0.693	63.5	37.1
31	Kato and Mukai (1985)	3	C	5.91×5.91×0.236	10.63×10.63	4	1.18	1.18	—	0.618	0.630	0.693	66.1	39.6
32	Kato and Mukai (1985)	4	C	5.91×5.91×0.236	10.63×10.63	4	1.18	1.18	—	0.728	0.630	0.693	66.3	38.4
33	Kato and Mukai (1985)	5	C	5.91×5.91×0.236	10.63×10.63	4	1.18	1.18	—	0.842	0.630	0.693	64.1	36.4
34	Kato and Mukai (1985)	8	C	5.91×5.91×0.236	10.63×10.63	4	1.18	1.18	—	0.350	0.787	0.850	71.2	59.6
35	Kato and Mukai (1985)	9	C	5.91×5.91×0.236	10.63×10.63	4	1.18	1.18	—	0.449	0.787	0.850	63.5	58.0
36	Kato and Mukai (1985)	10	C	5.91×5.91×0.236	10.63×10.63	4	1.18	1.18	—	0.602	0.787	0.850	67.4	59.8
37	Kato and Mukai (1985)	11	C	5.91×5.91×0.236	10.63×10.63	4	1.18	1.18	—	0.728	0.787	0.850	66.3	59.8
38	Kato and Mukai (1985)	12	C	5.91×5.91×0.236	10.63×10.63	4	1.18	1.18	—	0.882	0.787	0.850	62.8	58.2
39	Kato and Mukai (1985)	13	C	5.91×5.91×0.236	10.63×10.63	4	1.18	1.18	—	0.992	0.787	0.850	62.9	58.9
40	Kato and Mukai (1985)	14	C	5.91×5.91×0.236	10.63×10.63	4	1.18	1.18	—	0.449	0.787	0.850	63.5	58.0
41	Kato and Mukai (1985)	15	C	5.91×5.91×0.236	10.63×10.63	4	1.18	1.18	—	0.992	0.787	0.850	62.9	58.9
42	Kato and Mukai (1985)	16	C	7.87×7.87×0.315	12.6×12.6	4	1.18	1.18	—	0.449	0.787	0.850	63.5	58.0
43	Kato and Mukai (1985)	17	C	7.87×7.87×0.315	12.6×12.6	4	1.18	1.18	—	0.606	0.787	0.850	65.5	59.8
44	Kato and Mukai (1985)	18	C	7.87×7.87×0.315	12.6×12.6	4	1.18	1.18	—	0.729	0.787	0.850	66.3	59.8
45	Kato and Mukai (1985)	19	C	7.87×7.87×0.315	12.6×12.6	4	1.18	1.18	—	0.882	0.787	0.850	62.8	58.2
46	Kato and Mukai (1985)	20	C	7.87×7.87×0.315	12.6×12.6	4	1.18	1.18	—	0.941	0.787	0.850	68.3	58.9
47	Kato and Mukai (1985)	21	C	7.87×7.87×0.315	12.6×12.6	4	1.18	1.18	—	0.606	0.945	1.01	65.5	84.5
48	Kato and Mukai (1985)	22	C	7.87×7.87×0.315	12.6×12.6	4	1.18	1.18	—	0.728	0.945	1.01	66.3	88.6
49	Kato and Mukai (1985)	23	C	7.87×7.87×0.315	12.6×12.6	4	1.18	1.18	—	0.882	0.945	1.01	62.8	85.4
50	Kato and Mukai (1985)	24	C	7.87×7.87×0.315	12.6×12.6	4	1.18	1.18	—	0.940	0.945	1.01	68.3	88.1
51	Kato and Mukai (1985)	25	C	7.87×7.87×0.315	12.6×12.6	4	1.18	1.18	—	1.08	0.945	1.01	61.5	84.1
52	Willibald et al. (2002)	2-7	C	6.02×6.02×0.370	12.25×12.25	4	1.59	1.52	—	0.496	0.744	0.807	74.8	57.6
53	Willibald et al. (2002)	2-8	C	6.02×6.02×0.370	12.25×12.25	4	1.57	1.53	—	0.622	0.744	0.807	74.3	55.6
54	Willibald et al. (2002)	2-9	C	6.02×6.02×0.370	12.25×12.25	4	1.38	1.72	—	0.496	0.744	0.807	74.8	57.6
55	Willibald et al. (2002)	2-10	C	6.02×6.02×0.370	12.25×12.25	4	1.38	1.73	—	0.622	0.744	0.807	74.3	55.7

Table 2. Validation of the Proposed Analysis Method

No.	a' (in.)	b' (in.)	ρ	$*P_i$ (in.)	$*P_{i,max}$ (in.)	δ	t_{cx} (in.)	α'	T_u (kip)	N_u (kip)	N_{ux} (kip)	β_{ux} (%)	N_{ux}/N_u
1	1.71	1.05	0.615	4.08	6.81	0.833	0.716	0.194	33.2	265	249	15.7	0.939
2	1.72	1.04	0.606	4.07	6.78	0.833	0.680	–0.195	34.2	274	261	4.8	0.954
3	1.71	1.05	0.615	4.08	6.81	0.833	0.716	0.182	33.3	266	279	3.2	1.05
4	1.74	1.05	0.604	4.08	6.85	0.833	0.683	–0.191	34.2	274	268	2.1	0.980
5	1.88	1.26	0.671	4.24	7.96	0.840	0.702	0.715	24.8	198	203	22.2	1.02
6	1.89	1.25	0.662	4.24	7.93	0.839	0.700	0.710	24.9	199	213	16.4	1.07
7	1.67	1.26	0.756	4.24	7.69	0.840	0.702	0.637	24.5	196	190	30.5	0.968
8	1.68	1.45	0.864	4.39	8.52	0.845	0.733	0.235	26.4	211	213	13.4	1.01
9	1.63	1.45	0.891	4.39	8.46	0.845	0.740	0.790	22.9	183	198	25.3	1.08
10	1.66	1.45	0.875	4.39	8.50	0.845	0.733	0.234	26.4	211	229	5.5	1.08
11	1.50	0.865	0.579	4.86	5.72	0.858	0.645	0.640	30.8	246	234	26.8	0.95
12	1.50	0.865	0.579	4.86	5.72	0.858	0.623	0.053	35.9	287	264	11.5	0.919
13	1.50	0.865	0.579	4.86	5.72	0.858	0.642	–0.164	38.4	307	299	2.7	0.973
14	1.50	0.865	0.579	4.86	5.72	0.858	0.643	–0.331	36.5	292	286	2.1	0.979
15	1.50	0.865	0.579	4.86	5.72	0.858	0.653	–0.418	37.7	302	302	–0.1	1.00
16	1.57	0.787	0.500	4.86	5.45	0.825	0.741	6.409	12.2	97	143	233.4	1.47
17	1.57	0.787	0.500	4.86	5.45	0.825	0.738	3.488	20.6	165	270	77.5	1.64
18	1.57	0.787	0.500	4.86	5.45	0.825	0.758	0.474	52.5	420	367	30.6	0.874
19	1.57	0.787	0.500	4.86	5.45	0.825	0.765	0.083	58.0	464	416	15.2	0.896
20	1.57	0.787	0.500	4.86	5.45	0.825	0.775	–0.184	58.3	466	—	—	—
21	1.57	0.787	0.500	4.86	5.45	0.825	0.778	–0.310	58.9	471	—	—	—
22	2.03	1.067	0.525	3.58	7.27	0.808	0.729	0.275	29.9	240	209	25.6	0.873
23	1.72	1.458	0.846	4.30	8.61	0.840	0.771	0.937	23.9	239	232	41.4	0.971
24	1.73	1.458	0.841	4.30	8.63	0.840	0.760	0.313	27.0	270	259	22.4	0.960
25	1.92	1.248	0.649	4.17	7.95	0.835	0.724	0.847	25.8	258	249	31.7	0.963
26	1.91	1.258	0.658	4.18	7.99	0.835	0.717	0.233	28.6	286	279	13.6	0.975
27	1.72	1.051	0.611	4.37	6.82	0.844	0.692	0.119	34.1	273	236	22.0	0.865
28	1.72	1.051	0.611	4.37	6.82	0.844	0.659	–0.220	34.1	273	256	6.6	0.938
29	1.50	0.865	0.579	7.76	5.72	0.879	0.620	1.480	23.1	92	97.6	53.7	1.06
30	1.50	0.865	0.579	7.76	5.72	0.879	0.595	0.544	31.3	125	126	17.8	1.01
31	1.50	0.865	0.579	7.76	5.72	0.879	0.602	–0.036	39.6	158	155	202	0.98
32	1.50	0.865	0.579	7.76	5.72	0.879	0.592	–0.244	38.4	154	154	–0.3	1.00
33	1.57	0.787	0.500	7.76	5.45	0.844	0.573	–0.409	36.4	146	149	–2.3	1.02
34	1.57	0.787	0.500	7.76	5.45	0.844	0.695	2.326	27.9	111	144	65.6	1.29
35	1.57	0.787	0.500	7.76	5.45	0.844	0.726	1.276	40.9	164	167	38.9	1.021
36	1.57	0.787	0.500	7.76	5.45	0.844	0.716	0.326	54.0	216	214	11.8	0.991
37	1.57	0.787	0.500	7.76	5.45	0.844	0.722	–0.014	59.8	239	236	1.4	0.987
38	1.57	0.787	0.500	7.76	5.45	0.844	0.731	–0.247	58.2	233	235	–0.9	1.009
39	1.57	0.787	0.500	7.76	5.45	0.844	0.735	–0.356	58.9	236	235	0.3	0.997
40	1.57	0.787	0.500	7.76	5.45	0.844	0.726	1.276	40.9	164	164	41.5	1.003
41	1.57	0.787	0.500	7.76	5.45	0.844	0.735	–0.356	58.9	236	233	1.1	0.989
42	1.57	0.787	0.500	9.72	5.45	0.844	0.726	1.276	40.9	164	172	34.9	1.05
43	1.57	0.787	0.500	9.72	5.45	0.844	0.726	0.344	53.8	215	209	14.4	0.97
44	1.57	0.787	0.500	9.72	5.45	0.844	0.722	–0.016	59.8	239	238	0.5	0.995
45	1.57	0.787	0.500	9.72	5.45	0.844	0.738	–0.237	59.2	237	237	–0.1	1.001
46	1.57	0.787	0.500	9.72	5.45	0.844	0.706	–0.346	58.9	236	234	0.7	0.993
47	1.65	0.708	0.428	9.72	5.17	0.805	0.840	0.803	72.3	289	262	29.0	0.905
48	1.65	0.708	0.428	9.72	5.17	0.805	0.855	0.331	81.3	325	298	18.9	0.917
49	1.65	0.708	0.428	9.72	5.17	0.805	0.863	–0.037	85.4	342	333	2.6	0.975
50	1.65	0.708	0.428	9.72	5.17	0.805	0.840	–0.175	88.1	352	348	1.3	0.988
51	1.65	0.708	0.428	9.72	5.17	0.805	0.865	–0.311	84.1	336	332	1.3	0.987
52	1.96	1.148	0.585	8.41	7.56	0.893	0.706	0.725	46.8	187	191	20.6	1.02
53	1.94	1.158	0.596	8.42	7.58	0.894	0.678	0.132	52.6	210	215	4.0	1.02
54	1.75	1.348	0.769	8.72	8.18	0.901	0.713	0.667	44.7	179	178	29.4	0.996
55	1.75	1.358	0.775	8.74	8.22	0.902	0.704	0.175	50.4	201	205	8.7	1.02

*i = A, B or C based on bolt pattern type; see Column Heading "Type" in Table 1

Shaded Indicates outlier not included in statistical analysis

Table 3 Statistical Analysis				
Type	Mean (μ)	$\sum(\mu - x_i)^2$	*n*	COV (%)
A	0.977	0.075	22	5.99
B	0.902	0.001	2	2.87
C	1.00	0.010	26	1.96

in the design method. This is indicated by the large N_{ux}/N_u for these specimens, 1.47 and 1.64, respectively. In scanning Tables 1 and 2 and comparing t_p to d, it can be seen that reasonable prying ratios β_{ux} occur when $t_p/d > ½$. In addition to the two type A specimens that do not satisfy this criterion, there is one type C specimen that does not. This is specimen 34, which has a prying ratio of 65.6% and a N_{ux}/N_u ratio of 1.29. The author considers these three specimens, numbers—16, 17 and 34—to be outliers that skew the mean of N_{ux}/N_u in a desirable direction—that is, $\mu > 1$—but this skewing is not correct. Thus, they are discounted in the Table 3 statistical analysis. Table 3 shows the mean, μ, the sum of the squares of the deviation from the mean, $\sum_i(\mu - x_i)^2$, and the covariance as a percentage, COV(%), for each of the bolt group types, A, B and C, with the outliers excluded. The means (μ) for types A and C are 0.977 and 1.00, respectively, with covariances of 5.99% and 1.96%, respectively. These values indicate excellent agreement of theory and test results and that designs performed with the proposed type A and C yield lines can be used with confidence.

Type B

The sample size for this type of connection is too small to provide confidence in its use. The mean is 0.902, which, being less than 1.0, indicates that this type will yield unconservative results. As such, its use is not recommended. This same observation is made by Willibald et al. (2002). They recognize that the corner bolts do not share the load equally with the side bolts. The side bolts fail first and reduce the connection capacity below what it would be if all bolts were equally loaded. The low mean value of 0.902 is suggestive of this observation.

The statistical data for type B is included in Table 3 only for completeness. The sample is too small for these data to be meaningful.

Further Discussion and Observations

Note that type C has p_{max} controlling in all specimens. This indicates that this type should be used only for small HSS, say, 3×3 and 4×4. For HSS5×5 and larger, there is no reason not to use a type A configuration.

From the data of Table 2, a correlation between α' and β_{ux} can be observed. When $\alpha' < 0$, the bolts theoretically control the design, which requires that β_{ux} be zero or small. That this is the case can be seen in Table 2. When $0 < \alpha' < 1$, the largest value of β_{ux} is 41.4%. In this range of α', both the plate and the bolts are active in controlling the design capacity. The β_{ux} value of 41.4% indicates that prying is taking place but that no separation or excessive deformations are occurring. When $\alpha' > 1$, the plate controls the design capacity. If the plate is too thin relative to bolt size, say, $t_p/d <$ ½, large values of α' and β_{ux} occur. Table 2 shows that if $\alpha' \le 1.5$, reasonable values of prying ratio, less than approximately 50%, occur. (Specimen 29, with $\alpha' = 1.48$ and $\beta_{ux} =$ 53.7%, is slightly over this 50% limit, but it is accepted here as a viable design.) Note that the outliers all have large values of α'.

The correlation of α' to β_{ux} is important. The ideal parameter to test a design is β_{ux}, but this is an experimental parameter that is not available to the designer. The parameter α', which mirrors the β_{ux} experimental values, is available to the designer. The author recommends, based on the Table 2 results, that the designer control α' to be ≤ 1.5. If $\alpha' > 1.5$, a thicker plate should be used.

When rectangular HSS are used, the bolt spacing should be kept uniform around the perimeter of the HSS. This will ensure that the bolts and HSS wall are uniformly loaded, as is assumed in the design of the HSS member. The parameter c shown in Figure 1 for pattern A is used to guarantee this.

CONCLUSIONS

Design and analysis procedures for end plate connected HSS tension members have been developed. The methods use yield lines matched to the end plate bolt pattern. The methods use the end plate tensile strength F_u rather than the end plate yield strength F_y, thereby bringing them into conformance with the AISC *Manual* (2011) procedure for prying action. The method recommends that, for end plated HSS tension members, the calculation parameter α' be limited to 1.5.

EXAMPLE PROBLEM—DESIGN

Given:

Determine the end plate thickness and the weld size, and the bolts required to resist forces of 16 kips dead load and 50 kips live load on an ASTM A500 Grade B HSS4×4×¼ section. The end plate is ASTM A36. Use E70 electrodes.

Solution:

From AISC *Manual* Tables 2-4 and 2-5, the material properties are:

HSS strut
F_y = 46 ksi
F_u = 58 ksi

End plate
F_y = 36 ksi
F_u = 58 ksi

From AISC *Manual* Table 1-12, the geometric properties are as follows:

HSS4×4×¼
t = 0.233 in.
A = 3.37 in.^{2}

Find the required end plate thickness, t_p.

From Chapter 2 of ASCE/SEI 7 (ASCE, 2016), the required tensile strength is:

P_u = 1.2(16.0 kips) + 1.6(50.0 kips)
= 99.2 kips

From Figure 5,
a = 1.5 in
b = 1.5 in.

A1. Check $a \le 1.25b$:
a = 1.50 in.
1.25b = 1.25(1.50 in.)
= 1.88 in.
$a \le 1.25b$ **o.k.**

A2. Calculate a', b', ρ, d':

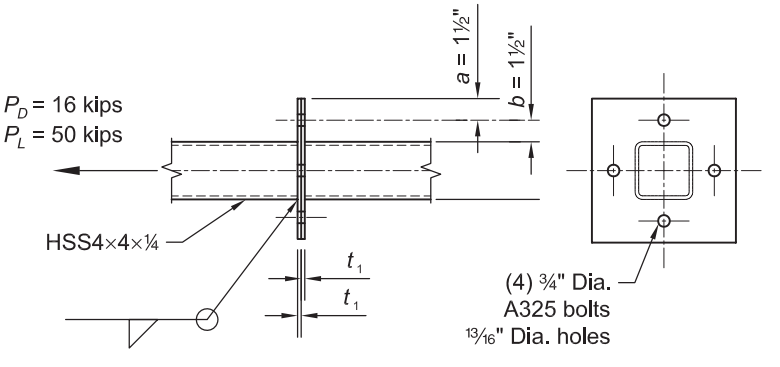

Fig. 5. Data for example problem.

$$a' = a + \frac{d}{2} \tag{12}$$
$$= 1.50 \text{ in.} + \frac{(0.75 \text{ in.})}{2}$$
$$= 1.88 \text{ in.}$$

$$b' = b - \frac{d}{2} \tag{13}$$
$$= 1.50 \text{ in.} - \frac{(0.75 \text{ in.})}{2}$$
$$= 1.13 \text{ in.}$$

$$\rho = \frac{b'}{a'} \tag{14}$$
$$= \frac{1.13 \text{ in.}}{1.88 \text{ in.}}$$
$$= 0.600$$

$$d' = d + 1/16 \text{ in.} \tag{15}$$
$$= 3/4 \text{ in.} + 1/16 \text{ in.}$$
$$= 13/16 \text{ in.}$$

A3. The tributary length per bolt for pattern C is:

$$p_c = \frac{2(w_i + h_i + \pi b)}{n} \tag{8}$$
$$= \frac{2\left[4.00 \text{ in.} + 4.00 \text{ in.} + \pi(1.50 \text{ in.})\right]}{4}$$
$$= 6.36 \text{ in.}$$

A4. Check p_{max}:

$$p_{max} = 4\sqrt{b'(a+b)} \tag{11}$$
$$= 4\sqrt{1.13 \text{ in.}(1.50 + 1.50 \text{ in.})}$$
$$= 7.35 \text{ in.}$$

Because $p_c < p_{max}$, the pattern C can be developed. Use $p = p_c = 6.36$ in.

A5. Calculate δ:

$$\delta = 1 - \frac{d'}{p} \tag{16}$$
$$= 1 - \frac{13/16 \text{ in.}}{6.36 \text{ in.}}$$
$$= 0.872$$

A6. Calculate t_c:

From AISC *Manual* Table 7-2, the design strength per bolt is:

$B = 29.8$ kips.

$$t_c = \sqrt{\frac{4Bb'}{\phi p F_u}} \tag{17}$$
$$= \sqrt{\frac{(4)(29.8 \text{ kip/bolt})(1.13 \text{ in.})}{(0.90)(6.36 \text{ in.})(58 \text{ ksi})}}$$
$$= 0.636 \text{ in.}$$

D1. Check $T \le B$:

The required tension per bolt, T, is:

$$T = \frac{P_u}{n}$$
$$= \frac{99.2 \text{ kips}}{4 \text{ bolts}}$$
$$= 24.8 \text{ kips}$$

Because $T < B$, the procedure can continue.

D2. Calculate β:

$$\beta = \frac{1}{\rho}\left(\frac{B}{T} - 1\right) \tag{21}$$
$$= \frac{1}{0.600}\left(\frac{29.8 \text{ kips}}{24.8 \text{ kips}} - 1\right)$$
$$= 0.336$$

D3. Because $0 < \beta < 1$,

$$\alpha^* = \min\left[\frac{1}{\delta}\left(\frac{\beta}{1-\beta}\right), 1\right] \tag{22}$$
$$= \frac{1}{0.872}\left(\frac{0.336}{1-0.336}\right)$$
$$= 0.580$$

D4. Calculate t_p:

$$t_p = t_c\sqrt{\frac{T}{B}\left(\frac{1}{1+\delta\alpha^*}\right)} \tag{23}$$
$$= 0.636 \text{ in.}\sqrt{\frac{24.8 \text{ kips}}{29.8 \text{ kips}}\left(\frac{1}{1+0.872(0.580)}\right)}$$
$$= 0.473 \text{ in.}$$

Use a ½-in. A36 end plate.

D5. Calculate α':

$$\alpha' = \frac{1}{\delta(1+\rho)}\left[\left(\frac{t_c}{t_p}\right)^2 - 1\right] \tag{18}$$
$$= \frac{1}{0.872\,(1+0.600)}\left[\left(\frac{0.636 \text{ in.}}{0.500 \text{ in.}}\right)^2 - 1\right]$$
$$= 0.443$$

D6. Check α':

$\alpha' = 0.443 < 1.5$ **o.k.**

Therefore, the ½-in. A36 end plate is adequate.

Design the weld of the end plate to the HSS

From AISC *Manual* Table 1-12, the surface area of the HSS 4×4×¼ = 1.27 ft^2/ft

Length of weld = l_w = (1.27 ft^2/ft)(12 in./ft)
= 15.2 in.

From the AISC *Specification* Section J2.4 (AISC, 2016):

$F_{nw} = 0.60F_{EXX}(1.0 + 0.50\sin^{1.5}\theta)$ (*Spec*. Eq. J2-5)

With $\theta = 90°$:

$1.0 + 0.50\sin^{1.5} 90 = 1.5$

The weld size required, D, is then:

$$D = \frac{P_u}{1.392(1.5)l_w}$$ (from *Manual* Eq. 8-2a)

$$= \frac{99.2 \text{ kips}}{1.392(1.5)(15.2 \text{ in.})}$$

= 3.12 sixteenths

Use ¼-in. fillet weld.

EXAMPLE PROBLEM—ANALYSIS

Find the design strength of the previous example when a ½-in. A36 end plate is specified.

From the calculations of the previous problem:
t_c = 0.636 in.
$\alpha' = 0.443$

A7. Because $0 < \alpha' < 1$, bolts and plate control

$$T_u = B\left(\frac{t_p}{t_c}\right)^2(1+\delta\alpha') \quad (19)$$

$$= (29.8 \text{ kip/bolt})\left(\frac{0.500 \text{ in.}}{0.636 \text{ in.}}\right)^2\left[1+(0.872)(0.443)\right]$$

= 25.5 kip/bolt

A8. Calculate N_u:

$N_u = nT_u$ (20)
= (4 bolts)(25.5 kip/bolt)
= 102 kips

A9. Because N_u = 102 kips > P_u = 99.2 kips, the design is satisfactory.

SYMBOLS

B Design bolt tensile strength, $\phi F_{nt} A_b$, used for routine analysis design calculations, kips [The notation used here is that of the AISC *Specification*, ANSI/AISC 360-10; see the AISC *Manual* (2011), Part 16, Table J3.2.]

B_u Measured bolt tensile strength, Table 1, kips

F_u End plate tensile strength, measured values for Table 2 calculations, specified minimum values for routine analysis and design calculations, ksi

F_y End plate yield strength, ksi

N_u Predicted connection axial capacity, nT_u, kips

N_{ux} Experimental connection capacity, kips

P_u Required axial tension strength for the design problems and the yield line nominal tensile strengths for patterns A, B and C, kips

T Required tensile strength per bolt, kips

T_u Predicted tensile capacity per bolt, or design strength, kips

a Plate dimension from bolt center to edge of end plate, in.

a' $a + d/2$, in.

b Plate dimension from bolt center to edge of HSS member, in.

b' $b - d/2$, in.

c Reported bolt spacing in type A bolt pattern specimens, in. (Not explicitly used in this study, but see the discussion in the "Further Discussion and Observations" section.)

d Bolt diameter, in.

d' Hole size (bolt diameter plus 1/16 in., except measured values for specimens 23–26), in.

h_i Dimension of HSS, in.

h_p Dimension of end plate, in.

l Length of equivalent straight line yield line, in.

n Number of bolts in bolt pattern or number of specimens in statistical sample

p Tributary length of end plate per bolt, in.

p_i Tributary length of end plate per bolt for the ith pattern, A, B or C, in.

$p_{i,max}$ Maximum bolt spacing for the ith pattern, in.

t_c End plate thickness that will develop the design bolt strength B, in.

t_{cx} End plate thickness that will develop the experimental bolt strength B_u, in.

t_p End plate thickness, in.

w_i Dimension of HSS, in.

w_p Dimension of end plate, in.

x_i Specific datum value, $(N_{ux}/N_u)_i$, for the ith datum value

α^* Calculation parameter for the proposed design method

α' Calculation parameter for the proposed analysis method, representing the theoretical point at which the bolt strength and the plate strength are equal

β Calculated prying ratio, $\frac{1}{\rho}\left(\frac{B}{T} - 1\right)$, Eq. 9-25 of the AISC *Manual* (2011)

β_{ux} Experimental prying ratio, $\frac{nB_u - N_{ux}}{N_{ux}}(100)$, % [similar to AISC *Manual* (2011), Eq. 9-25]

δ Factor in analysis and design methods that removes the bolt holes, $1 - d'/p$

ϕ Resistance factor from AISC *Manual* (2011) Eq. 9-30a

μ Mean value of a data set

ρ Parameter in analysis and design methods, b'/a'

REFERENCES

AISC (1980), *Manual of Steel Construction*, 8th Ed., American Institute of Steel Construction, Chicago, IL.

AISC (2005), *Manual of Steel Construction*, 13th Ed., American Institute of Steel Construction, Chicago, IL.

AISC (2011), *Manual of Steel Construction*, 14th Ed., American Institute of Steel Construction, Chicago, IL.

AISC (2016), *Specification for Structural Steel Buildings*, ANSI/AISC 360-16, American Institute of Steel Construction, Chicago, IL.

ASCE (2016), *Minimum Design Loads and Associated Criteria for Buildings and Other Structures,* ASCE/SEI 7-16, American Society of Civil Engineers, Reston, VA.

Caravaggio, A. (1988), "Tests on Steel Roof Joints for Toronto Sky Dome," Master of Applied Science Thesis, University of Toronto, Toronto, Canada.

Douty, R.T. and McGuire, W. (1965), "High Strength Bolted Moment Connections," *Journal of the Structural Division,* ASCE, Vol. 91, No. ST2, pp. 101–128.

Dowswell, B. (2011), "A Yield Line Component Method for Bolted Flange Connections," *Engineering Journal*, AISC, Vol. 48, No. 2, pp. 93–115.

Kapp, R. H. (1974), "Yield Line Analysis of a Web Connection in Direct Tension," *Engineering Journal*, AISC, Vol. 11, No. 2, pp. 38–41.

Kato, B. and McGuire, W. (1973), "Analysis of T-Stub Flange to Column Connections," *Journal of the Structural Division*, ASCE, Vol. 99, No. ST5, pp. 865–888.

Kato, B., and Mukai, A. (1985), "Bolted Tension Flanges Joining Square Hollow Section Members," *Journal of Constructional Steel Research*, Vol. 5, pp. 163–177.

Packer, J., Sherman, D. and Lecce, M. (2010), Design Guide 24, *Hollow Structural Section Connections*, American Institute of Steel Construction, Chicago, IL.

Save, M.A. and Massonnet, C.E. (1972), *Plastic Analysis and Design of Plates, Shells and Disks*, North Holland, Amsterdam, pp. 225–265.

Struik, J.H.A. and deBack, J. (1969), "Tests on Bolted T-Stubs with Respect to a Bolted Beam to Column Connection," Stevin Laboratory Report 6-69-B, Delft University of Tech, Delft, The Netherlands.

Swanson, J. (2002), "Ultimate Strength Prying Models for Bolted Tee Stub Connections," *Engineering Journal*, AISC, Vol. 39, No. 3, pp. 136–147.

Thornton, W.A. (1985), "Prying Action—A General Treatment," *Engineering Journal*, AISC, Vol. 22, No. 2, pp. 67–75.

Thornton, W.A. (1992), "Strength and Serviceability of Hanger Connections," *Engineering Journal*, AISC, Vol. 29, No. 4, pp. 145–149.

Thornton, W.A. (1996), "Strength and Serviceability of Hanger Connections," Errata, *Engineering Journal*, AISC, Vol. 33, No. 1, pp. 39–40.

Willibald, S., Packer, J.A. and Puthli, R.S. (2002), "Experimental Study of Bolted HSS Flange-Plate Connections in Axial Tension," *Journal of Structural Engineering,* ASCE, Vol. 128, No. 3, pp. 328–336.

Willibald, S., Packer, J.A. and Puthli, R.S. (2003), "Design Recommendations for Bolted Rectangular HSS Flange Plate Connections in Axial Tension," *Engineering Journal*, AISC, Vol. 40, No. 1, pp. 15–24.

Design of Wrap-Around Gusset Plates

BO DOWSWELL, FOUAD FOUAD, JAMES DAVIDSON and ROBERT WHYTE

ABSTRACT

This paper addresses the design of wrap-around gusset plates, which are commonly used where a horizontal brace connects at a beam-to-column intersection. Wrap-around gusset plates must be cut around the column, which can lead to high flexural stresses near the reentrant corner.

A rational design method is developed in this paper, based on the results of 15 experimental tests and the corresponding finite element models. The design method, which models the gusset legs as rectangular beams, considers the strength of each leg independently. Because the buckled shapes included both out-of-plane translation and twisting along the leg, the stability behavior is evaluated using a lateral-torsional buckling model according to AISC *Specification* Section F11. Based on the buckled shape of the specimens and finite element models, design buckling lengths are recommended. Information is also included for calculating the strength of wrap-around gusset plates with the interior corner cut on a diagonal. Three examples are provided to illustrate the proposed design procedure.

Keywords: wrap-around gusset plate, horizontal braced, design buckling length.

INTRODUCTION

In most commercial buildings, floor and roof diaphragms are used to distribute loads in the horizontal plane of the structure to the lateral load-resisting system. Due to the open nature of most industrial structures, diaphragms are not present, and horizontal bracing is often used to distribute the loads in the horizontal plane. Horizontal bracing is also used in commercial structures, where a diaphragm is not present or where the strength or stiffness of the diaphragm is not adequate. A simple horizontal bracing system is shown in Figure 1.

Connection Details

Figure 2a shows a typical horizontal bracing connection at a beam-to-beam intersection. Where a horizontal brace connects at a beam-to-column intersection, the gusset plate is typically cut around the column as shown in Figure 2b. At locations with large columns and beam clip angles, as shown in Figure 2c, a significant portion of the gusset plate must be cut out. The optional diagonal cut shown at the inside corner of the plate can increase the bending strength of the gusset plate. The optional cut at the outside corner is used to ensure compliance with the maximum edge distance requirements in AISC *Specification* (AISC, 2010) Section J3.5.

Objective

A consistent design method for wrap-around gusset plates has not been established. The objective of this paper is to develop a rational design method, based on the results of 15 experimental tests and the corresponding finite element models (Dowswell, 2005). The tests and finite element models were also documented by Dowswell and Fouad (2006), Dowswell et al. (2006) and Dowswell and Fouad (2007). This paper is focused on design information; therefore, only a brief discussion of the pertinent research data will be presented. Three examples are provided to illustrate the proposed design procedure.

LOAD DISTRIBUTION

Due to the geometry of wrap-around gusset plates, shear and flexural stresses develop in the plate that must be accounted for in design. Because the force distribution in horizontal brace connections is indeterminate, simplifying assumptions are required for connection design. The load distribution can be determined using a stiffness analysis, but modeling the entire connection using finite elements is not practical for design. Localized yielding in bracing connections begins in the early stages of loading and the load distribution changes

Bo Dowswell, P.E., Ph.D., ARC International, LLC, Birmingham, AL. Email: bo@arcstructural.com (corresponding)

Fouad H. Fouad, Ph.D., P.E., Professor and Chair, Department of Civil, Construction and Environmental Engineering, The University of Alabama at Birmingham, Birmingham, AL. Email: ffouad@uab.edu

James S. Davidson, Ph.D., Professor, Auburn University, Auburn, AL. Email: jim.davidson@auburn.edu

Robert Whyte, P.E., S.E., Project Manager, LBYD Inc., Birmingham, AL. Email: rwhyte@lbyd.com

Paper No. 2016-02

as the brace force increases. Further complicating the analysis are the effects of frame action, foundation settlements, thermal expansion, erection stresses, etc. Therefore, the loads used in connection design should be based on the ultimate strength condition.

Interface Loads

The lower-bound theorem of limit analysis states that a load calculated based on an assumed load distribution that satisfies equilibrium conditions with forces nowhere exceeding the capacity will be less than or equal to the true limit load. Using the lower-bound theorem for a given connection, the strength calculated using the load distribution that results in the highest strength is closest to the actual strength. In practical terms, this means that engineers can choose any load distribution that is convenient if the following conditions are satisfied:

1. All framing members and connection elements must be in equilibrium.
2. All elements in the load path must have adequate strength to resist the assumed loads.
3. All elements in the joint must have adequate ductility to allow the loads to redistribute so the assumed distribution can be achieved.

The assumed load distribution must be consistent throughout the connection and member design. If the aforementioned conditions are satisfied, the loads can be distributed in any convenient manner. Because this is critical to the economy of the connection, selecting a reasonable load distribution often requires significant experience and judgment.

For the connection in Figure 2b, Figure 3 shows two potential methods to distribute the axial load in the brace to the gusset-to-beam interfaces. Using a deformation compatibility approach, the interface forces shown in Figure 3a are incorrect. This is because the gusset-to-beam interfaces are typically much stiffer when loaded in the plane of the web relative to out-of-plane loading. The out-of-plane flexibility can be caused by weak-axis bending of the beams, local bending of the web, and bending (prying) of the clip angles.

If the forces perpendicular to the web at both interfaces are deemed negligible, the resulting interface forces are shown in Figure 3b. The load distribution in Figure 3b uses the simplest and most direct path to get the components of the brace force directly into the beams, and it is considered standard practice for these connections.

Even if deformation compatibility were not an issue, there are several negative consequences for selecting the load distribution in Figure 3a:

1. The connection angles and beam webs must be designed for the forces perpendicular to the webs, $F_E/2$ or $F_N/2$. This will require thicker connection angles and will likely require stiffeners in the beam webs.
2. The beams may be overstressed because they are not typically designed for weak-axis bending and weak-axis shear.
3. In addition to any transfer force and beam end reaction, the beam-to-column connections would be subjected to a horizontal shear force.

Internal Loads

The load distribution in wrap-around gusset plate connections is shown in Figure 4. The plate legs are subject to flexure, and each leg is modeled independently as a rectangular beam with a linearly varying moment diagram. The

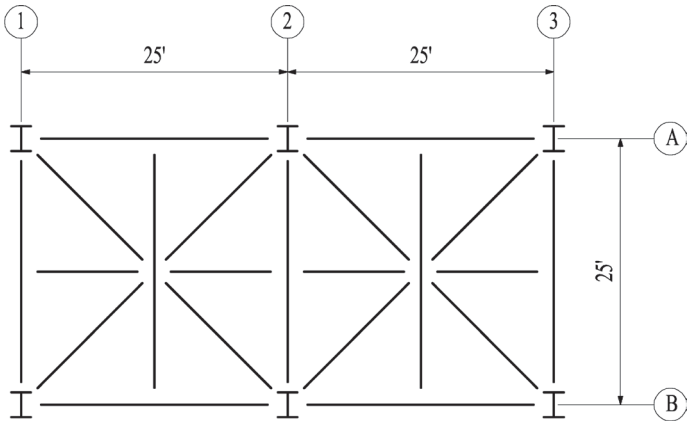

Fig. 1. Plan view of a horizontal bracing system.

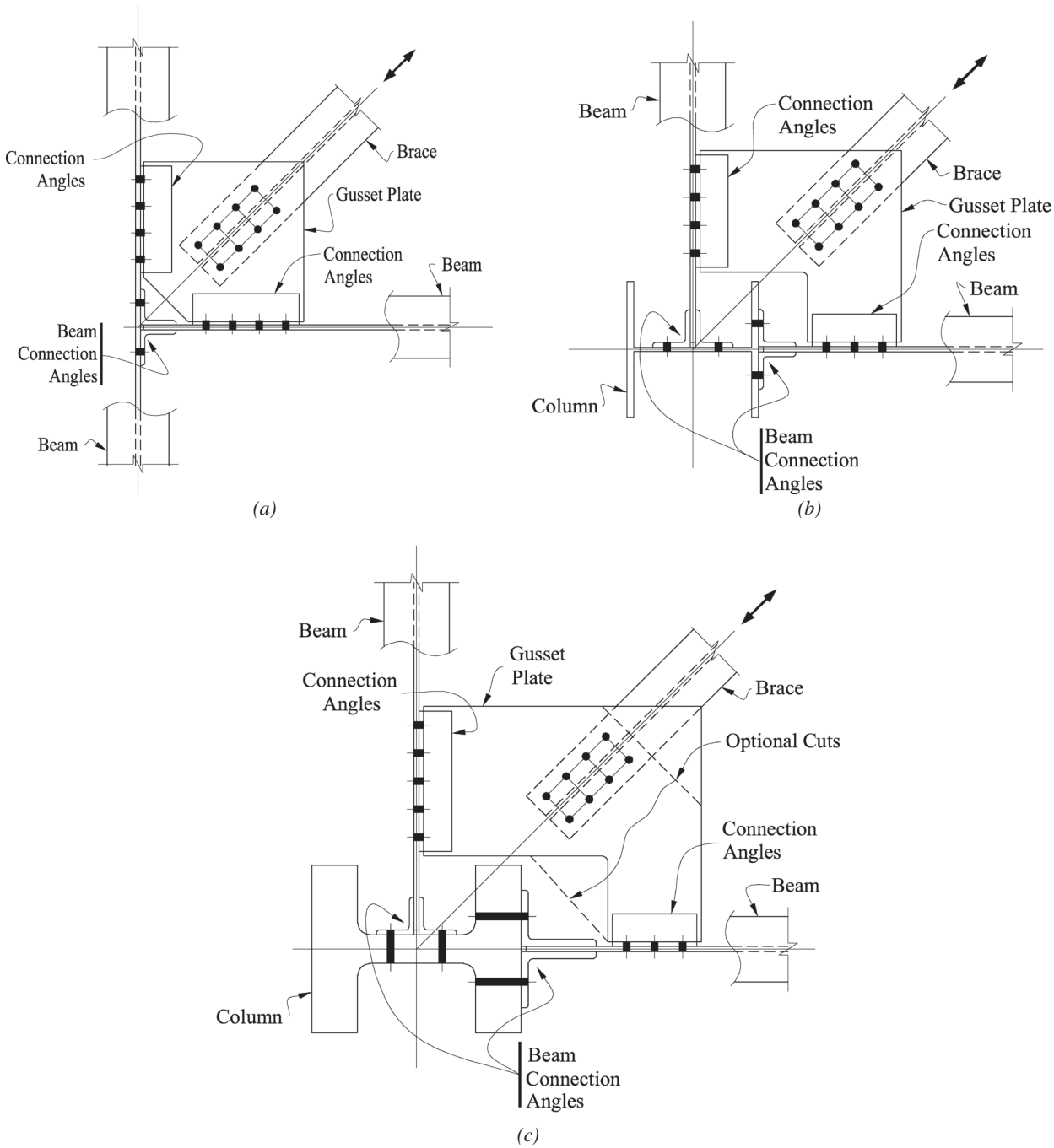

Fig. 2. Horizontal brace gusset plates: (a) beam-to-beam interface; (b) beam-to-column interface with wrap-around gusset plate; (c) wrap-around gusset plate with a large cutout and optional diagonal cuts.

maximum moments are located at the interior face of the adjacent leg. Equations 1a and 1b, which may be conservative for some gusset plate geometries, can be used to calculate the required moments at the critical section of each leg.

For leg 1

$$M_{r1} = P_1 e_2 \quad (1a)$$

For leg 2

$$M_{r2} = P_2 e_1 \quad (1b)$$

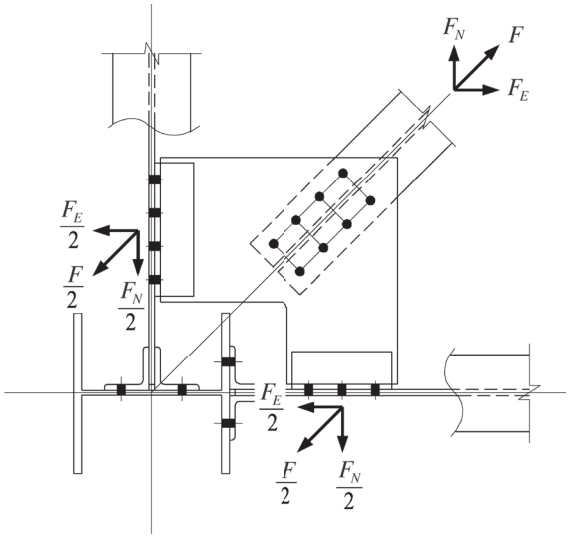

(a)

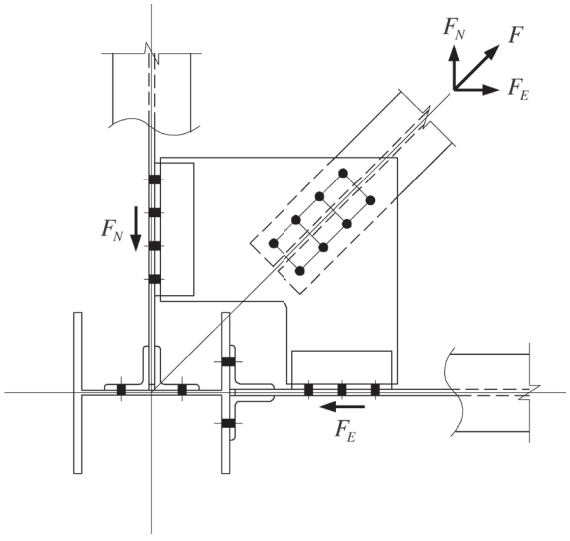

(b)

Fig. 3. Interface loads at a horizontal brace connection: (a) inefficient; (b) efficient.

where

P_1 = component of the brace load, P, at leg 1, kips

P_2 = components of the brace load, P, at leg 2, kips

e_1 = cutout dimension perpendicular to leg 1, in.

e_2 = cutout dimension perpendicular to leg 2, in.

FLEXURAL STRENGTH

Each leg of the plate is subject to limit states common to flexural members; therefore, the legs are modeled independently, as separate beams. In addition to the flexural strength, including lateral-torsional buckling, the shear strength of each leg should be considered in the design.

Stress

Each leg of the gusset plate must resist the moments generated by the load system in Figure 4. This results in maximum bending stresses at the reentrant corner where the two legs meet. Figure 5 shows the stress contour plots for a finite element model loaded in tension. Figure 5a shows maximum von Mises stresses at the reentrant corner. The normal stresses in the *x*- and *y*-directions are shown in Figures 5b and 5c, respectively. As expected, the maximum stresses are at the edges of each leg and at the intersection of the two legs—where the maximum moments occur. Because the brace load was in tension, the flexural stresses are compressive at the inner edges and tensile at the outer edges. The stresses in the *y*-direction are higher than the stresses in the *x*-direction because of the larger cutout dimension in the *y*-direction.

The stress patterns from 15 finite element models and the strain gage data from the corresponding experimental specimens verified the accuracy of the load system in

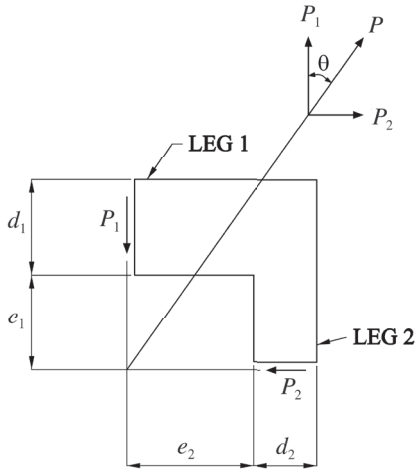

Fig. 4. Internal loads for wrap-around gusset plates.

Figure 4. At the failure load, the strain gage data and finite element models indicated some yielding. Although most of the plates had a substantial amount of material above the proportional limit, none of the plates reached full plasticity before buckling.

Lateral-Torsional Buckling

Although five of the 15 specimens were tested with tensile brace loads, the gusset leg flexural loads caused buckling in all of the experimental specimens and finite element models as shown in Figures 6 and 7, respectively. Figure 6a shows the permanent deformation after testing for specimen 2T, which was tested in tension. Figure 6b shows the permanent deformation after testing for specimen 7C, which was tested in compression. For both specimens, the maximum out-of-plane translation corresponds to the location of maximum compressive stress. The buckled shapes included both out-of-plane translation and twisting along the leg.

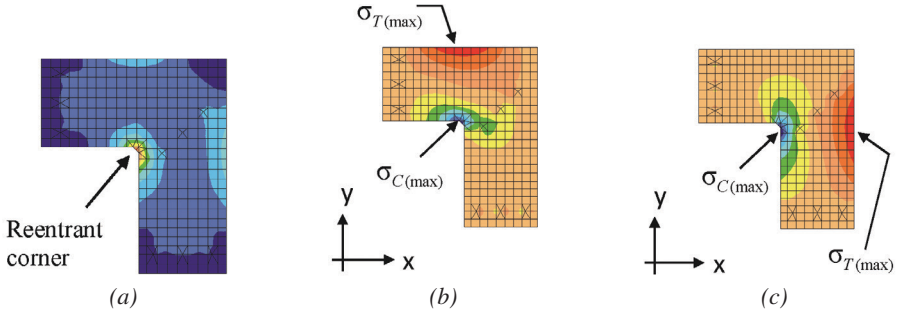

Fig. 5. Elastic stress contours for a typical model loaded in tension: (a) von Mises stresses; (b) x-x normal stresses; (c) y-y normal stresses.

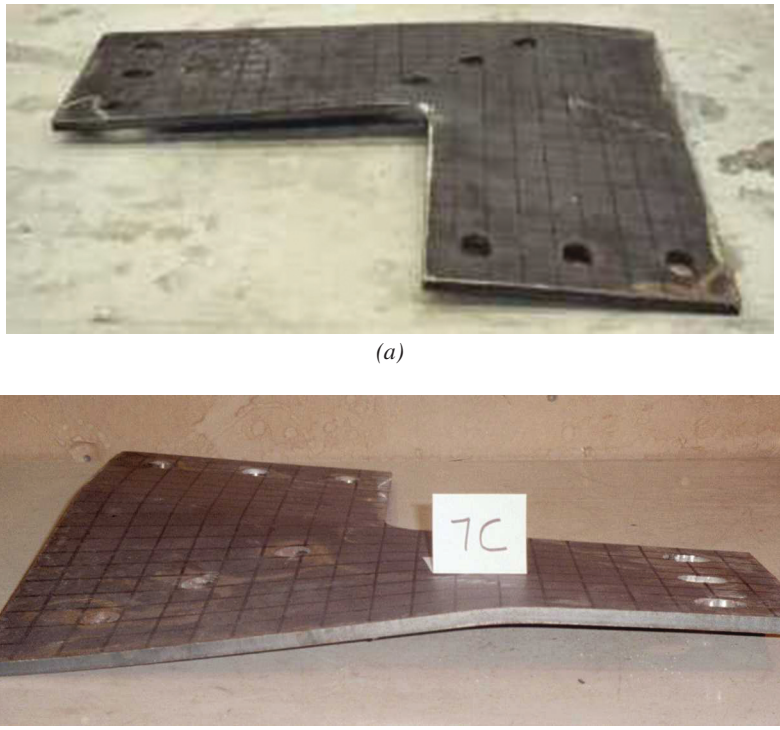

Fig. 6. Specimens 2T and 7C after testing: (a) specimen 2T; (b) specimen 7C.

Effect of Diagonal Cut at the Interior Corner

Wrap-around gusset plates can have the interior corner cut on a diagonal as shown in Figure 2c. To determine the effect of the diagonal cut, test specimens 8 and 10, shown in Figure 8, were fabricated with identical geometry, except for the diagonal cut on specimen 10. The tests and finite element models showed a strength increase of about 20% due to the diagonal cut.

For each leg, the critical section could be located at either end of the diagonal cut; therefore, the flexural strength at both sections should be considered. Figures 9a and 9b show the normal stress contours for specimen 10 in the x- and y-directions, respectively. Because the gusset plate is loaded in tension, the interior edges of the cutout are subjected to compression stresses. The maximum x-direction stresses are located at the reentrant corner farthest from the beam center at leg 1. In this case, the critical section is subjected to a moment equal to P_1e_2. The maximum y-direction stresses are located at the reentrant corner closest to the beam center at leg 2. In this case, the critical section is subjected to a moment equal to P_2e_{r1}. These results show the importance of calculating the flexural strength for each leg at both cross-sections located at the reentrant corners of the diagonal cut.

DESIGN

The experimental and finite element results validate the practice of treating each leg of the gusset plate as a rectangular beam. Because the buckled shapes included both out-of-plane translation and twisting along the leg, the stability behavior can be evaluated using a lateral-torsional buckling model. Dowswell (2016) verified that AISC *Specification* Section F11 can be used for designing connection elements subjected to lateral-torsional buckling. Dowswell and Whyte (2014) suggested this approach for calculating the local flexural strength of double-coped beams, which had buckled shapes that are similar to those of wrap-around gusset plate

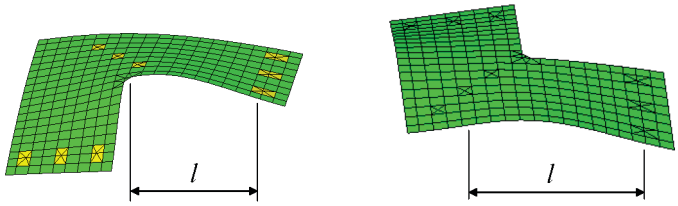

Fig. 7. Buckled shapes of finite element models: (a) tension load; (b) compression load.

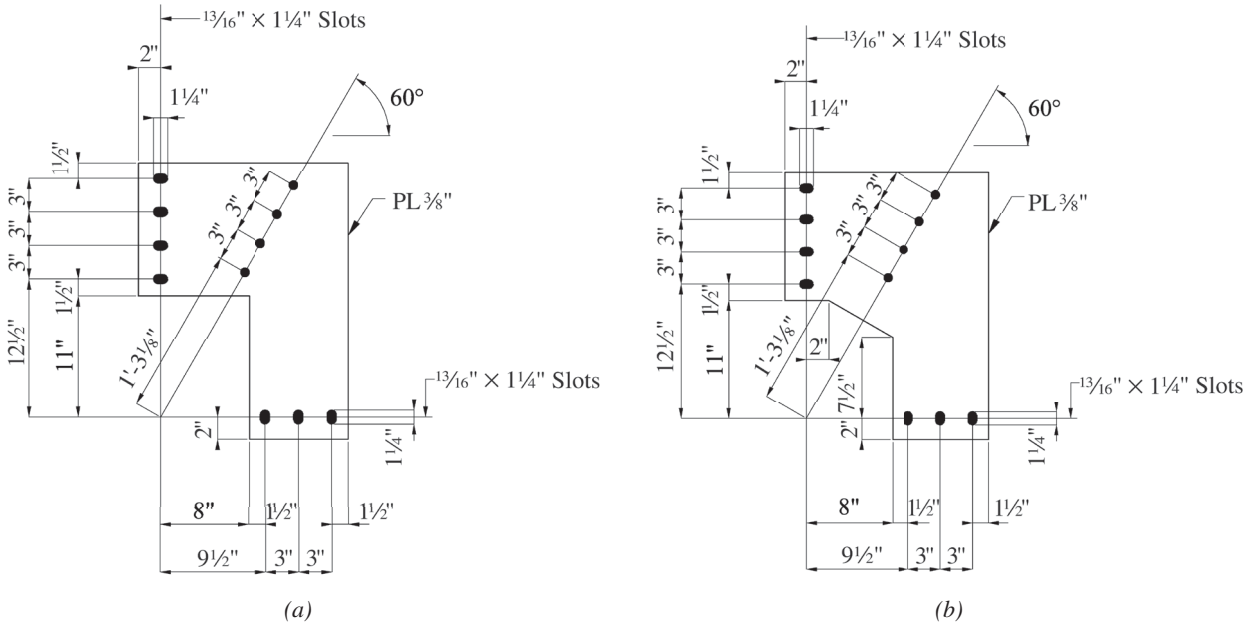

Fig. 8. Details of specimens 8 and 10: (a) specimen 8; (b) specimen 10.

legs. The shear strength of each leg is calculated according to AISC *Specification* Section J4.2.

AISC *Specification* Section F11

AISC *Specification* (AISC, 2010) Section F11 defines the flexural strength of rectangular members. The nominal strength is the lower value obtained according to the limit states of yielding and lateral-torsional buckling.

For $\frac{L_b d}{t^2} \le \frac{0.08E}{F_y}$, yielding is the controlling limit state. The nominal strength is:

$$M_n = M_p = F_y Z \le 1.6 M_y \qquad \text{(Spec. Eq. F11-1)}$$

For $\frac{0.08E}{F_y} < \frac{L_b d}{t^2} \le \frac{1.9E}{F_y}$, inelastic lateral-torsional buckling is the controlling limit state.

$$M_n = C_b \left[1.52 - 0.274 \left(\frac{L_b d}{t^2} \right) \frac{F_y}{E} \right] M_y \le M_p \qquad \text{(Spec. Eq. F11-2)}$$

For $\frac{L_b d}{t^2} > \frac{1.9E}{F_y}$, elastic lateral-torsional buckling is the controlling limit state.

$$M_n = F_{cr} S_x \le M_p \qquad \text{(Spec. Eq. F11-3)}$$

where

$$F_{cr} = \frac{1.9EC_b}{\frac{L_b d}{t^2}} \qquad \text{(Spec. Eq. F11-4)}$$

C_b = lateral-torsional buckling modification factor for nonuniform moment diagrams

E = modulus of elasticity of steel = 29,000 ksi (200 000 MPa)

F_y = specified minimum yield stress, ksi (MPa)

L_b = distance between braces, in. (mm)

M_p = plastic bending moment, kip-in. (N-mm)

M_y = moment at yielding of the extreme fiber, kip-in. (N-mm)

S_x = elastic section modulus taken about the x-axis, in.^{3} (mm^3)

Z = plastic section modulus about the axis of bending, in.^{3} (mm^3)

d = depth of the gusset plate leg, in. (mm)

t = thickness of the gusset plate, in. (mm)

General Design Method

Because the buckling strength in AISC *Specification* Section F11 is dependent on both L_b and C_b, appropriate values for these variables were developed to provide the best estimate of the true strength and behavior of the specimens. To determine the buckling length, L_b, the buckled shape of the specimens and finite element models was observed. A general trend was observed, where the buckling length of the tension specimens was limited to the cutout dimension and the buckling length of the compression specimens extended approximately to the mid-depth of the adjacent leg. The following buckling lengths are applicable when the plate is loaded in tension: $L_{b1} = e_2$ for leg 1, and $L_{b2} = e_1$ for leg 2. For plates loaded in compression, the following buckling lengths

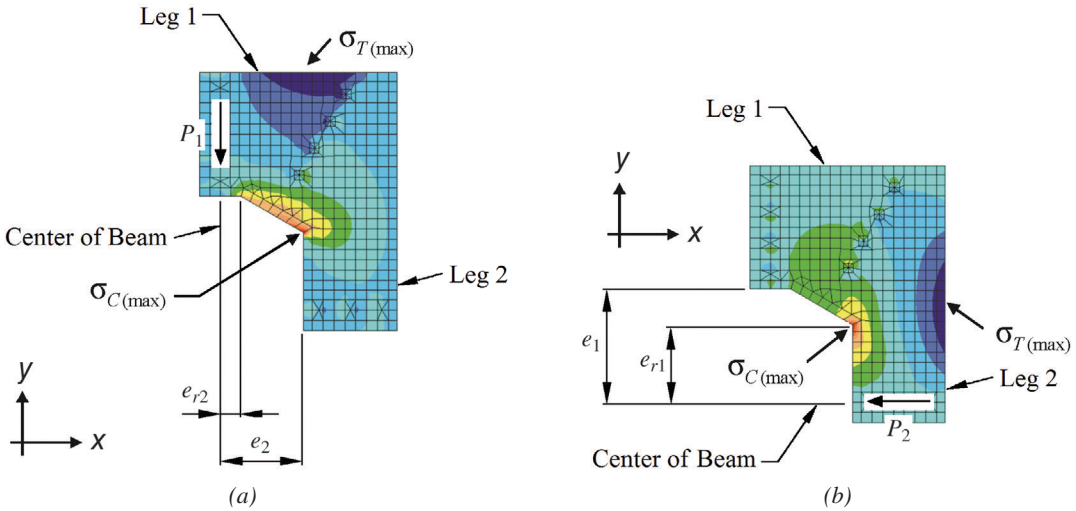

Fig. 9. Elastic stress contours for specimen 10, which was loaded in tension: (a) x-direction normal stresses; (b) y-direction normal stresses.

are applicable: $L_{b1} = e_2 + d_2/2$ for leg 1, and $L_{b2} = e_1 + d_1/2$ for leg 2. As shown in Figure 4, d_1 and d_2 are the depths of legs 1 and 2, respectively.

According to equations developed by Dowswell (2004), $C_b = 1.84$ for a rectangular cantilever beam loaded at the shear center with bracing at each end and a concentrated load at the tip. However, the experimental and finite element results show that the legs can be assumed fully braced at both ends only under certain conditions. For gusset plates carrying tensile brace loads, $C_b = 1.84$.

For many gusset plates carrying compressive brace loads, both legs will not reach their critical load simultaneously. Therefore, the noncritical leg can provide restraint to the critical leg, and $C_b = 1.84$ provides accurate results. Conversely, when the critical load ratio of both legs are similar, full bracing cannot be assumed, and $C_b = 1.00$ is more accurate. For gusset plates carrying compressive brace loads, C_b, can be determined based on the critical load ratio, α, which was developed by Dowswell (2012).

For gusset plates with $\alpha > 1.6$ or $\alpha < 1/1.6$, $C_b = 1.84$

For gusset plates with $1/1.6 \le \alpha \le 1.6$, $C_b = 1.00$

where

$$\alpha = \frac{(M_{cr}/M_r)_2}{(M_{cr}/M_r)_1} = \frac{d_1 L_{b2} P_2 e_1}{d_2 L_{b1} P_1 e_2} = \frac{d_1 L_{b2} e_1}{d_2 L_{b1} e_2} \tan\theta \quad (2)$$

$(M_{cr}/M_r)_1$ = critical moment to required moment ratio at leg 1

$(M_{cr}/M_r)_2$ = critical moment to required moment ratio at leg 2

$M_{cr} = F_{cr} S_x$

θ = angle between the brace and the beam connected to leg 1 (Figure 4)

For plates with a diagonal cut, L_b and C_b are calculated the same as plates with square cutouts. Plate leg depths, d_1 and d_2, are the dimensions between the parallel edges, without consideration of the diagonal cut. For buckling calculations, d_1 and d_2 are used to calculate the sectional properties. The required moments for buckling at the legs can be calculated using Equations 1a and 1b with e_{m1} and e_{m2} substituted for e_1 and e_2, respectively. The variables e_{m1} and e_{m2} are the distances along the adjacent leg, from the work point to the midpoint of the diagonal cut, as shown in Figure 10. The flexural yielding strength, using the available plastic moment, should also be checked at the reentrant corners of the diagonal cut.

The strength of each specimen was calculated using the general design method, with the results summarized in the second column of Table 1. All of the loads are expressed as the brace load based on the minimum strength of the two legs. All loads were calculated using the actual plate thickness and yield strength measured before testing. The predicted failure modes are listed in the third column. The specimen numbers are suffixed with "T" if the plate was loaded in tension and "C" if it was loaded in compression.

The experimental loads are listed in the fourth and fifth columns of Table 1. P_{ep} is the experimental load at the proportional limit, determined using a line offset 1/32 in. from the linear portion of the experimental curve. P_{eu} is the maximum experimental load. The experimental failure modes are listed in the sixth column. The experimental-to-calculated strength ratios, P_{ep}/P_c and P_{eu}/P_c, are listed in the seventh and eighth columns of Table 1, respectively. P_{ep}/P_c varies from 0.786 to 1.89, with an average of 1.15 and a standard deviation of 0.302. P_{eu}/P_c varies from 0.880 to 2.01, with an average of 1.40 and a standard deviation of 0.312.

Simplified Design Method

To simplify the design process, $C_b = 1.00$ can be used for all gusset plates with compressive brace loads. Using $C_b = 1.84$ for gusset plates with tensile brace loads, four of the five experimental specimens were predicted to fail at the plastic strength. These four specimens were 3/8-in. thick. Specimen 6T, which had a predicted failure mode of elastic buckling, was only 1/4-in. thick. Because gusset plates in steel structures are usually at least 3/8-in. thick, these gusset plates can be designed assuming the legs are fully braced against lateral-torsional buckling.

The strength of each specimen was calculated using the simplified design method, with the results summarized in the second column of Table 2. All of the loads are expressed as the brace load based on the minimum strength of the

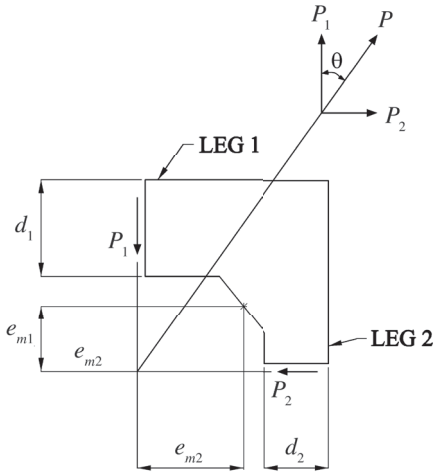

Fig. 10. Dimensions for wrap-around gusset plates with a diagonal cut.

Table 1. Calculated and Experimental Loads (General Design Method)							
Specimen No.	P_c, kips	Predicted Failure Mode	P_{ep}, kips	P_{eu}, kips	Experimental Failure Mode	$\frac{P_{ep}}{P_c}$	$\frac{P_{eu}}{P_c}$
2T	49.7	P	69.0	89.9	I	1.39	1.81
6T	45.1	E	42.3	53.6	I	0.938	1.19
8T	69.0	P	85.3	91.2	I	1.24	1.32
9T	53.6	P	51.5	63.6	I	0.961	1.19
10T	82.7	P	96.2	110.0	I	1.16	1.33
1C	39.5	I	33.3	45.8	I	0.843	1.16
2C	49.3	I	47.3	63.9	I	0.960	1.30
3C	41.9	I	46.6	64.2	I	1.11	1.53
4C	16.9	E	32.0	32.0	E	1.89	1.89
5C	23.3	E	28.7	46.8	I	1.23	2.01
6C	15.7	E	25.3	25.3	E	1.61	1.61
7C	52.9	I	46.4	46.5	I	0.877	0.880
8C	48.9	I	38.4	60.8	I	0.786	1.24
9C	37.3	I	44.4	51.5	I	1.19	1.38
10C	57.0	I	57.0	66.5	I	1.00	1.17

P_c = calculated strength, kips
P_{ep} = experimental load at proportional limit (1/32 in. offset), kips
P_{eu} = maximum experimental load, kips
E: Elastic buckling
I: Inelastic buckling
P: Plastic flexural strength

Table 2. Calculated and Experimental Loads (Simplified Design Method)							
Specimen No.	P_c, kips	Predicted Failure Mode	P_{ep}, kips	P_{eu}, kips	Experimental Failure Mode	$\frac{P_{ep}}{P_c}$	$\frac{P_{eu}}{P_c}$
2T	49.7	P	69.0	89.9	I	1.39	1.81
6T	47.7	P	42.3	53.6	I	0.887	1.12
8T	69.0	P	85.3	91.2	I	1.24	1.32
9T	53.6	P	51.5	63.6	I	0.960	1.19
10T	82.7	P	96.2	110.0	I	1.16	1.33
1C	28.4	I	33.3	45.8	I	1.17	1.61
2C	35.9	I	47.3	63.9	I	1.32	1.78
3C	41.9	I	46.6	64.2	I	1.11	1.53
4C	9.2	E	32.0	32.0	E	3.48	3.48
5C	12.6	E	28.7	46.8	I	2.28	3.71
6C	15.7	E	25.3	25.3	E	1.61	1.61
7C	52.9	I	46.4	46.5	I	0.877	0.880
8C	48.9	I	38.4	60.8	I	0.785	1.24
9C	37.3	I	44.4	51.5	I	1.19	1.38
10C	57.0	I	57.0	66.5	I	1.00	1.17

P_c = calculated strength, kips
P_{ep} = experimental load at proportional limit (1/32 in. offset), kips
P_{eu} = maximum experimental load, kips
E: Elastic buckling
I: Inelastic buckling
P: Plastic flexural strength

two legs. All loads were calculated using the actual plate thickness and yield strength measured before testing. The predicted failure modes are listed in the third column. The experimental loads are listed in the fourth and fifth columns, and the experimental failure modes are listed in the sixth column. The P_{ep}/P_c and P_{eu}/P_c ratios are listed in the seventh and eighth columns of Table 2, respectively. P_{ep}/P_c varies from 0.786 to 3.48, and P_{eu}/P_c varies from 0.880 to 3.70. The highest experimental-to-nominal load ratios are for cases where the general design method could be used to increase C_b from 1.00 to 1.84.

SUMMARY

A rational design method for wrap-around gusset plates was developed in this paper, based on the results of 15 experimental tests and the corresponding finite element models. The design method, which models the gusset legs as rectangular beams, considers the strength of each leg independently.

Because the buckled shapes included both out-of-plane translation and twisting along the leg, the buckling strength of each leg is evaluated using a lateral-torsional buckling model according to AISC *Specification* Section F11. Appropriate values for L_b and C_b were developed to provide the best estimate of the true strength and behavior of the specimens. Three examples are provided to illustrate the proposed design procedure.

For many practical geometries, the noncritical leg can provide restraint against lateral-torsional buckling of the critical leg. In these cases, including gusset plates carrying tensile brace loads, C_b = 1.84 is recommended for design. Otherwise, C_b = 1.00 is applicable. At the maximum experimental load, the mean experimental-to-calculated strength ratio is 1.40 with a standard deviation of 0.312.

A simplified design method was also discussed, where C_b = 1.00 for all gusset plates carrying compressive brace loads. For gusset plates with tensile brace loads, the limit state of lateral-torsional buckling is neglected, and the flexural strength is calculated using the plastic moment capacity. At the maximum experimental load, the experimental-to-calculated strength ratios varied from 0.880 to 3.70. However, the highest experimental-to-nominal load ratios are for cases where the general design method could be used to increase C_b from 1.00 to 1.84.

EXAMPLE 1—SIMPLIFIED DESIGN METHOD

In this example, the strength the gusset plate shown in Figure 11 is calculated using the simplified design method. The gusset plate is ⅜-in.-thick ASTM A572 Grade 50 material. The LRFD and ASD loads are 50.0 kips tension/30 kips compression and 33.3 kips tension/20 kips compression, respectively.

From AISC *Manual* Table 2-4, the yield strength is F_y = 50 ksi.

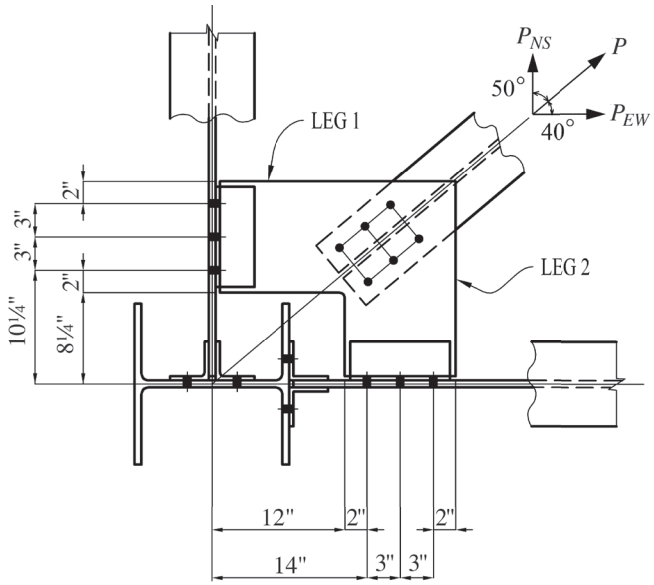

Fig. 11. Wrap-around gusset plate for Example 1.

Tension Brace Load

The brace axial load is:

LRFD	ASD
$P_u = 50.0$ kips (tension)	$P_a = 33.3$ kips (tension)

The north–south and east–west brace components are:

LRFD	ASD
$P_{NS} = (50 \text{ kips})\sin 40° = 32.1$ kips $P_{EW} = (50 \text{ kips})\cos 40° = 38.3$ kips	$P_{NS} = (33.3 \text{ kips})\sin 40° = 21.4$ kips $P_{EW} = (33.3 \text{ kips})\cos 40° = 25.5$ kips

Flexural Strength of Leg 1

The required moment at the interior face of the adjacent leg is:

LRFD	ASD
$M_u = P_{NS}e_2$ (from Eq. 1a) $= (32.1 \text{ kips})(12.0 \text{ in.})$ $= 385$ kip-in.	$M_a = P_{NS}e_2$ (from Eq. 1a) $= (21.4 \text{ kips})(12.0 \text{ in.})$ $= 257$ kip-in.

When the brace is in tension, the legs are assumed to be fully braced; therefore, the nominal flexural strength according to AISC *Specification* Section F11 is:

$$M_n = M_p = F_y Z \qquad \text{(Spec. Eq. F11-1)}$$

$$= (50 \text{ ksi})\left[\frac{(⅜ \text{ in.})(10.0 \text{ in.})^2}{4}\right]$$

$$= 469 \text{ kip-in.}$$

The available flexural strength is:

LRFD	ASD
$\phi M_n = (0.90)(469 \text{ kip-in.})$ $= 422 \text{ kip-in.} > 385 \text{ kip-in.}$ **o.k.**	$\frac{M_n}{\Omega} = \frac{469 \text{ kip-in.}}{1.67}$ $= 281 \text{ kip-in.} > 257 \text{ kip-in.}$ **o.k.**

Shear Yielding of Leg 1

$$V_n = 0.60F_y A_{gv} \qquad \text{(from Spec. Eq. J4-3)}$$

$$= (0.60)(50 \text{ ksi})(10.0 \text{ in.})(⅜ \text{ in.})$$

$$= 113 \text{ kips}$$

The available shear strength is:

LRFD	ASD
$\phi V_n = (1.00)(113 \text{ kips})$ $= 113 \text{ kips} > 32.1 \text{ kips}$ **o.k.**	$\frac{V_n}{\Omega} = \frac{113 \text{ kips}}{1.50}$ $= 75.3 \text{ kips} > 21.4 \text{ kips}$ **o.k.**

Flexural Strength of Leg 2

The required moment at the interior face of the adjacent leg is:

LRFD	ASD
$M_u = P_{EW}e_1$ (from Eq. 1b) $= (38.3 \text{ kips})(8¼ \text{ in.})$ $= 316 \text{ kip-in.}$	$M_a = P_{EW}e_1$ (from Eq. 1b) $= (25.5 \text{ kips})(8¼ \text{ in.})$ $= 210 \text{ kip-in.}$

When the brace is in tension, the legs are assumed to be fully braced; therefore, the nominal flexural strength according to AISC *Specification* Section F11 is:

$$M_n = M_p = F_y Z \quad \text{(Spec. Eq. F11-1)}$$

$$= (50 \text{ ksi})\left[\frac{(⅜ \text{ in.})(10.0 \text{ in.})^2}{4}\right]$$

$$= 469 \text{ kip-in.}$$

The available flexural strength is:

LRFD	ASD
$\phi M_n = (0.90)(469 \text{ kip-in.})$ $= 422 \text{ kip-in.} > 316 \text{ kip-in.}$ **o.k.**	$\frac{M_n}{\Omega} = \frac{469 \text{ kip-in.}}{1.67}$ $= 281 \text{ kip-in.} > 210 \text{ kip-in.}$ **o.k.**

Shear Yielding of Leg 2

$$V_n = 0.60F_yA_{gv} \quad \text{(from Spec. Eq. J4-3)}$$
$$= (0.60)(50 \text{ ksi})(10.0 \text{ in.})(⅜ \text{ in.})$$
$$= 113 \text{ kips}$$

The available shear strength is:

LRFD	ASD
$\phi V_n = (1.00)(113 \text{ kips})$ $= 113 \text{ kips} > 38.3 \text{ kips}$ **o.k.**	$\frac{V_n}{\Omega} = \frac{113 \text{ kips}}{1.50}$ $= 75.3 \text{ kips} > 25.5 \text{ kips}$ **o.k.**

Compression Brace Load

The brace axial load is:

LRFD	ASD
$P_u = 30.0$ kips (compression)	$P_a = 20.0$ kips (compression)

The north–south and east–west brace components are:

LRFD	ASD
$P_{NS} = (30.0 \text{ kips})\sin 40° = 19.3 \text{ kips}$ $P_{EW} = (30.0 \text{ kips})\cos 40° = 23.0 \text{ kips}$	$P_{NS} = (20.0 \text{ kips})\sin 40° = 12.9 \text{ kips}$ $P_{EW} = (20.0 \text{ kips})\cos 40° = 15.3 \text{ kips}$

Flexural Strength of Leg 1

$$S_x = \frac{(3/8 \text{ in.})(10.0 \text{ in.})^2}{6}$$
$$= 6.25 \text{ in.}^3$$

$$M_p = F_y Z \qquad \text{(from } \textit{Spec.} \text{ Eq. F11-1)}$$
$$= (50 \text{ ksi})\left[\frac{(3/8 \text{ in.})(10.0 \text{ in.})^2}{4}\right]$$
$$= 469 \text{ kip-in.}$$

The required moment at the interior face of the adjacent leg is:

LRFD	ASD
$M_u = P_{NS} e_2$ (from Eq. 1b)	$M_a = P_{NS} e_2$ (from Eq. 1b)
$= (19.3 \text{ kips})(12.0 \text{ in.})$	$= (12.9 \text{ kips})(12.0 \text{ in.})$
$= 232$ kip-in.	$= 155$ kip-in.

Using $C_b = 1.00$ and $L_{b1} = e_2 + d_2/2 = 12 \text{ in.} + 5 \text{ in.} = 17.0 \text{ in.}$:

$$\frac{L_{b1} d_1}{t^2} = \frac{(17.0 \text{ in.})(10.0 \text{ in.})}{(3/8 \text{ in.})^2}$$
$$= 1{,}210$$

$$\frac{1.9E}{F_y} = \frac{(1.9)(29{,}000 \text{ ksi})}{(50 \text{ ksi})}$$
$$= 1{,}100$$

Because 1,210 > 1,100, elastic lateral-torsional buckling is the controlling limit state, and the critical stress is:

$$F_{cr} = \frac{1.9EC_b}{\frac{L_{b1} d_1}{t^2}} \qquad \text{(}\textit{Spec.}\text{ Eq. F11-4)}$$
$$= \frac{(1.9)(29{,}000 \text{ ksi})(1.00)}{1{,}210}$$
$$= 45.5 \text{ ksi}$$

And thus the nominal flexural strength is:

$$M_n = F_{cr} S_x \le M_p \qquad \text{(}\textit{Spec.}\text{ Eq. F11-3)}$$
$$= (45.5 \text{ ksi})(6.25 \text{ in.}^3) \le 469 \text{ kip-in.}$$
$$= 284 \text{ kip-in.}$$

The available flexural strength is:

LRFD	ASD
$\phi M_n = (0.90)(284 \text{ kip-in.})$	$\frac{M_n}{\Omega} = \frac{284 \text{ kip-in.}}{1.67}$
$= 256 \text{ kip-in.} > 232 \text{ kip-in.}$ **o.k.**	$= 170 \text{ kip-in.} > 155 \text{ kip-in.}$ **o.k.**

Shear Yielding of Leg 1

$V_n = 0.60F_yA_{gv}$ (from *Spec.* Eq. J4-3)
$= (0.60)(50 \text{ ksi})(10.0 \text{ in.})(⅜ \text{ in.})$
$= 113 \text{ kips}$

The available shear strength is:

LRFD	ASD
$\phi V_n = (1.00)(113 \text{ kips})$ $= 113 \text{ kips} > 19.3 \text{ kips}$ **o.k.**	$\frac{V_n}{\Omega} = \frac{113 \text{ kips}}{1.50}$ $= 75.3 \text{ kips} > 12.9 \text{ kips}$ **o.k.**

Flexural Strength of Leg 2

$$S_x = \frac{(⅜ \text{ in.})(10.0 \text{ in.})^2}{6}$$
$$= 6.25 \text{ in.}^3$$

$M_y = F_yS_x$
$= (50 \text{ ksi})(6.25 \text{ in.}^3)$
$= 313 \text{ kip-in.}$

$M_p = F_yZ$ (from *Spec.* Eq. F11-1)

$$= (50 \text{ ksi})\left[\frac{(⅜ \text{ in.})(10.0 \text{ in.})^2}{4}\right]$$
$$= 469 \text{ kip-in.}$$

The required moment at the interior face of the adjacent leg is:

LRFD	ASD
$M_u = P_{EW}e_1$ (from Eq. 1b) $= (23.0 \text{ kips})(8¼ \text{ in.})$ $= 190 \text{ kip-in.}$	$M_a = P_{EW}e_1$ (from Eq. 1b) $= (15.3 \text{ kips})(8¼ \text{ in.})$ $= 126 \text{ kip-in.}$

Using $C_b = 1.00$ and $L_{b2} = e_1 + d_1/2 = 8¼ \text{ in.} + 5 \text{ in.} = 13¼ \text{ in.}$:

$$\frac{L_{b2}d_2}{t^2} = \frac{(13¼ \text{ in.})(10.0 \text{ in.})}{(⅜ \text{ in.})^2}$$
$$= 942$$

$$\frac{0.08E}{F_y} = \frac{(0.08)(29{,}000 \text{ ksi})}{(50 \text{ ksi})}$$
$$= 46.4$$

$$\frac{1.9E}{F_y} = \frac{(1.9)(29{,}000 \text{ ksi})}{(50 \text{ ksi})}$$
$$= 1{,}100$$

Because $46.4 < 942 < 1{,}100$, inelastic lateral-torsional buckling is the controlling limit state, and the nominal flexural strength is:

$$M_n = C_b\left[1.52 - 0.274\left(\frac{L_{b2}d_2}{t^2}\right)\frac{F_y}{E}\right]M_y \le M_p \quad \text{(from } \textit{Spec.} \text{ Eq. F11-2)}$$

$$= (1.00)\left[1.52 - (0.274)(942)\left(\frac{50 \text{ ksi}}{29{,}000 \text{ ksi}}\right)\right](313 \text{ kip-in.}) \le 469 \text{ kip-in.}$$

$$= 336 \text{ kip-in.}$$

The available flexural strength is:

LRFD	ASD
$\phi M_n = (0.90)(336 \text{ kip-in.})$ $= 302 \text{ kip-in.} > 190 \text{ kip-in.}$ **o.k.**	$\frac{M_n}{\Omega} = \frac{336 \text{ kip-in.}}{1.67}$ $= 201 \text{ kip-in.} > 126 \text{ kip-in.}$ **o.k.**

Shear Yielding of Leg 2

$$V_n = 0.60F_yA_{gv} \quad \text{(from } \textit{Spec.} \text{ Eq. J4-3)}$$

$$= (0.60)(50 \text{ ksi})(10.0 \text{ in.})(\tfrac{3}{8} \text{ in.})$$

$$= 113 \text{ kips}$$

The available shear strength is:

LRFD	ASD
$\phi V_n = (1.00)(113 \text{ kips})$ $= 113 \text{ kips} > 23.0 \text{ kips}$ **o.k.**	$\frac{V_n}{\Omega} = \frac{113 \text{ kips}}{1.50}$ $= 75.3 \text{ kips} > 15.3 \text{ kips}$ **o.k.**

EXAMPLE 2—GENERAL DESIGN METHOD

In this example, the strength of the gusset plate in Example 1 is calculated using the general design method.

Tension Brace Load

Flexural Strength of Leg 1

$$S_x = \frac{(\tfrac{3}{8} \text{ in.})(10.0 \text{ in.})^2}{6}$$

$$= 6.25 \text{ in.}^3$$

$$M_y = F_yS_x$$

$$= (50 \text{ ksi})(6.25 \text{ in.}^3)$$

$$= 313 \text{ kip-in.}$$

$$M_p = F_yZ \quad \text{(from } \textit{Spec.} \text{ Eq. F11-1)}$$

$$= (50 \text{ ksi})\left[\frac{(\tfrac{3}{8} \text{ in.})(10.0 \text{ in.})^2}{4}\right]$$

$$= 469 \text{ kip-in.}$$

The required moment at the interior face of the adjacent leg is:

LRFD	ASD
$M_u = P_{NS}e_2$ (from Eq. 1a) $= (32.1 \text{ kips})(12.0 \text{ in.})$ $= 385 \text{ kip-in.}$	$M_a = P_{NS}e_2$ (from Eq. 1a) $= (21.4 \text{ kips})(12.0 \text{ in.})$ $= 257 \text{ kip-in.}$

Using $C_b = 1.84$ and $L_{b1} = e_2 = 12.0$ in.:

$$\frac{L_{b1}d_1}{t^2} = \frac{(12.0 \text{ in.})(10.0 \text{ in.})}{(⅜ \text{ in.})^2}$$
$$= 853$$

$$\frac{0.08E}{F_y} = \frac{(0.08)(29{,}000 \text{ ksi})}{(50 \text{ ksi})}$$
$$= 46.4$$

$$\frac{1.9E}{F_y} = \frac{(1.9)(29{,}000 \text{ ksi})}{(50 \text{ ksi})}$$
$$= 1{,}100$$

Because $46.4 < 853 < 1{,}100$, inelastic lateral-torsional buckling is the controlling limit state, and the nominal flexural strength is:

$$M_n = C_b\left[1.52 - 0.274\left(\frac{L_{b1}d_1}{t^2}\right)\frac{F_y}{E}\right]M_y \le M_p \quad \text{(from } \textit{Spec.} \text{ Eq. F11-2)}$$
$$= (1.84)\left[1.52 - (0.274)(853)\left(\frac{50 \text{ ksi}}{29{,}000 \text{ ksi}}\right)\right](313 \text{ kip-in.}) \le 469 \text{ kip-in.}$$
$$= 469 \text{ kip-in.}$$

The available flexural strength is:

LRFD	ASD
$\phi M_n = (0.90)(469 \text{ kip-in.})$ $= 422 \text{ kip-in.} > 385 \text{ kip-in.}$ **o.k.**	$\frac{M_n}{\Omega} = \frac{469 \text{ kip-in.}}{1.67}$ $= 281 \text{ kip-in.} > 257 \text{ kip-in.}$ **o.k.**

Shear Yielding of Leg 1

$$V_n = 0.60F_yA_{gv} \quad \text{(from } \textit{Spec.} \text{ Eq. J4-3)}$$
$$= (0.60)(50 \text{ ksi})(10.0 \text{ in.})(⅜ \text{ in.})$$
$$= 113 \text{ kips}$$

The available shear strength is:

LRFD	ASD
$\phi V_n = (1.00)(113 \text{ kips})$ $= 113 \text{ kips} > 32.1 \text{ kips}$ **o.k.**	$\frac{V_n}{\Omega} = \frac{113 \text{ kips}}{1.50}$ $= 75.3 \text{ kips} > 21.4 \text{ kips}$ **o.k.**

Flexural Strength of Leg 2

$$S_x = \frac{(3/8 \text{ in.})(10.0 \text{ in.})^2}{6}$$
$$= 6.25 \text{ in.}^3$$

$$M_y = F_y S_x$$
$$= (50 \text{ ksi})(6.25 \text{ in.}^3)$$
$$= 313 \text{ kip-in.}$$

$$M_p = F_y Z \qquad \text{(from } \textit{Spec.} \text{ Eq. F11-1)}$$
$$= (50 \text{ ksi})\left[\frac{(3/8 \text{ in.})(10.0 \text{ in.})^2}{4}\right]$$
$$= 469 \text{ kip-in.}$$

The required moment at the interior face of the adjacent leg is:

LRFD	ASD
$M_u = P_{EW} e_1$ (from Eq. 1b)	$M_a = P_{EW} e_1$ (from Eq. 1b)
$= (38.3 \text{ kips})(8\frac{1}{4} \text{ in.})$	$= (25.5 \text{ kips})(8\frac{1}{4} \text{ in.})$
$= 316 \text{ kip-in.}$	$= 210 \text{ kip-in.}$

Using $C_b = 1.84$ and $L_{b2} = e_1 = 8\frac{1}{4}$ in.:

$$\frac{L_{b2} d_2}{t^2} = \frac{(8\frac{1}{4} \text{ in.})(10.0 \text{ in.})}{(3/8 \text{ in.})^2}$$
$$= 587$$

$$\frac{0.08E}{F_y} = \frac{(0.08)(29{,}000 \text{ ksi})}{(50 \text{ ksi})}$$
$$= 46.4$$

$$\frac{1.9E}{F_y} = \frac{(1.9)(29{,}000 \text{ ksi})}{(50 \text{ ksi})}$$
$$= 1{,}100$$

Because $46.4 < 587 < 1{,}100$, inelastic lateral-torsional buckling is the controlling limit state, and the nominal flexural strength is:

$$M_n = C_b\left[1.52 - 0.274\left(\frac{L_{b2} d_2}{t^2}\right)\frac{F_y}{E}\right] M_y \le M_p \qquad \text{(from } \textit{Spec.} \text{ Eq. F11-2)}$$
$$= (1.84)\left[1.52 - (0.274)(587)\left(\frac{50 \text{ ksi}}{29{,}000 \text{ ksi}}\right)\right](313 \text{ kip-in.}) \le 469 \text{ kip-in.}$$
$$= 469 \text{ kip-in.}$$

The available flexural strength is:

LRFD	ASD
$\phi M_n = (0.90)(469 \text{ kip-in.})$ $= 422 \text{ kip-in.} > 316 \text{ kip-in.}$ **o.k.**	$\frac{M_n}{\Omega} = \frac{469 \text{ kip-in.}}{1.67}$ $= 281 \text{ kip-in.} > 210 \text{ kip-in.}$ **o.k.**

Shear Yielding of Leg 2

$V_n = 0.60F_yA_{gv}$ (from *Spec.* Eq. J4-3)
$= (0.60)(50 \text{ ksi})(10.0 \text{ in.})(\frac{3}{8} \text{ in.})$
$= 113 \text{ kips}$

The available shear strength is:

LRFD	ASD
$\phi V_n = (1.00)(113 \text{ kips})$ $= 113 \text{ kips} > 38.3 \text{ kips}$ **o.k.**	$\frac{V_n}{\Omega} = \frac{113 \text{ kips}}{1.50}$ $= 75.3 \text{ kips} > 25.5 \text{ kips}$ **o.k.**

Compression Brace Load

Critical Load Ratio

$\theta = 50°$

$$\alpha = \frac{d_1 L_{b2} e_1}{d_2 L_{b1} e_2} \tan\theta \quad (2)$$

$$= \frac{(10.0 \text{ in.})(13\frac{1}{4} \text{ in.})(8\frac{1}{4} \text{ in.})}{(10.0 \text{ in.})(17.0 \text{ in.})(12.0 \text{ in.})} \tan(50°)$$

$= 0.639$

Because $1/1.6 < 0.639 < 1.6$, $C_b = 1.00$ and the remaining calculations are identical to Example 1.

Both the tension and compression strength is the same as for Example 1, which used the simplified design method.

EXAMPLE 3—GUSSET WITH DIAGONAL CUT

In this example, a diagonal cut is added to the gusset plate in Figure 11 as shown in Figure 12. The simplified design method is used to calculate the strength. The gusset plate is ⅜-in.-thick ASTM A572 Grade 50 material. The LRFD and ASD loads are 60.0 kips tension/35.0 kips compression and 40.0 kips tension/23.3 kips compression, respectively.

From AISC *Manual* Table 2-4, $F_y = 50$ ksi.

Tension Brace Load

The brace axial load is:

LRFD	ASD
$P_u = 60.0$ kips (Tension)	$P_a = 40.0$ kips (Tension)

The north–south and east–west brace components are:

LRFD	ASD
P_{NS} = (60 kips)sin40° = 38.6 kips P_{EW} = (60 kips)cos40° = 46.0 kips	P_{NS} = (40.0 kips)sin40° = 25.7 kips P_{EW} = (40.0 kips)cos40° = 30.6 kips

Flexural Strength of Leg 1

The required moment at the reentrant corner of the diagonal cut is:

LRFD	ASD
$M_u = P_{NS}e_2$ (from Eq. 1a) = (38.6 kips)(8.00 in.) = 309 kip-in.	$M_a = P_{NS}e_2$ (from Eq. 1a) = (25.7 kips)(8.00 in.) = 206 kip-in.

When the brace is in tension, the legs are assumed to be fully braced; therefore, the nominal flexural strength according to AISC *Specification* Section F11 is:

$$M_p = F_y Z \quad \text{(from } \textit{Spec.} \text{ Eq. F11-1)}$$

$$= (50 \text{ ksi})\left[\frac{(\frac{3}{8} \text{ in.})(10.0 \text{ in.})^2}{4}\right]$$

$$= 469 \text{ kip-in.}$$

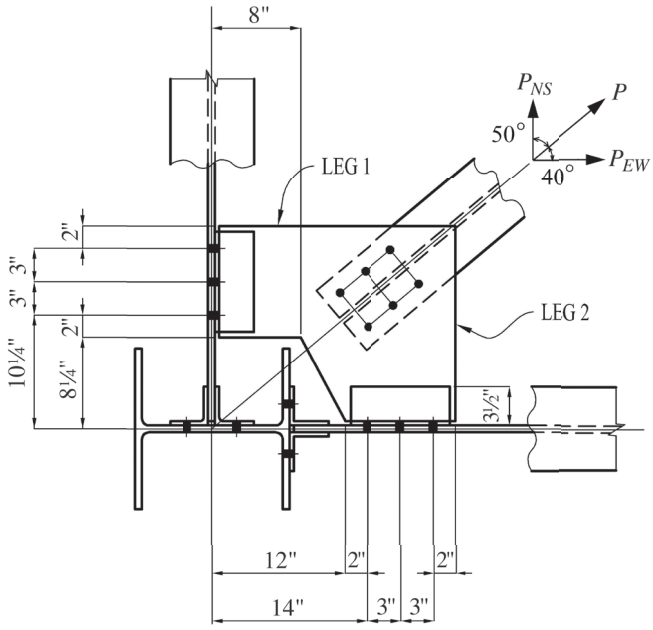

Fig. 12. Wrap-around gusset plate for Example 3.

The available flexural strength is:

LRFD	ASD
$\phi M_n = (0.90)(469 \text{ kip-in.})$ $= 422 \text{ kip-in.} > 309 \text{ kip-in.}$ **o.k.**	$\frac{M_n}{\Omega} = \frac{469 \text{ kip-in.}}{1.67}$ $= 281 \text{ kip-in.} > 206 \text{ kip-in.}$ **o.k.**

Shear Yielding of Leg 1

$V_n = 0.60F_yA_{gv}$ (from *Spec.* Eq. J4-3)
$= (0.60)(50 \text{ ksi})(10.0 \text{ in.})(\frac{3}{8} \text{ in.})$
$= 113 \text{ kips}$

The available shear strength is:

LRFD	ASD
$\phi V_n = (1.00)(113 \text{ kips})$ $= 113 \text{ kips} > 38.6 \text{ kips}$ **o.k.**	$\frac{V_n}{\Omega} = \frac{113 \text{ kips}}{1.50}$ $= 75.3 \text{ kips} > 25.7 \text{ kips}$ **o.k.**

Flexural Strength of Leg 2

The required moment at the interior face of the adjacent leg is:

LRFD	ASD
$M_u = P_{EW}e_1$ (from Eq. 1b) $= (46.0 \text{ kips})(8\frac{1}{4} \text{ in.})$ $= 380 \text{ kip-in.}$	$M_a = P_{EW}e_1$ (from Eq. 1b) $= (30.6 \text{ kips})(8\frac{1}{4} \text{ in.})$ $= 252 \text{ kip-in.}$

The depth of leg 2 at the interior face of the adjacent leg is 14 in. When the brace is in tension, the legs are assumed to be fully braced; therefore, the nominal flexural strength according to AISC *Specification* Section F11 is:

$M_p = F_yZ$ (from *Spec.* Eq. F11-1)

$$= (50 \text{ ksi})\left[\frac{(\frac{3}{8} \text{ in.})(14.0 \text{ in.})^2}{4}\right]$$

$= 919 \text{ kip-in.}$

The available flexural strength is:

LRFD	ASD
$\phi M_n = (0.90)(919 \text{ kip-in.})$ $= 827 \text{ kip-in.} > 380 \text{ kip-in.}$ **o.k.**	$\frac{M_n}{\Omega} = \frac{919 \text{ kip-in.}}{1.67}$ $= 550 \text{ kip-in.} > 252 \text{ kip-in.}$ **o.k.**

Shear Yielding of Leg 2

The shear strength will be analyzed at a plane immediately beyond the clip angle leg. The gusset plate leg width at this location is:

$d_{2V} = 10.0 \text{ in} + (4.00 \text{ in.})(3.50 \text{ in.}/8.25 \text{ in.})$
$= 11.7 \text{ in.}$

$V_n = 0.60F_yA_{gv}$ (from *Spec.* Eq. J4-3)
$= (0.60)(50 \text{ ksi})(11.7 \text{ in.})(0.375 \text{ in.})$
$= 132 \text{ kips}$

The available shear strength is:

LRFD	ASD
$\phi V_n = (1.00)(132 \text{ kips})$ $= 132 \text{ kips} > 46.0 \text{ kips}$ **o.k.**	$\frac{V_n}{\Omega} = \frac{132 \text{ kips}}{1.50}$ $= 88.0 \text{ kips} > 30.6 \text{ kips}$ **o.k.**

Compression Brace Load

The brace axial load is:

LRFD	ASD
$P_u = 35.0 \text{ kips (compression)}$	$P_a = 23.3 \text{ kips (compression)}$

The north–south and east–west brace components are:

LRFD	ASD
$P_{NS} = (35.0 \text{ kips})\sin 40° = 22.5 \text{ kips}$ $P_{EW} = (35.0 \text{ kips})\cos 40° = 26.8 \text{ kips}$	$P_{NS} = (23.3 \text{ kips})\sin 40° = 15.0 \text{ kips}$ $P_{EW} = (23.3 \text{ kips})\cos 40° = 17.8 \text{ kips}$

Flexural Strength of Leg 1

$$S_x = \frac{(\frac{3}{8} \text{ in.})(10.0 \text{ in.})^2}{6}$$
$$= 6.25 \text{ in.}^3$$

$M_p = F_yZ$ (from *Spec.* Eq. F11-1)
$$= (50 \text{ ksi})\left[\frac{(\frac{3}{8} \text{ in.})(10.0 \text{ in.})^2}{4}\right]$$
$= 469 \text{ kip-in.}$

The required moment at the mid-point of the diagonal cut is:

LRFD	ASD
$M_u = P_{NS}e_{m2}$ (from Eq. 1a) $= (22.5 \text{ kips})(10.0 \text{ in.})$ $= 225 \text{ kip-in.}$	$M_a = P_{NS}e_{m2}$ (from Eq. 1a) $= (15.0 \text{ kips})(10.0 \text{ in.})$ $= 150 \text{ kip-in.}$

Using $C_b = 1.00$ and $L_{b1} = e_2 + d_2/2 = 12 \text{ in.} + 5 \text{ in.} = 17.0 \text{ in.}$:

$$\frac{L_{b1}d_1}{t^2} = \frac{(17.0 \text{ in.})(10.0 \text{ in.})}{(\frac{3}{8} \text{ in.})^2}$$
$$= 1{,}210$$

$$\frac{1.9E}{F_y} = \frac{(1.9)(29{,}000 \text{ ksi})}{(50 \text{ ksi})}$$
$$= 1{,}100$$

Because 1,210 > 1,100, elastic lateral-torsional buckling is the controlling limit state, and the critical stress is:

$$F_{cr} = \frac{1.9EC_b}{\frac{L_{b1}d_1}{t^2}} \quad \text{(from } \textit{Spec.} \text{ Eq. F11-4)}$$
$$= \frac{(1.9)(29{,}000 \text{ ksi})(1.00)}{1{,}210}$$
$$= 45.5 \text{ ksi}$$

The nominal flexural strength is:

$$M_n = F_{cr}S_x \le M_p \quad \text{(}\textit{Spec.}\text{ Eq. F11-3)}$$
$$= (45.5 \text{ ksi})(6.25 \text{ in.}^3) \le 469 \text{ kip-in.}$$
$$= 284 \text{ kip-in.}$$

The available flexural strength is:

LRFD	ASD
$\phi M_n = (0.90)(284 \text{ kip-in.})$ $= 256 \text{ kip-in.} > 225 \text{ kip-in.}$ **o.k.**	$\frac{M_n}{\Omega} = \frac{284 \text{ kip-in.}}{1.67}$ $= 170 \text{ kip-in.} > 150 \text{ kip-in.}$ **o.k.**

Shear Yielding of Leg 1

$$V_n = 0.60F_yA_{gv} \quad \text{(from } \textit{Spec.} \text{ Eq. J4-3)}$$
$$= (0.60)(50 \text{ ksi})(10.0 \text{ in.})(\tfrac{3}{8} \text{ in.})$$
$$= 113 \text{ kips}$$

The available shear strength is:

LRFD	ASD
$\phi V_n = (1.00)(113 \text{ kips})$ $= 113 \text{ kips} > 22.5 \text{ kips}$ **o.k.**	$\frac{V_n}{\Omega} = \frac{113 \text{ kips}}{1.50}$ $= 75.3 \text{ kips} > 15.0 \text{ kips}$ **o.k.**

Flexural Strength of Leg 2

$$S_x = \frac{(\tfrac{3}{8} \text{ in.})(10.0 \text{ in.})^2}{6}$$
$$= 6.25 \text{ in.}^3$$

$$M_y = F_yS_x$$
$$= (50 \text{ ksi})(6.25 \text{ in.}^3)$$
$$= 313 \text{ kip-in.}$$

$$M_p = F_y Z \qquad \text{(from } \textit{Spec.} \text{ Eq. F11-1)}$$
$$= (50 \text{ ksi})\left[\frac{(⅜ \text{ in.})(10.0 \text{ in.})^2}{4}\right]$$
$$= 469 \text{ kip-in.}$$

The required moment at the mid-point of the diagonal cut is:

LRFD	ASD
$M_u = P_{EW} e_{m1}$ (from Eq. 1b)	$M_a = P_{EW} e_1$ (from Eq. 1b)
$= (26.8 \text{ kips})(4⅜ \text{ in.})$	$= (17.8 \text{ kips})(4⅜ \text{ in.})$
$= 117$ kip-in.	$= 77.9$ kip-in.

Using $C_b = 1.00$ and $L_{b2} = e_1 + d_1/2 = 8¼$ in. + 5 in. = 13¼ in.:

$$\frac{L_{b2} d_2}{t^2} = \frac{(13¼ \text{ in.})(10.0 \text{ in.})}{(⅜ \text{ in.})^2}$$
$$= 942$$

$$\frac{0.08E}{F_y} = \frac{(0.08)(29{,}000 \text{ ksi})}{(50 \text{ ksi})}$$
$$= 46.4$$

$$\frac{1.9E}{F_y} = \frac{(1.9)(29{,}000 \text{ ksi})}{(50 \text{ ksi})}$$
$$= 1{,}100$$

Because $46.4 < 942 < 1{,}100$, inelastic lateral-torsional buckling is the controlling limit state, and the nominal flexural strength is:

$$M_n = C_b\left[1.52 - 0.274\left(\frac{L_{b2} d_2}{t^2}\right)\frac{F_y}{E}\right] M_y \le M_p \qquad \text{(from } \textit{Spec.} \text{ Eq. F11-2)}$$
$$= (1.00)\left[1.52 - (0.274)(942)\left(\frac{50 \text{ ksi}}{29{,}000 \text{ ksi}}\right)\right](313 \text{ kip-in.}) \le 469 \text{ kip-in.}$$
$$= 336 \text{ kip-in.}$$

The available flexural strength is:

LRFD	ASD
$\phi M_n = (0.90)(336 \text{ kip-in.})$	$\frac{M_n}{\Omega} = \frac{336 \text{ kip-in.}}{1.67}$
$= 302$ kip-in. > 117 kip-in. **o.k.**	$= 201$ kip-in. > 77.9 kip-in. **o.k.**

The required moment at the interior face of the adjacent leg is:

LRFD	ASD
$M_u = P_{EW} e_1$ (from Eq. 1b)	$M_a = P_{EW} e_1$ (from Eq. 1b)
$= (26.8 \text{ kips})(8¼ \text{ in.})$	$= (17.8 \text{ kips})(8¼ \text{ in.})$
$= 221$ kip-in.	$= 147$ kip-in.

The depth of leg 2 at the reentrant corner is 14 in. For yielding at the reentrant corner, the legs are assumed to be fully braced; therefore, the nominal flexural strength according to AISC *Specification* Section F11 is:

$$M_p = F_y Z \qquad \text{(from } \textit{Spec.} \text{ Eq. F11-1)}$$

$$= (50 \text{ ksi}) \left[\frac{(\frac{3}{8} \text{ in.})(14.0 \text{ in.})^2}{4} \right]$$

$$= 919 \text{ kip-in.}$$

The available flexural strength is:

LRFD	ASD
$\phi M_n = (0.90)(919 \text{ kip-in.})$	$\frac{M_n}{\Omega} = \frac{919 \text{ kip-in.}}{1.67}$
$= 827 \text{ kip-in.} > 221 \text{ kip-in.}$ **o.k.**	$= 550 \text{ kip-in.} > 147 \text{ kip-in.}$ **o.k.**

Shear Yielding of Leg 2

The shear strength will be analyzed at a plane immediately beyond the clip angle leg. The gusset plate leg width at this location is:

$$d_{2V} = 10.0 \text{ in} + (4.00 \text{ in.})(3.50 \text{ in.}/8.25 \text{ in.})$$
$$= 11.7 \text{ in.}$$

$$V_n = 0.60 F_y A_{gv} \qquad \text{(from } \textit{Spec.} \text{ Eq. J4-3)}$$
$$= (0.60)(50 \text{ ksi})(11.7 \text{ in.})(0.375 \text{ in.})$$
$$= 132 \text{ kips}$$

The available shear strength is:

LRFD	ASD
$\phi V_n = (1.00)(132 \text{ kips})$	$\frac{V_n}{\Omega} = \frac{132 \text{ kips}}{1.50}$
$= 132 \text{ kips} > 26.8 \text{ kips}$ **o.k.**	$= 88.0 \text{ kips} > 17.8 \text{ kips}$ **o.k.**

REFERENCES

AISC (2010), *Specification for Structural Steel Buildings*, ANSI/AISC 360-10, American Institute of Steel Construction, Chicago, IL.

AISC (2011), *Steel Construction Manual*, 14th Ed., American Institute of Steel Construction, Chicago, IL.

Dowswell, B. (2004), "Lateral-Torsional Buckling of Wide Flange Cantilever Beams," *Engineering Journal*, AISC, Vol. 41, No. 2, pp. 135–147.

Dowswell, B. (2005), *Design of Wrap-Around Steel Gusset Plates*, Ph.D. Dissertation, Department of Civil and Environmental Engineering, The University of Alabama at Birmingham, Birmingham, AL.

Dowswell, B. (2012), "Connection Design for Industrial Structures—Problems and Solutions," *Proceedings of the Structures for Mining and Related Materials Handling Conference*, South African Institute of Steel Construction, October 15-18, Vanderbijlpark, South Africa.

Dowswell, B. (2016), "Stability of Rectangular Connection Elements," *Engineering Journal*, AISC, accepted for publication.

Dowswell, B. and Fouad, F. (2006), "Testing of Wrap-Around Gusset Plates in Tension," *Proceedings of the Annual Stability Conference*, San Antonio, TX, Structural Stability Research Council.

Dowswell, B. and Fouad, F. (2007), "Design of Wrap-Around Gusset Plates," *Proceedings of the Annual Stability Conference*, New Orleans, LA, Structural Stability Research Council.

Dowswell, B. and Whyte, R. (2014), "Local Stability of Double-Coped Beams," *Engineering Journal*, AISC, Vol. 51, No. 1.

Dowswell, B., Whyte, R., Davidson, J. and Fouad, F. (2006), "Finite Element Modeling of Wrap-Around Gusset Plates in Tension," *Proceedings of the Structures Congress*, St. Louis, MO, American Society of Civil Engineers.

Effective Shear Plane Model for Tearout and Block Shear Failure of Bolted Connections

LIP H. TEH and GREGORY G. DEIERLEIN

ABSTRACT

In spite of many revisions to the block shear requirements of the AISC *Specification*, the model in the current *Specification* can result in calculated strengths and failure modes that are inconsistent with published test data. The inconsistencies are primarily related to the assumed interaction of tensile and shear resisting mechanisms, combined with the definition of net and gross shear planes that are unrealistic. Using recently published test results of single-bolt connections in mild and high-strength steel plates, the shear failure planes are observed to be neither the assumed net nor gross shear planes, which are the basis of the current design provision, but rather effective shear planes with a calculated area that is between the net and gross areas. Based on the tensile rupture and shear yielding mechanism, and assuming that the steel on the effective shear planes is fully strain hardened, a simpler and more accurate block shear design equation is proposed. The new equation is straightforward to implement as it requires a simple rearrangement of existing design variables to determine an effective shear failure area. Through verifications against 161 gusset plate specimens, tested by independent researchers around the world, the proposed equation is shown to be significantly more accurate than the current AISC, Canadian, European and Japanese block shear design provisions. A resistance factor of 0.85 is recommended for use with the proposed equation, based on the available statistics from tests and well-established LRFD reliability principles. An example is presented to illustrate the impact of the proposed design provision, which can result in significantly fewer bolts per connection and/or smaller gusset plates, leading to simpler and more economical designs.

Keywords: block shear, bolted connections, gusset plates, shear-out, shear planes, tearout.

INTRODUCTION

The block shear failure mode of bolted connections was first identified by Birkemoe and Gilmor (1978) and was incorporated in the 1978 AISC *Specification for Structural Steel Buildings* (AISC, 1978), which was still in the allowable stress design (ASD) format. Since then, the design provision to check block shear failures of bolted connections changed with every edition of the load and resistance factor design (LRFD) *Specification* until 2005, as summarized in Table 1 for concentrically loaded gusset plates. These changes were primarily motivated by ambiguities regarding the interaction of tension and shear behavior on assumed gross or net yield and rupture planes. In all of these specifications, there has been a presumption of yielding on gross areas and rupture on net areas, where the gross and net areas are A_{gt} and A_{nt} for tension and A_{gv} and A_{nv} for shear, and the corresponding stress limits for yielding and rupture are the tension yield stress, F_y, and ultimate stress, F_u. As will be described later, these basic assumptions about characterizing behavior are much the reason for the perennial debate about block shear design provisions.

It may be noted that since the 2005 S*pecification* (AISC, 2005), there is a nonuniform stress distribution factor, denoted U_{bs}, applied to the tensile strength component, F_uA_{nt}, of the block shear resistance. This reduction factor is equal to unity in most cases, including a concentrically loaded gusset plate, and is therefore not shown in the equations contained in this paper.

The absence of changes in the block shear design provision since 2005 masks a curiosity of the current provision (AISC, 2016), which suggests that the load required to fail a bolted connection by simultaneous tensile and shear ruptures can be lower than that required for the tensile rupture and shear yielding mechanism. The practical outcome of this incongruence is that the design provision can underestimate the actual block shear strength by almost 20% on average and up to 40% in certain cases.

There are several reasons for the repeated amendments and for the fact that the latest design provision is still substantially inaccurate, even though it represents an improvement over earlier provisions. This paper reviews the evolution of the block shear design provisions in the AISC *Specifications* since the first LRFD edition (AISC, 1986). Based on physical reasoning, the authors contend that the underlying premises of the *Specification* equations are incorrect. In particular, the available evidence suggests that the shear failure planes

Lip Teh, Associate Professor, School of Civil, Mining and Environmental Engineering, University of Wollongong, Wollongong, NSW, Australia. Email: lteh@uow.edu.au (corresponding)

Gregory Deierlein, Professor, Department of Civil and Environmental Engineering, Stanford University, Stanford, CA. Email: ggd@stanford.edu

Paper No. 2016-09

Table 1. AISC *Specification* Block Shear Design Provisions, 1978–2016	
1978	$R_n = F_uA_{nt} + 0.6F_uA_{nv}$
1986	$R_n = \max(F_uA_{nt} + 0.6F_yA_{gv}; F_yA_{gt} + 0.6F_uA_{nv})$
1993	If $F_uA_{nt} \geq 0.6F_uA_{nv}$: $R_n = F_uA_{nt} + 0.6F_yA_{gv}$ If $F_uA_{nt} < 0.6F_uA_{nv}$: $R_n = F_yA_{gt} + 0.6F_uA_{nv}$
1999	If $F_uA_{nt} \geq 0.6F_uA_{nv}$: $R_n = \min(F_uA_{nt} + 0.6F_uA_{nv}; F_uA_{nt} + 0.6F_yA_{gv})$ If $F_uA_{nt} < 0.6F_uA_{nv}$: $R_n = \min(F_uA_{nt} + 0.6F_uA_{nv}; F_yA_{gt} + 06F_uA_{nv})$
2005 2010 2016	$R_n = \min(F_uA_{nt} + 0.60F_uA_{nv}; F_uA_{nt} + 0.60F_yA_{gv})$

in bolted connections are neither the net nor the gross shear planes, as defined in the AISC *Specifications*. This evidence includes contact finite element analyses (Clements and Teh, 2013) and connection tests (Cai and Driver, 2010) that fail in shear tearout.

The determination of the effective shear planes resolves the ambiguity involving the net and gross shear planes used in the current block shear design provision (AISC, 2016). In addition, Teh and Yazici (2013) provide an explanation, substantiated by tests and analysis, that there is only one feasible mechanism for conventional block shear failures in bolted connections, which involves tensile rupture and shear yielding. In fact, the simultaneous tensile and shear rupture mechanism postulated by the first equation in the bottom row of Table 1 has never been observed in published laboratory tests. However, Teh and Uz (2015a) have demonstrated that the ductile shear yielding in a block shear failure is typically accompanied by significant strain hardening, such that the assumed yield stress can be significantly larger than $0.6F_y$, up to or even beyond $0.6F_u$. Based on these three observations, this paper proposes a design equation against the block shear failure mode of bolted connections that (1) is more accurate than existing models, including one proposed by Teh and Yazici (2013) and Teh and Uz (2015a); (2) is logical and straightforward to implement; and (3) is determined using parameters in current design provisions that are familiar to engineers.

This paper presents a comprehensive verification of block shear failure models of bolted connections in gusset plates composed of structural steel (Hardash and Bjorhovde, 1985; Rabinovitch and Cheng, 1993; Udagawa and Yamada, 1998; Aalberg and Larsen, 1999; Nast et al., 1999; Swanson and Leon, 2000; Puthli and Fleischer, 2001; Huns et al., 2002; Mullin, 2002; Moze and Beg, 2014) and aluminum alloy (Menzemer et al., 1999). The exercise includes both conventional and the less conventional "split" block shear failure mode. Comparisons are made against the design provisions found in the 2010 and 2016 AISC *Specifications* (AISC 2010, 2016) and the Canadian (CSA, 2014), European (ECS, 2005) and Japanese (AIJ, 2002) standards.

Design Provisions of AISC *Specifications*

As shown in Table 1, the first edition of the AISC LRFD *Specification* (AISC, 1986) specified that the larger of the following two resistances is to be used in determining the nominal block shear strength of bolted connections:

$$R_n = F_uA_{nt} + 0.6F_yA_{gv} \quad (1a)$$

$$R_n = F_yA_{gt} + 0.6F_uA_{nv} \quad (1b)$$

The net and gross shear and tension planes, as defined by the *Specification* are indicated in Figure 1. The accompanying Commentary argued that the provision was more conservative than the equation given in the earlier ASD *Specification* (AISC, 1978), which "implies that ultimate fracture strength on both planes occur simultaneously." The 1978 equation, rewritten in the limit state format is as follows:

$$R_n = F_uA_{nt} + 0.6F_uA_{nv} \quad (2)$$

In contrast to the 1986 Commentary's claim of being more conservative, depending on the relative values of F_y and F_u, the 1978 equation can result in a lower resistance than the 1986 equation due to the its smaller shear area, as demonstrated by Teh and Yazici (2013).

Therefore, there are two fundamental problems with the 1986 provision (AISC, 1986). First, contrary to its intention of adopting a more conservative model, it often results in a less conservative design against the block shear failure mode compared to the original equation (AISC, 1978). Second, its prescription that "the controlling equation is one that produces the larger force" is contrary to well-established design conventions of choosing the lowest of multiple possible failure modes. The Commentary (AISC, 1986) attempts to explain the oddity of the design check by way of two extreme examples, shown in Figure 2. According

to the Commentary, Equation 1a gives a lower resistance than Equation 1b for the connection shown in Figure 2a. However, considering that the total force is resisted primarily by shear, the Commentary argues that shear fracture, not shear yielding, should control the block shear failure mode, and therefore, Equation 1b should be used for the connection in Figure 2a. A reverse argument is applied by the Commentary to the other connection. The Commentary further states that "when it is not obvious which failure plane fractures, it is easier just to use the larger of the two formulas."

There are two points that have been overlooked in the 1986 Commentary. First, as with the comparison between Equations 1a and 2, Equation 1a does not, in general, give a lower resistance than Equation 1b for the connection shown in Figure 2a. Second, there is no evidence to support the contention that fracture will take place first in the primary resistance plane (i.e., tension or shear). In fact, the connection in Figure 2a will fracture first in the tension plane irrespective of the steel material ductility (Teh and Yazici, 2013). The connection in Figure 2b, on the other hand, will fail in individual shear tearout of the bolts rather than block shear if the tensile resistance is sufficiently larger than the shear resistance.

The second LRFD *Specification* (AISC, 1993) recognizes the first point described in the preceding paragraph and qualifies the use of Equations 1a and 1b as shown in Table 1. The *Specification* Commentary modifies the 1986 prescription to "the controlling equation is one that produces the larger *rupture* force." However, this modified prescription does not have a clear justification either, except that the 1993 Commentary repeats the earlier Commentary's statement that "block shear is a rupture or tearing phenomenon not a yielding limit state."

The 1993 Commentary has an additional argument for the form of Equations 1a and 1b that survives into the latest Commentary (AISC, 2016). It argues that the equations are consistent with the philosophy of tension member design, "where gross area is used for the limit state of yielding and net area is used for rupture." However, the gross area is used for the tension member design in conjunction with the yield

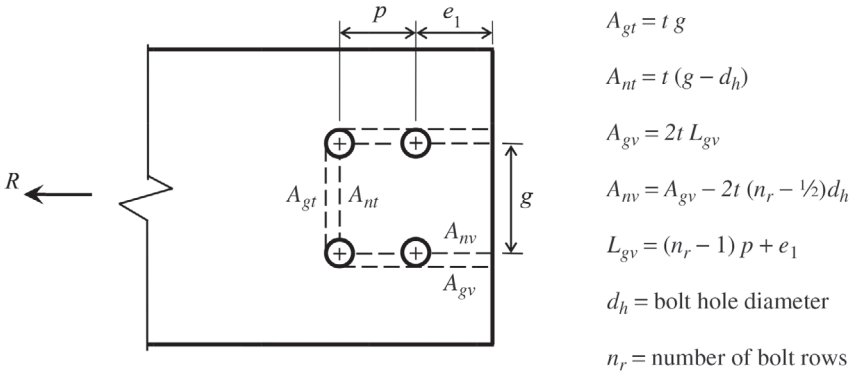

Fig. 1. Gross and net planes.

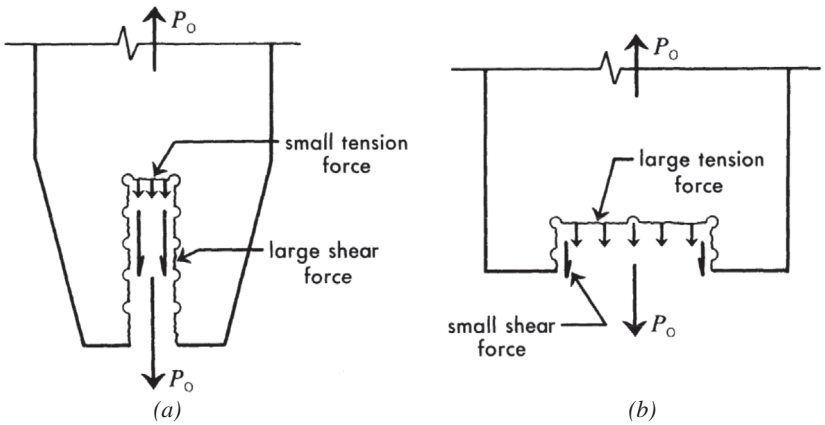

Fig. 2. Two extreme block shear examples cited in the AISC Commentary (AISC, 1986): (a) shear-resistance dominant; (b) tensile-resistance dominant.

stress to prevent excessive member elongation due to yielding along the member. This condition is not present in the design against a block shear failure, where yielding is local to the connection region only.

The third LRFD *Specification* (AISC, 1999) recognizes the fact that Equation 2 may give a lower resistance than either Equation 1a or 1b. Accordingly, as noted in Table 1, the 1999 *Specification* requires the checking of Equation 2 in applying Equations 1a and 1b.

Two further changes to the block shear design provision have been incorporated in the 2005 *Specification* (AISC, 2005). First, the governing block shear strength is changed to simply the lower resistance computed from the prescribed equations. Second, the tensile yielding and shear rupture mechanism, Equation 1b, is no longer considered. The rationale for the removal of Equation 1b is explained by Teh and Yazici (2013), who point out that a conventional block shear failure cannot occur through tensile yielding and shear rupture.

Despite the first improvement mentioned in the preceding paragraph, the resulting block shear design provision, which remains the same in the 2010 and 2016 *Specifications* (AISC, 2010, 2016), often reduces to Equation 2 for modern structural steels, where the ratio of tensile strength F_u to yield stress F_y is not particularly high. As will be evident in the next section, the net shear area A_{nv} used in the equation is significantly smaller than the more realistic value given by the effective shear area. The practical outcome is that the design provision can be very conservative, relative to physical test data.

Effective Shear Planes

If one looks at Figures 1 and 2 closely, it will be become apparent that the shear failure planes cannot coincide with the centerlines of the bolt holes in the direction of loading, where shear stresses would be minimal due to the bolts bearing "symmetrically" on the respective holes. This indication has been confirmed by the contact finite element analysis results of Clements and Teh (2012), which show that maximum in-plane shear stresses take place between the net and the gross shear planes.

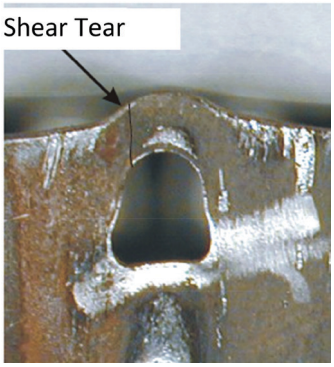

Fig. 3. A downstream bolt failing in shear tearout (Cai and Driver, 2010).

This assertion is clearly evident in the observed failure mode in laboratory tests of bolted connections failing in shear tearout. For example, consider the failure mode shown in Figure 3 for the downstream bolt of a serial bolted connection tested by Cai and Driver (2010). In a shear tearout failure, full strain hardening can be expected along the two shear failure planes, enabling the determination of their location and effective area based on simple calculation checks under the limiting stress of $0.6F_u$. Moreover, from the photo in Figure 3, the shear tearout plane can be seen to be roughly midway between the net and the gross shear planes. For the shear tearout failure, the net A_{nv}, gross A_{gv}, and effective A_{ev} shear planes are shown in Figure 4. Note that in contrast to the gross and effective shear planes, the literal interpretation of the net area is that it can have only one failure plane.

The Canadian steel design standard (CSA, 2014) determines the nominal shear tearout strength of bolts from the following equation:

$$R_n^* = 0.6\left(\frac{F_u + F_y}{2}\right)(2A_{gv}) \tag{3}$$

which assumes partial strain hardening along the total area of two gross shear planes ($2A_{gv}$).

The shear tearout equation of the current AISC *Specification* (AISC, 2016) and the North American cold-formed steel structures *Specification* (AISI, 2012) are described as follows,

$$R_n^* = 1.2F_uA_{nv} \tag{4}$$

While it is obviously impossible to have the two shear failure planes coinciding with the centerlines of the bolt hole, two net shear planes are implied by the limiting shear stress, $1.2F_u$. Note that this shear tearout equation corresponds to the case in the AISC *Specification* where deformations are to be controlled. As an aside, the AISC shear tearout equation for the case where deformations are not controlled has a limiting stress of $1.5F_u$, which implies a failure stress of $0.75F_u$ on each net shear plane. The authors are not aware of test evidence to support the use of $0.75F_u$, and moreover, Teh and Uz (2015b) have pointed out that test evidence supports a limiting shear tearout stress of $0.6F_u$ on each effective shear area.

Following Teh and Uz (2015b), if each shear failure plane is taken to be midway between the gross and the net shear planes, then the nominal shear tearout strength is calculated as:

$$R_n^* = 0.6F_u(2A_{ev}) \tag{5a}$$

where

$$A_{ev} = \frac{A_{gv} + A_{nv}}{2} \quad (5b)$$

Equations 3, 4, and 5 have been verified by Teh and Uz (2015b) against independent laboratory test results. However, at the time, they were not aware of the single-bolt connection test results obtained by Moze and Beg (2010, 2014), which provide even stronger evidence that Equation 5 is significantly more accurate than Equations 3 and 4. Table 2 lists the geometric and material variables of the Moze and Beg tests, which included specimens of mild and high-strength steels with bolt holes ranging from 18 to 30 mm. The table summarizes ratios of ultimate test load P_t to the predicted shear tearout strength R_n^* (such a ratio is called the "professional factor") given by Equations 3, 4 and 5. The variable d_h is the bolt hole diameter, e_1 is the distance between the center of the bolt hole and the downstream end, and t is the plate thickness. An empty cell indicates that the data in the above cell applies. The summary statistics are separated between tests of mild steel specimens, where the ratio F_u/F_y is 1.36, and tests of high-strength steel specimens, where the ratio is 1.04. This distinction is important to help differentiate between the assumed ultimate stresses versus shear failure planes used in the models. It should be noted that the reported F_y and F_u values are all measured, as opposed to nominal, values.

The results in Table 2 show that, despite the assumption of only partial strain hardening, Equation 3 specified in the Canadian steel design standard (CSA, 2014) unconservatively overestimates the shear tearout strengths of the mild steel specimens by about 10% on average. For the high-strength steel specimens, the largest overestimation is over 35% ($1/0.73 = 1.37$). These overestimations are due to the optimistic assumption that the shear failure planes are the gross shear planes, rather than the absence of shear strain hardening in the test specimens.

Conversely, even though full strain hardening is considered by Equation 4, as specified in the AISC *Specification* (AISC, 2016) and the cold-formed steel specification (AISI, 2012), the use of the net shear planes leads to excessive conservatism in the predicted strengths.

Equation 5, which is based on the effective shear planes, calculated as the mean between the net and the gross shear planes, is consistently more accurate than both Equations 3 and 4. Thus, these data indicate that the shear failure planes lie midway between the net and the gross shear planes—a conclusion that is consistent with the design recommendation of Tolbert and Hackett (1974) for pin lugs.

Proposed Equation against Block Shear Failure

Having established strong evidence that the effective shear failure planes are located between the net and the gross shear planes, the block shear failure mechanism can be revised to the one shown Figure 5.

The reasoning for this model is substantiated by Teh and Yazici (2013), who explain why there is only one feasible mechanism for the conventional block shear failure mode—namely, the tensile rupture and shear yielding mechanism. Teh and Uz (2015a) have further pointed out that shear yielding in a block shear failure is typically accompanied by full strain hardening ($0.6F_u$), even though shear fracture very rarely, if ever, is the triggering failure mechanism. This can be explained by the large ductility of steel in shear, where the steel in the shear yielding zone can strain harden up to

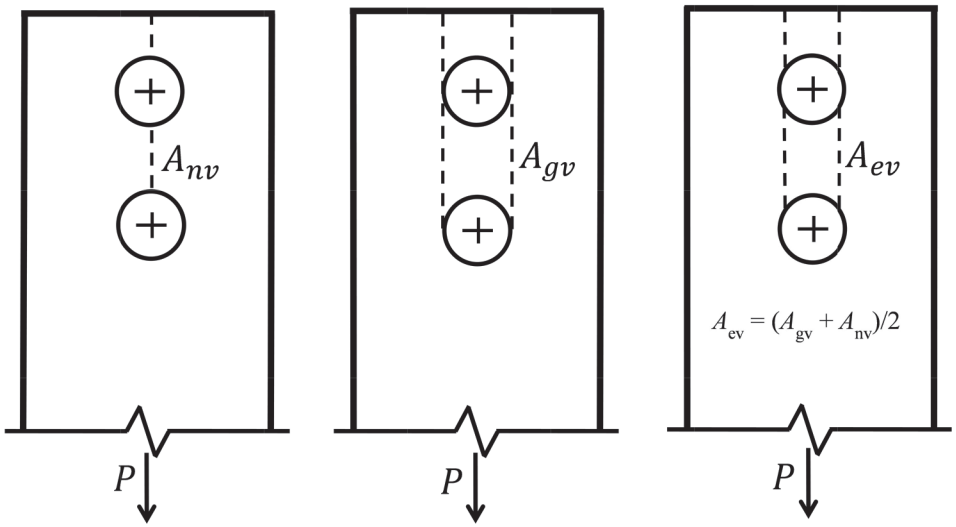

Fig. 4. Illustration of net, gross and effective shear planes for shear tearout.

Table 2. Comparison of Shear-Out Equations with Tests by Moze and Beg (2010, 2014)								
Specimen	F_y, ksi (MPa)	F_u, ksi (MPa)	t, in. (mm)	d_h, in. (mm)	e_1, in. (mm)	P_t/R_n^* of Equations		
						3	4	5
M101	45.4 (313)	61.6 (425)	0.472 (12)	1.02 (26)	1.26 (32)	0.89	1.30	0.97
M104	—	—	—	—	1.02 (26)	0.90	1.57	1.05
M105	—	—	—	—	1.26 (32)	0.97	1.41	1.05
M109	—	—	—	0.71 (18)	0.71 (18)	0.88	1.53	1.02
M110	—	—	—	—	0.87 (22)	0.89	1.31	0.97
M111	—	—	—	—	1.06 (27)	0.90	1.17	0.94
Moze and Beg (2014)					Mean	0.90	1.38	1.00
					COV	0.034	0.109	0.047
B109	122 (847)	128 (885)	0.39 (10)	1.18 (30)	1.18 (30)	0.73	1.43	0.95
B118	—	—	—	—	1.81 (46)	0.82	1.19	0.96
Moze and Beg (2010)					Mean	0.78	1.31	0.96
					COV	0.082	0.127	0.005

F_u and sustain large strains without the necking and rupture behavior that occurs in standard tensile coupons.

Based on this reasoning, the following block shear equation is proposed:

$$R_n = F_u A_{nt} + 0.6 F_u A_{ev} \quad (6)$$

This equation, in which the effective shear area A_{ev} is simply the mean between the gross and the net shear areas, as shown in Equation 5b, is slightly more accurate than a similar equation proposed by Teh and Yazici (2013) and Teh and Uz (2015a), which computes the shear areas from the shear plane length that ignores a quarter of the bolt hole diameter. In addition to being more accurate, the concept of an effective shear area is intuitive and straightforward to implement.

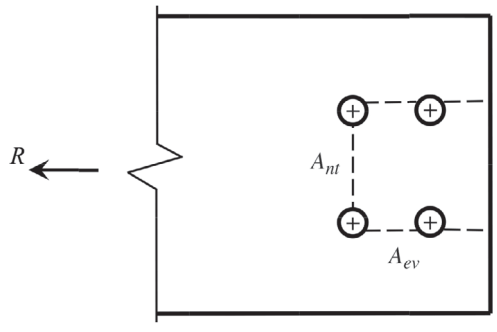

Fig. 5. Net tension and effective shear failure planes for proposed block shear model.

Verifications of Block Shear Equations

Strengths calculated using the proposed block shear Equation 6 and the current AISC provision (AISC, 2016) are compared to previously published test data in Table 3. The table covers 155 tests by 11 independent research teams, including tests of 20 aluminum specimens by Menzemer et al. (1999). Due to the large number of specimens involved, it is not practical to provide the details of individual specimens in the manner given by Table 2. In addition to the mean professional factors P_t/R_n, Table 3 provides the number of tests by each research group (N), their maximum number of bolt rows (n_{rmax}) and number of bolt lines (n_{lmax}), the range of their bolt hole diameters (d_h), the range of their ratios of measured tensile strength to yield stress (F_u/F_y), and the range of their ratios of ultimate test load to tensile strength component [$P_t/(F_u A_{nt})$]. The overall mean values and the coefficients of variation (COV) given at the bottom of the table refer to the professional factors of individual specimens, not the mean professional factors of the 11 test programs. All the specimens in the table failed in a conventional block shear mode along the failure planes illustrated in Figure 5.

It can be seen from Table 3 that strengths calculated by the proposed Equation 6 are consistently accurate across reported tests, where the overall mean professional factor of 1.01 has a 5% coefficient of variation. In contrast, the current AISC equation (AISC, 2016) has an overall mean professional factor of 1.18. Thus, the AISC provision is conservative by about 20%. Interestingly, the AISC results are almost always governed by Equation 2, simultaneous fracture on the net tension and shear areas, which is somewhat counterintuitive as being more conservative than the

Table 3. Comparison between Test Data and Strengths Calculated by the Proposed and AISC Block Shear Equations								
	N	n_{rmax}	n_{1max}	d_h, (mm)	F_u/F_y	$P_t/(F_uA_{nt})$	Mean P_t/R_n	
							AISC	Proposed
Hardash and Bjorhovde (1985)	28	5	2	14–17	1.30–1.41	2.2–6.7	1.20	1.03
Rabinovitch and Cheng (1993)	5	5	2	22	1.20	7.5–8.5	1.17	0.99
Udagawa and Yamada (1998)	72	4	4	18	1.08–1.70	1.7–6.0	1.18	0.99
Aalberg and Larsen (1999)	8	4	2	19	1.05–1.44	4.0–7.1	1.20	0.99
Menzemer et al. (1999)	20	7	2	17.5	1.12	3.7–14.0	1.16	1.00
Nast et al. (1999)	3	5	2	22	1.17	8.2–8.5	1.23	1.04
Swanson and Leon (2000)	1	4	2	24	1.33	4.1	1.30	1.05
Puthli and Fleischer (2001)	6	1	2	30	1.23	2.1–2.4	1.18	1.01
Huns et al. (2002)	5	3	4	21	1.34	2.6–8.0	1.26	1.08
Mullin (2002)	5	8	2	21	1.37	2.6–7.8	1.14	1.00
Moze and Beg (2014)	2	1	2	22	1.36	2.3–3.1	1.24	1.08
						Overall mean	1.18	1.01
						COV	0.051	0.048
Note: 1 in. = 25.4 mm								

combined yielding-fracture condition. The performance of Equation 1a is included in the Appendix.

As noted previously, Table 3 only includes bolted connection specimens that failed in a conventional block shear mode along the failure planes illustrated in Figure 5. However, depending on the geometry, it is possible for a bolted gusset plate to fail in the "split" block shear mode along the planes indicated in Figure 6. In addition to testing six specimens that failed in the conventional (C) block shear mode, Puthli and Fleischer (2001) tested six specimens that failed in the split (S) mode. The split mode occurred in gusset plate specimens where the gauge length, g, was more than twice the edge distance, e_2. Results for the 12 specimens tested by Puthli and Fleischer (2001) are summarized in Table 4, including the six that failed in the conventional mode and are also included in Table 3. All the specimens had a plate thickness, t, of 17.5 mm, a bolt hole diameter, d_h, of 30 mm, an end distance, e_1, of 36 mm, and one row of two bolts. The measured yield stress, F_y, and tensile strength, F_u, were 524 MPa and 645 MPa, respectively.

For determining the split block shear strength, the "normal" block shear equations are still applicable provided the appropriate net tension area, A_{nt}, is used. Similar to the comparisons of Table 3, the results in Table 4 demonstrate that the strengths based on the proposed Equation 6 are significantly more accurate than those determined using the AISC (AISC, 2016), Canadian (CSA, 2014), European (ECS, 2005) and Japanese (AIJ, 2002) equations for both the conventional and the split block shear modes. Further details and discussion of the Canadian, European and Japanese standard equations are given in the Appendix.

Resistance Factor

In conjunction with the proposed new model for determining shear tearout and block shear, the comparisons with test data can be used to evaluate an appropriate resistance factor. The reliability analysis methodology and the statistical parameters are adopted from Driver et al. (2006), who evaluated the required resistance factor ϕ using the following equation proposed by Fisher et al. (1978):

$$\phi = (0.0062\beta^2 - 0.131\beta + 1.338)M_mF_mP_me^{-p} \qquad (7)$$

in which β is the target reliability index, M_m is the mean value of the material factor equal to 1.11 (Schmidt and Bartlett 2002), F_m is the mean value of the fabrication factor equal to 1.00 (Hardash and Bjorhovde 1985), and P_m is the mean value of the professional factor.

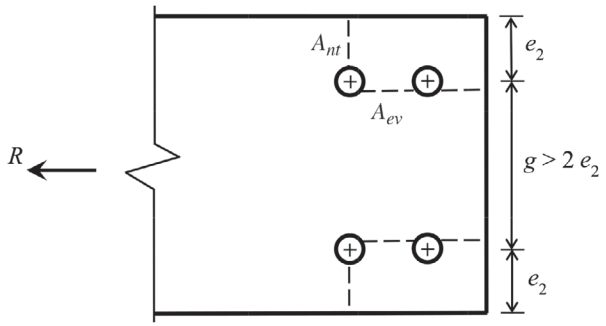

Fig. 6. Split block shear failure planes.

Table 4. Comparison of Model Equations for Tests That Failed in Both Conventional (C) and Split (S) Block Shear (Puthli and Fleischer, 2001)								
Specimen	g, (mm)	e_2, (mm)	Mode	P_t/R_n				
				AISC	Eq. (6)	CSA	ECS	AIJ
12	54	36	C	1.16	0.98	0.90	1.28	1.07
13	—	40.5	—	1.16	0.98	0.90	1.28	1.07
14	—	45	—	1.19	1.01	0.93	1.32	1.10
17	63	36	—	1.19	1.03	0.96	1.29	1.11
18	—	40.5	—	1.21	1.05	0.97	1.32	1.13
19	—	45	—	1.19	1.03	0.96	1.30	1.11
20	72	27	S	1.23	1.04	0.96	1.36	1.14
21	—	31.5	—	1.21	1.05	0.97	1.31	1.13
22	81	27	—	1.18	1.00	0.92	1.31	1.09
23	—	31.5	—	1.19	1.03	0.96	1.29	1.11
24	90	27	—	1.20	1.01	0.93	1.33	1.11
25	—	31.5	—	1.19	1.03	0.96	1.30	1.12
Puthli and Fleischer (2001)			Mean	1.19	1.02	0.94	1.31	1.11
			COV	0.017	0.023	0.027	0.017	0.019

The exponential term p in Equation 7 is computed from

$$p = \alpha_R \beta \sqrt{V_m^2 + V_F^2 + V_P^2} \quad (8)$$

in which α_R is the separation variable equal to 0.55 (Ravindra and Galambos, 1978), V_M is the coefficient of variation of the material factor equal to 0.054 (Schmidt and Bartlett 2002), V_F is the coefficient of variation of the fabrication factor equal to 0.05 (Hardash and Bjorhovde, 1985), and V_P is the coefficient of variation of the professional factor.

The mean professional factor P_m of the proposed Equation 6 for the 141 structural steel specimens included in Tables 3 and 4 is 1.01, and its coefficient of variation V_P is 0.051. The aluminum specimens tested by Menzemer et al. (1999) were not included in the reliability analysis, although it would have made little difference to the computed resistance factor. Using these values, along with a target reliability index β of 4.0, a resistance factor ϕ of 0.84 was computed per Equation 7. Accordingly, and based on the large number of test comparisons covering a very diverse range of connection geometry and steel grades, a resistance factor ϕ rounded up to 0.85 is recommended.

BLOCK SHEAR DESIGN EXAMPLE

Shown in Figure 7 is a connection between a pair of back-to-back C6×13 tension braces and an ASTM A572 Grade 50 ⅝-in.-thick gusset plate (F_y of 50 ksi; F_u of 65 ksi). The gusset plate thickness is selected so as to have sufficient bolt bearing strength to develop the full design shear strength of each ¾-in. ASTM F3125 Grade A325 bolt of 45.1 kips (double shear, bearing). The bolted gusset plate, which has two lines of bolts with a hole diameter equal to 13⁄16 in., is to be designed against the block shear failure mode under a factored load of R_u = 270 kips. The pitch, p, and gauge, g, are all equal to 2½ in., while the end distance e_1 is 1½ in. These values satisfy the requirements prescribed in Sections J3.3 and J3.4 of the AISC *Specification* (AISC, 2016).

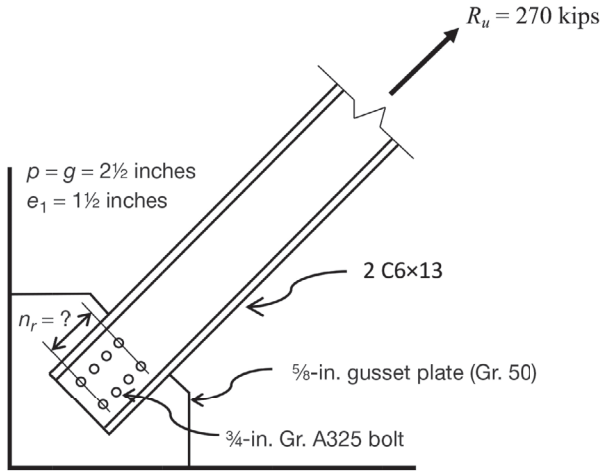

Fig. 7. Block shear design example.

Based on the bolt shear strength, six bolts are required to resist the factored load of 270 kips. The following calculations determine the number of bolt rows, n_r, required according to the AISC *Specification* (AISC, 2016) and the proposed block shear equation. For all block shear designs, the net tension area, A_{nt}, is constant at 1.02 in.^{2}. In all calculations, 1⁄16 in. is added to the nominal bolt hole diameter in accordance with Section B4.3b of the *Specification*.

Try $n_r = 3 \rightarrow A_{gv} = 8.12$ in.^{2}; $A_{nv} = 5.39$ in.^{2}:

AISC:
$\phi R_n = 0.75 \times \min$
$(F_u A_{nt} + 0.60 F_u A_{nv}; F_u A_{nt} + 0.60 F_y A_{gv}) = 207$ kips **n.g.**

Proposed:
$\phi R_n = 0.85 \times$
$[F_u A_{nt} + 0.6 F_u (A_{nv} + A_{gv})/2] = 280$ kips **o.k.**

Try $n_r = 4 \rightarrow A_{gv} = 11.2$ in.^{2}; $A_{nv} = 7.42$ in.^{2}:

AISC: $\phi R_n = 267$ kips < 270 kips

In this example, the AISC block shear check of the gusset plate requires much more than the minimum number of six bolts based on the bolt shear capacity. It requires five rows of bolts (10 bolts), whereas the proposed block shear model requires only three rows of bolts (six bolts). These calculations assume that plate thickness, bolt pitch, and end distance are to be maintained.

An alternative to increasing the number of bolt rows in the current AISC block shear check is to increase the bolt pitch (there is a very limited scope for increasing the bolt gage since the clear width of each channel brace is only 5.31 in.). In order to resist the factored load of $R_u = 270$ kips, the bolt pitch must be increased to 3½ in. in step increases of ½ in. each.

Try $p = 3½$ in. $\rightarrow A_{gv} = 10.62$ in.^{2}; $A_{nv} = 8.09$ in.^{2}:

AISC: $\phi R_n = 280$ kips **o.k.**

In either AISC solution, the resulting gusset plate dimension is larger than that given by the proposed block shear solution.

While it can be argued that this example is not necessarily representative of a typical condition, it demonstrates how the proposed block shear check can result in more economical connections.

COPED BEAM SHEAR CONNECTIONS

In essence, all of the changes to the AISC block shear design provisions listed in Table 1 and discussed in the section "Design Provisions of AISC *Specifications*" relate to tension members. While the block shear failure mode was first discovered by Birkemoe and Gilmor (1978) for coped beam shear connections, the coped beam condition may involve another level of complexity that clouds the basic behavior of block shear. The nonuniform stress distribution factor, U_{bs}, contained in the AISC block shear design provision since 2005 (AISC, 2005), is believed to arise from the in-plane load eccentricity of the coped beam shear connection, which is outside the scope of this paper.

Nevertheless, a reviewer of this paper has suggested that a verification of Equation 6 be made against the recent coped beam test results of Fang et al. (2013). The experimental program of Fang et al. is well documented and interesting in that it included not only single- and double-line bolted connections, but also single- and double-sided angle cleat connections on the beam web. The single- and the double-line bolted connections are believed to result in uniform ($U_{bs} = 1.0$) and nonuniform ($U_{bs} = 0.5$) tensile stress distributions, respectively, as illustrated in Figure 8 adapted from the 2016 *Specification* (AISC, 2016). The single-sided cleat connections, on the other hand, result in out-of-plane load eccentricity.

Table 5 shows the professional factors of Equation 6 for the coped beam shear connections of Fang et al. (2013). The geometric variables are defined in Figure 8, with the bolt pitch, p, being uniform at 75 mm for all specimens except for T1-1-3-a. The first seven specimens were single-line bolted,

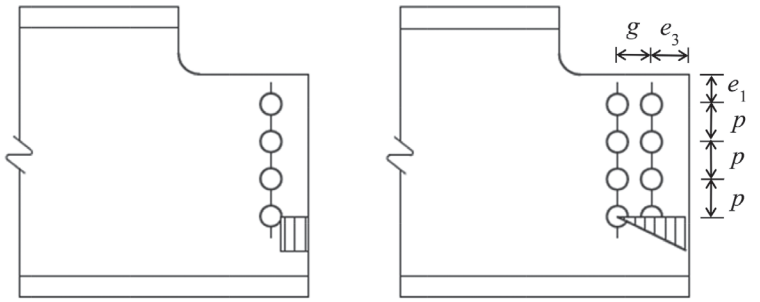

Fig. 8. AISC tensile stress distribution factor: (a) $U_{bs} = 1.0$*; (b)* $U_{bs} = 0.5$ *(AISC, 2016).*

Table 5. Verification against Coped Beam Test Results of Fang et al. (2013), p = 75 mm									
Specimen	g, (mm)	e_3, (mm)	e_1, (mm)	t, (mm)	F_u, (MPa)	Bolt Lines	Single Sided?	P_t, (kN)	P_t/ Eq. (6)
A1-1-3-a	N/A	28	28	6.6	459	Single	N	305	0.96
T1-1-3-a*	—	28	28	—	459	—	Y	332	1.05
A1-1-3-b	—	50	27	—	459	—	N	393	1.03
T1-1-3-b	—	50	28	—	459	—	Y	415	1.08
T2-1-3-a	–	27	28	6.8	464	—	Y	358	1.09
T2-1-3-b	—	51	28	—	464	—	Y	485	1.20
A1-1-3-a-S	—	28	29	—	459	—	Y	319	1.02
A2-2-2-a	75	28	27	—	464	Double	N	384	1.04
T1-2-2-a	—	28	28	—	464	—	Y	380	1.02
T2-2-2-a	—	28	27	—	459	—	Y	329	0.90
								Mean	1.04
								COV	0.077
* The upper pitch is equal to 74 mm.									

while the last three were double-line bolted. No nonuniform stress distribution factor was applied to any specimen. In this table, the ultimate test loads, P_t, are explicitly given in order to avoid potential confusion with the "Ultimate load P_{test}" given in Table 4 of Fang et al. (2013), the latter referring to the ultimate load applied on the beam, which had two end connections (not carrying the same amount of load). In that paper, the ultimate block shear load, P_t, of each shear connection of the tested beam is called "ultimate connection reaction," measured by a load cell. It can be seen that Equation 6 resulted in reasonable estimates of the ultimate block shear loads, including those of the double-line bolted, single-sided cleat connections.

The slightly conservative estimates by Equation 6—despite the equivalent use of U_{bs} = 1.0 in the presence of in-plane and out-of-plane load eccentricities, especially for Specimen T2-1-3-b—might have been due to the fact that the bolts were snug tightened. It may also be noted that Fang et al. (2013) have found that all the AISC, Canadian, European and Japanese block shear design provisions for coped beams were excessively conservative. The maximum professional factors of the international design specifications for the specimens in Table 5 were computed by Fang et al. (2013) to be 1.66, 1.62, 2.05 and 1.63, respectively.

The only significant overestimation by Equation 6 concerns specimen T2-2-2-a, for which the professional factor is 0.90. However, Fang et al. (2013) suggested that this specimen might have suffered from an "erratic test setup alignment" because it was similar to specimen T1-2-2-a (except for a slightly lower tensile strength F_u), but the latter had an ultimate test load that was 15% higher. In fact, the ultimate beam load of specimen T2-2-2-a obtained in the laboratory test was about 15% lower than the finite element prediction of Fang et al. (2013).

It may be noted that, in addition to the "erratic" test result discussed in the preceding paragraph, test results involving coped beam shear connections have been known to be quite variable for nominally identical specimens. Such results include those obtained by Franchuk et al. (2003), which were among the few well-documented coped beam shear tests available in the literature.

Due to the limited verification against coped beam test results, the authors do not propose amending the current nonuniform stress distribution factor U_{bs}, which means that the proposed block shear design provision tends to be conservative for a double-line bolted coped beam shear connection.

CONCLUSIONS

In spite of changes to the block shear design provisions in the AISC *Specifications* over four decades, the current provision is shown to underestimate the block shear strength of bolted connections by about 20%, compared to published test data. The Canadian, European and Japanese block shear design provisions all have unique equations of their own, yet comparisons with these also reveal significant errors on either side of conservatism when verified against the independent test results, as cited in this paper, including those presented in the Appendix. All the *Specification* equations share two fundamental shortcomings. First, they use either the net area (too conservative) or the gross area (too optimistic) for the shear failure planes, neither of which is a reliable representation of the shear failure plane. Second, none of the provisions recognize that shear yielding in a block shear

failure is typically accompanied by full strain hardening, prior to rupture of the net tension failure plane.

Observed deformations and failure modes in shear tearout tests of bolted connections suggest that the effective shear failure plane lies midway between the net and the gross shear planes. This is further substantiated by comparisons between the measured failure loads and the strengths calculated assuming different failure plane areas under the maximum shear stress of $0.6F_u$. Accordingly, the effective shear area for evaluating shear tearout failure can be calculated as the mean between the gross and the net shear areas.

The proposed block shear model (Equation 6) is based on failure due to the tensile rupture and shear yielding mechanism, which is supported by test data and basic mechanics. The model assumes full strain hardening (plastic flow stress of $0.6F_u$) along the effective shear planes, up to the point of tensile fracture on the net tension plane. The calculated strengths agree well with data from 161 block shear tests of bolted gusset plates conducted by 11 independent research teams, including specimens composed of mild and high-strength steels, an aluminum alloy, and both conventional and split block shear failure modes. Based on the observed variability in calculated to measured strengths and well-established reliability indices for connections, a resistance factor of 0.85 is recommended for use with the proposed block shear strength equation. The proposed equation for calculating block shear can also be adapted to provide more consistent strengths for shear tearout failure of bolts.

Although the proposed equation resulted in reasonable estimates for the studied coped beam shear connections, including those with a double line of bolts without the application of any nonuniform stress distribution factor, more research is required to determine the accurate nonuniform stress distribution factor if it is necessary at all. By retaining the existing nonuniform stress distribution factor $U_{bs} = 0.5$ for a double-line bolted coped beam connection, the proposed block shear provision tends to err on the safe side for such a connection.

Relative to the block shear design provisions in the current AISC *Specification* (2016), the use of the proposed provision will facilitate structural designs that are more reliable and economical. This is demonstrated in a gusset plate example, where the proposed block shear equation leads to a significant reduction in the number of required bolt rows or in the bolt pitch and, therefore, smaller gusset plate dimensions than the current provision.

ACKNOWLEDGMENTS

The authors would like to thank the Australian Government Department of Education and Training, for providing a 2016 Endeavour Research Fellowship to the first author, and Tufel Musyadad of Scope Global, for managing the fellowship. The authors also thank Veysel Yazici and Mehmet Uz, for collecting the laboratory test results, and Ronald Ziemian, for suggesting the use of the mean value between the net and the gross shear areas in lieu of the active shear area previously used by the first author. Any opinions expressed in this paper are those of the authors alone and do not necessarily reflect the views of other parties.

REFERENCES

Aalberg, A. and Larsen, P.K. (1999), *Strength and Ductility of Bolted Connections in Normal and High Strength Steels*, Report N-7034, Department of Structural Engineering, Norwegian University of Science and Technology, Trondheim, Norway.

AIJ (2002), *Recommendation for the Design and Fabrication of Light Weight Steel Structures*, Architectural Institute of Japan, Tokyo, Japan.

AISC (1978), *Specification for the Design, Fabrication and Erection of Structural Steel for Buildings*, American Institute of Steel Construction, Chicago, IL.

AISC (1986), *Load and Resistance Factor Design Specification for Structural Steel Buildings*, American Institute of Steel Construction, Chicago, IL.

AISC (1993), *Load and Resistance Factor Design Specification for Structural Steel Buildings*, American Institute of Steel Construction, Chicago, IL.

AISC (1999), *Load and Resistance Factor Design Specification for Structural Steel Buildings*, American Institute of Steel Construction, Chicago, IL.

AISC (2005), *Specification for Structural Steel Buildings*, ANSI/AISC 360-05, American Institute of Steel Construction, Chicago, IL.

AISC (2010), *Specification for Structural Steel Buildings*, ANSI/AISC 360-10, American Institute of Steel Construction, Chicago, IL.

AISC (2016), *Specification for Structural Steel Buildings*, ANSI/AISC 360-16, American Institute of Steel Construction, Chicago, IL.

AISI (2012), *North American Specification for the Design of Cold-Formed Steel Structural Members*, ANSI/AISI S100-12, American Iron and Steel Institute, Washington DC.

Birkemoe, P.C. and Gilmor, M.I. (1978), "Behavior of Bearing-Critical Double-Angle Beam Connections," *Engineering Journal*, AISC, Vol. 15, No. 3, pp. 109–115.

Cai, Q. and Driver, R.G. (2010), "Prediction of Bolted Connection Capacity for Block Shear Failures along Atypical Paths," *Engineering Journal*, AISC, Vol. 47, No. 4, pp. 213–221.

Clements, D.D.A. and Teh, L.H. (2012), "Active Shear Planes of Bolted Connections Failing in Block Shear," *Journal of Structural Engineering*, ASCE, Vol. 139, No. 3, pp. 320–327.

CSA (2014), *Design of Steel Structures*, CSA-S16-14, Canadian Standards Association, Toronto, ON.

Driver, R.G., Grondin, G.Y. and Kulak, G.L. (2006), "Unified Block Shear Equation for Achieving Consistent Reliability," *Journal of Constructional Steel Research*, Vol. 62, No. 3, pp. 210–222.

ECS (2005), *Eurocode 3: Design of Steel Structures, Part 1.8: Design of Joints*, EN 1993-1-8, European Committee for Standardisation, Brussels, Belgium.

Fang, C., Lam, A.C.C., Yam, M.C.H. and Seak, S.K. (2013), "Block Shear Strength of Coped Beams with Single-Sided Bolted Connection," *Journal of Constructional Steel Research*, Vol. 86, pp. 153–166.

Fisher, J.W., Galambos, T.V., Kulak, G.L. and Ravindra, M.K. (1978), "Load and Resistance Factor Design Criteria for Connectors," *Journal of the Structural Division*, ASCE, Vol. 104, No. ST9, pp. 1427–1441.

Franchuk, C.R., Driver, R.G. and Grondin, G.Y. (2003), "Experimental Investigation of Block Shear Failure in Coped Steel Beams," *Canadian Journal of Civil Engineering*, Vol. 30, pp. 871–881.

Hardash, S.G. and Bjorhovde, R. (1985), "New Design Criteria for Gusset Plates in Tension," *Engineering Journal*, AISC, Vol. 22, No. 2, pp. 77–94.

Huns, B.B.S., Grondin, G.Y. and Driver, R.G. (2002), *Block Shear Behaviour of Bolted Gusset Plates*, Structural Engineering Report No. 248, Department of Civil and Environmental Engineering, University of Alberta, Edmonton, AB.

Menzemer, C.C., Fei, L. and Srivatsan, T.S. (1999), "Design Criteria for Bolted Connection Elements in Aluminum Alloy 6061," *Journal of Mechanical Design*, Vol. 121, No. 9, pp. 348–358.

Moze, P. and Beg, D. (2010), "High Strength Steel Tension Splices with One or Two Bolts," *Journal of Constructional Steel Research*, Vol. 66, pp. 1000–1010.

Moze, P. and Beg, D. (2014), "A Complete Study of Bearing Stress in Single Bolt Connections," *Journal of Constructional Steel Research*, Vol. 95, pp. 126–140.

Mullin, D. (2002), Unpublished test data, Department of Civil and Environmental Engineering, University of Alberta, Edmonton, AB.

Nast, T.E., Grondin, G.Y. and Cheng, R.J.J. (1999), *Cyclic Behaviour of Stiffened Gusset Plate-Brace Member Assemblies*, Structural Engineering Report No. 229, Department of Civil and Environmental Engineering, University of Alberta, Edmonton, AB.

Puthli, R. and Fleischer, O. (2001), "Investigations on Bolted Connections for High Strength Steel Members," *Journal of Constructional Steel Research*, Vol. 57, No. 3, pp. 313–326.

Rabinovitch, J.S. and Cheng, J.J.R. (1993), *Cyclic Behaviour of Steel Gusset Plate Connections*, Structural Engineering Report No. 191, Department of Civil and Environmental Engineering, University of Alberta, Edmonton, AB.

Ravindra, M.K. and Galambos, T.V. (1978), "Load and Resistance Factor Design for Steel," *Journal of the Structural Division*, ASCE, Vol. 104, No. ST9, pp. 1337–1353.

Schmidt, B.J. and Bartlett, F.M. (2002), "Review of Resistance Factor for Steel: Data Collection," *Canadian Journal of Civil Engineering*, Vol. 29, No. 1, pp. 98–108.

Swanson, J.A. and Leon, R.T. (2000), "Bolted Steel Connections: Tests on T-Stub Components," *Journal of Structural Engineering*, ASCE, Vol. 126, No. 1, pp. 50–56.

Teh, L.H. and Uz, M.E. (2015a), "Block Shear Failure Planes of Bolted Connections—Direct Experimental Verifications," *Journal of Constructional Steel Research*, Vol. 111, pp. 70–74.

Teh, L.H. and Uz, M.E. (2015b), "Ultimate Shear-Out Capacity of Structural Steel Bolted Connections," *Journal of Structural Engineering*, ASCE, Vol. 141, No. 5.

Teh, L.H. and Yazici, V. (2013), "Block Shear Capacity of Bolted Connections in Hot-Rolled Steel Plates," *Connection Workshop VII*, European Convention for Constructional Steelwork Task Committee 10, pp. 91–100.

Timoshenko, S.P. (1953), *History of Strength of Materials*, McGraw-Hill, New York, NY.

Tolbert, R.N. and Hackett, R.M. (1974), "Experimental Investigation of Lug Stresses and Failure," *Engineering Journal*, AISC, Vol. 11, No. 2, pp. 34–37.

Udagawa, K. and Yamada, T. (1998), "Failure Modes and Ultimate Tensile Strength of Steel Plates Jointed with High-Strength Bolts," *Journal of Structural and Construction Engineering*, AIJ, Vol. 505, pp. 115–122.

APPENDIX—INTERNATIONAL SPECIFICATIONS

The block shear equation in the Canadian standard (CSA, 2014) is essentially the same as that originally proposed by Huns et al. (2002), which assumes partial strain hardening along the gross shear planes,

Table A-1. Effects of Assumptions and Approximations in Block Shear Equations									
Specimens	F_y, (MPa)	F_u, (MPa)	t, (mm)	n_r	P_t/R_n				
					Eq. (1a)	Eq. (6)	CSA	ECS	AIJ
T7	373	537	8.4	2	1.21	1.06	1.05	1.59	1.38
T9	—	—	—	3	1.18	1.03	1.01	1.65	1.36
T11	—	—	—	4	1.13	0.99	0.96	1.64	1.32
T15	—	—	—	3	1.12	0.98	0.95	1.56	1.29
T8	786	822	7.7	2	0.90	1.00	0.89	1.21	1.04
T10	—	—	—	3	0.86	0.97	0.84	1.22	1.00
T12	—	—	—	4	0.82	0.94	0.80	1.20	0.96
T16	—	—	—	3	0.83	0.94	0.82	1.18	0.97
Aalberg and Larsen (1999)				Mean	1.01	0.99	0.91	1.41	1.16
				COV	0.169	0.043	0.100	0.154	0.163
Note: d_h = 19 mm; e_1 = 38 mm; p = 48 mm; g = 48 mm									

$$R_n = F_u A_{nt} + \left(\frac{F_u + F_y}{2\sqrt{3}} \right) A_{gv} \quad \text{(A-1)}$$

except that the von Mises shear coefficient ($1/\sqrt{3} = 0.577$) is replaced by 0.6 in the standard

$$R_n = F_u A_{nt} + 0.6 \left(\frac{F_u + F_y}{2} \right) A_{gv} \quad \text{(A-2)}$$

Huns et al. (2002) found that Equation 1 was reasonably accurate for many of the specimens included in Table 3. However, this apparent accuracy has been due to the fact that the optimistic use of the gross shear area, A_{gv}, is offset by the pessimistic assumption of only partial strain hardening in specimens having high ratios of tensile strength to yield stress, F_u/F_y. The specimens of Puthli and Fleischer (2001) listed in Table 4 had a F_u/F_y ratio of 1.23, which is not particularly high, and the Canadian standard's equation (CSA, 2014) leads to overestimations as large as 10%, depending on the geometry. These overestimations are not due to the inability of the specimens to experience shear strain hardening, but rather are due to the assumption of gross shear planes.

Table A-1 lists the professional factors of alternative equations for the block shear specimens tested by Aalberg and Larsen (1999), where the first four specimens had material with a high F_u/F_y of 1.44 and the last four had a low F_u/F_y of 1.05. Data from the first four specimens might substantiate the Canadian standard's Equation A-2, which assumes partial strain hardening along the gross shear planes; however, the unconservative errors for the last four specimens, which have a low F_u/F_y ratio, highlight the overestimation of strengths that are based on the gross shear planes. This point is further supported by the results of Equation 1a, which assumes no shear strain hardening at all, where the results are similar to those of the Canadian equation for the specimens with a low F_u/F_y ratio. Lack of shear strain hardening is, therefore, not a factor. What is common to Equations 1a and A-2 is the use of gross shear planes, which are larger than the effective shear planes used by Equation 6. For specimens with relatively low ratios of F_u/F_y, the pessimistic assumption of nil, or only partial, strain hardening does not offset the excess of the gross shear areas over the effective shear areas.

In recent literature, the von Mises shear coefficient of $1/\sqrt{3}$ is sometimes identified as a more "correct" value than the commonly used shear coefficient of 0.6 for evaluating the shear fracture limit state, $0.6F_u$. For example, Moze and Beg (2014) proposed replacing the shear coefficient in the current AISC block shear provision (AISC, 2016) with the von Mises shear coefficient. However, given the discrepancies noted in Table 3, the practical difference of about 4% between $1/\sqrt{3}$(= 0.577) and 0.6 is insignificant. Moreover, while the von Mises shear coefficient of $1/\sqrt{3}$ has a theoretical basis for yielding behavior (i.e., Huber–von Mises–Hencky distortion energy theory, Timoshenko, 1953), there is no such theoretical basis for the ultimate shear coefficient.

While the Eurocode block shear design equation (ECS, 2005) uses the von Mises coefficient in conjunction with shear yielding along the net shear planes,

$$R_n = F_u A_{nt} + \frac{F_y A_{nv}}{\sqrt{3}} \quad \text{(A-3)}$$

as shown in Tables 4 and A-1, the Eurocode's Equation A-3 is often excessively conservative.

Among the models in current standards, the Japanese one (AIJ, 2002) is the most accurate for the results shown in Table 4, where it is only about 10% conservative as compared to the unconservative Canadian model (CSA, 2014) and the 20 to 30% conservatism in the AISC (AISC, 2016) and European (ECS, 2005) models. However, the AIJ equation, which assumes yielding along the gross shear planes with a reduced shear coefficient of 0.5 (AIJ, 2002)

$$R_n = F_u A_{nt} + 0.5 F_y A_{gv} \quad \text{(A-4)}$$

is quite conservative in most cases. In addition to the first four specimens listed in Table A-1, the conservatism of Equation A-4 is 30% or more for many of the specimens tested by Udagawa and Yamada (1998), Huns et al. (2002), Mullin (2002), and Moze and Beg (2014).

In line with the results shown in Tables 3 and 4, the proposed Equation 6 is shown to be reasonably accurate for all block shear specimens tested by Aalberg and Larsen (1999) and listed in Table A-1. It is the only equation that is consistently accurate across all gusset plate specimens tested by independent research groups around the world.

Analysis and Design of Cable-Stayed Steel Columns Using the Stiffness Probe Method

GERMAN GURFINKEL and SUDARSHAN KRISHNAN

ABSTRACT

The stiffness probe method (SPM) is a new numerical procedure that calculates buckling loads. SPM probes the local stiffness of a given structure at the point of application of a small transverse perturbation force as the applied load is increased. The local stiffness degrades from a maximum for an unloaded structure to zero at the buckling load. An artifice spring is added to the original structure that eventually absorbs the full perturbation force at a prescribed small deflection, thereby keeping structural deformations small as the buckling load is approached. As a result, using an indicator that approaches zero at buckling rather than having to rely on increasingly larger deflections at buckling as in conventional P-Δ methods, SPM ensures an accurate numerical result for the critical load. We use SPM herein to study the behavior of one and two cross-arm cable-stayed columns under applied load. A formula is given to calculate the minimum slenderness that justifies converting a tube into a cable-stayed column. Various factors such as cable prestrain, cable cross-sectional areas, and tiers of cross-arms affecting column strength are examined for a series of cable-stayed columns. We find that cable-stayed columns may buckle either in a one-lobe symmetrical mode or two-lobe anti-symmetrical mode, the latter case being contrary to conventional thinking. A design example for a given cable-stayed column using the AISC *Specification* is presented. The effect of optimum cable prestrain to enhance column buckling strengths is discussed. A strength enhancement ratio (SER) is defined that evaluates the additional column strength gained after transforming a given steel tube into a cable-stayed column.

Keywords: analysis, behavior, buckling modes, eigenvectors, cable (slackening, stays, optimum prestraining), columns, design (ASD, LRFD), elastic stability, failure mode, numerical methods, residual tension, cross-arms, load (applied, external), spring (augmented, parallel, series), steel, stiffness probe, strength (enhancement, nominal).

INTRODUCTION

Cable-stayed steel columns consist of a central steel tube, to which one or more sets of transverse cross-arms are welded at equal spacings along the length and to which prestressed steel cables are attached as required to enhance column strength. Review of the existing literature indicates a number of papers that have dealt with the subject in various attempts to understand and predict their behavior and strength. The following investigators have contributed to this field: R.J. Smith et al. (1975), Hafez et al. (1979), Hathout et al. (1979), Temple (1977), Temple et al. (1984), E.A. Smith (1985), and Saito and Wadee (2009). We present a new numerical approach to the subject that examines column behavior under axial load and calculates an accurate value of strength, followed by design using the 2010 AISC *Specification for Structural Steel Buildings* (AISC, 2010), hereafter referred to as the AISC *Specification*.

German Gurfinkel, Ph.D., Professor Emeritus of Structural Engineering, Department of Civil and Environmental Engineering, University of Illinois at Urbana-Champaign, Urbana, IL. Email: ggurfink@illinois.edu

Sudarshan Krishnan, Ph.D., Assistant Professor of Structures, Illinois School of Architecture, University of Illinois at Urbana-Champaign, Urbana, IL. Email: skrishnn@illinois.edu (corresponding)

Paper No. 2016-10

For this purpose, we first provide a simple introduction to the stiffness probe method (SPM), which was conceived jointly by the senior author and the late A.R. Robinson at the University of Illinois. R.E. Miller also contributed initially. Fundamentally, SPM is based on the incontrovertible fact that the stiffness of an axially compressed structure to resist the effects of a perturbation force or moment becomes zero only when subjected to its buckling load (Bleich et al., 1952; Hoff, 1941, 1956). We proceed to explain SPM first in full detail and then use the method specifically to calculate the buckling load of cable-stayed columns.

We recognize that two sets of internal forces are generated in any cable-stayed column—namely, compression in the central tube and tension in the stay cables. We identify these forces and provide equations for columns with one and two sets of cross-arms, respectively. We emphasize two distinct loading stages, initially at cable prestraining and finally at buckling. We also discuss two possible ways of specifying cable prestrains for use in the field and provide a formula to relate them both.

Cable slackening takes place as the external load increases because the applied compression on the tube causes shortening of both it and the cable stays. Ominous consequences to column stability may occur if total cable slackening takes place under service conditions. This effect could occur only if small amounts of cable prestrain were specified, a situation that must be prevented. We provide a formula to predict

the applied load at which total cable slackening occurs based on the initial amount of cable prestrain. For any case where the column load for total cable slackening is less than the column critical load, an enhancement of prestrain is required. We avoid this pitfall by specifying enough cable prestrain to make the load at which total cable slackening occurs to be greater than the column critical load by a reasonable margin.

We now calculate the critical load for a number of cable-stayed columns. We find that there are cases where the governing mode for a cable-stayed column may not be the conventional one-lobe symmetrical mode but, rather, the two-lobe anti-symmetrical mode. This counterintuitive situation calls for designers to always calculate and examine both modes and then use the smaller of the two as the critical value for design. We found that for a given stayed column, the critical mode depends on the initial cable pretension. There is a value of the latter that gives the same critical load, P_{cr}, for both modes. This value is usually but not always the optimum prestrain. Thus, we label as optimum only the actual prestrain value that gives the maximum P_{cr}.

The fact that an antisymmetric two-lobe mode could become the governing buckling mode, instead of the conventional symmetric one-lobe mode, was first pointed out for a given column using an analytical solution (Blumenthal, 1937) and later verified numerically (Newmark, 1943). Both papers found the buckling load of a double-hinged column subjected to two opposing compression loads not at the ends but at the column mid-third points instead. The governing buckling mode corresponding to the smallest buckling load was an anti-symmetrical, two-lobe configuration. Newmark remarked at that time that "It is of interest and importance that the critical load corresponding to the anti-symmetrical deflection is lower than that corresponding to the symmetrical configuration for the arrangement of loads chosen" and warned also that "this would not have been discovered if only symmetrical defection curves had been assumed." This caveat also applies to the calculation of the critical load for a cable-stayed column, a fact that has been verified by Smith et al. (1975) as well as by our own calculations using SPM. Further work using SPM showed that had the distance between the two compressive loads been $0.361L$ instead of $L/3$, both buckling modes would have provided the same critical load at $(\pi/0.361L)^2\ EI$.

For columns provided with cross-arms in a cruciform configuration, there are two principal axes about which buckling of the column may occur. One axis is defined by the tube diameter where two opposite cross-arms are located. The other axis is at 45° with respect to the cross-arms. We studied columns with one and two sets of cross-arms, including various areas of steel cables and prestrain levels, before concluding that the difference in buckling strength between the two axes is insignificant.

Designers shall not use the critical load, P_{cr}, to verify the strength of the supporting tube. Instead, they must use the actual compressive force, N_{cr}, in the tube, which is larger than P_{cr} by the amount of residual tension in the stay cables. We provide an example for this calculation using a given cable prestrain and find the AISC design strength for the given column for both LRFD and ASD values. For the sake of comparison, we now use the optimum cable prestrain and realize a major enhancement of the column design strength. Following this, we introduce the concept of a nominal strength enhancement ratio (*SER*) that effectively evaluates the additional strength gained by the unstayed-tube.

STIFFNESS PROBE METHOD

The stiffness probe method (SPM) is a new numerical procedure that can be used to evaluate the elastic stability of structures subjected to compressive forces. It is specifically used herein to calculate the buckling load of cable-stayed columns.

Consider a column made of a steel tube hinged at both ends and subjected to an axial load, *P*, (see Figure 1). The tube is reinforced with four steel cables, or rods, attached to each end and to the ends of horizontal cross-arms. The latter may be placed at either the mid-height of the column, at the mid-third points, or at equal spacing along the tube length as needed. Note that the cables are not continuous between the top and bottom ends of the tube but are segmental instead (see Figure 2). The schematic elevation and plan views of a one cross-arm column as shown in Figure 1 provide all necessary structural and geometric information to analyze the column for elastic stability. A one cross-arm column is used for the sake of simplicity. Both principal axes for flexural buckling—namely, *a-a* and *b-b*—are shown. Axis *a-a* is for bending about a cruciform configuration of the stay cables, and axis *b-b* is for bending about a two-paired configuration of stay cables. Two possible buckling modes—namely, a symmetric (one-lobe) and an anti-symmetric (two-lobe)—must always be calculated to ascertain the lowest critical load, as either mode may govern buckling. Calculations of higher modes using SPM is possible as shown herein, although modes with three or higher number of lobes will not govern column design.

Characteristic to SPM are a perturbation force, *PF*, and an elastic artifice spring of stiffness K_{spr}. After both are attached to a given column, the latter is transformed into an augmented structure (Figure 1). For any given value of load *P*, the force *PF* triggers a transverse displacement $\delta(P)$ at its location on the column. For any $P < P_{cr}$, the column achieves an equilibrium configuration. At $P = P_{cr}$, the column buckles while the augmented structure still remains stable because of the enhanced stiffness K_{spr} provided by the artifice spring. We note that all of the above would apply as well if a perturbation moment *PM* and an artifice rotational

spring of stiffness K_{rot} were used instead of PF and K_{spr}, respectively.

As PF is applied to the augmented structure in the presence of the external load P, it is resisted by both the column and the artifice spring K_{spr}. We recognize these two components of PF as PF_{col} and PF_{spr}, where $PF = PF_{col} + PF_{spr}$. Because the column and the artifice spring actually behave as a set of two parallel springs of stiffness $K_{col}(P)$ and K_{spr}, respectively, we find that for any given value of the transverse displacement $\delta(P)$, the two components PF_{col} and PF_{spr} can be calculated as follows:

$$PF_{col} = PF\frac{K_{col}(P)}{\left[K_{col}(P) + K_{spr}\right]} \tag{1}$$

and

$$PF_{spr} = PF\frac{K_{spr}}{\left[K_{col}(P) + K_{spr}\right]} \tag{2}$$

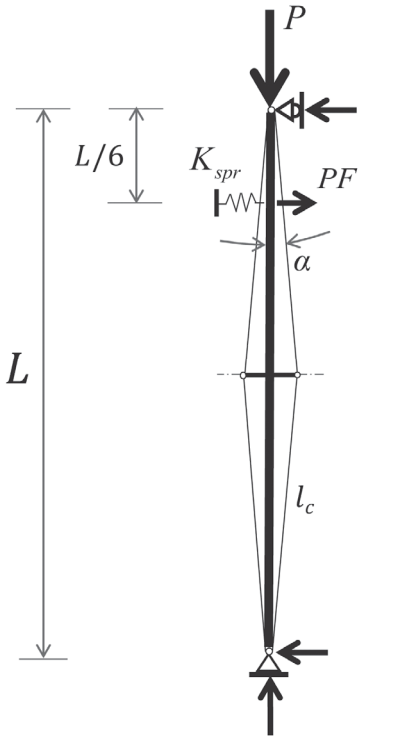

Column Elevation

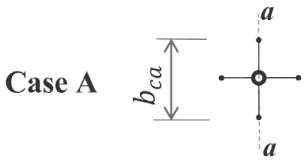

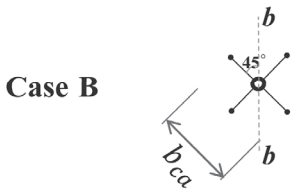

Column Plans

Column Data

Core: 12-in. outer dia × 0.5-in. thk. steel tube

L = 930.7 in.
E = 29,000 ksi
I = 299.2 in.^{4}
A = 18.06 in.^{2}
r = 4.07 in.
F_y = 42 ksi
$N_E = \pi^2 EI/L^2$ = 98.86 kips
$N_y = Af_y$ = 758.5 kips

Cross-arm: 4-in. outer dia × 0.33-in. thk. tube

E_{ca} = 29,000 ksi
A_{ca} = 3.81 in.^{2}
b_{ca} = 96 in.

Cable-stays

E_s = 24,000 ksi
A_s = 1 in.^{2} for each cable
F_y = 243 ksi
F_u = 20 ksi
l_c = 468 in.
$\alpha = \tan^{-1}\frac{b_{ca}}{L}$ = 5.8891°
$\varepsilon_{s_{spec}}$ = 0.002
$\varepsilon_{s_{ini}}$ = 0.00169

Stiffness-Probe Parameters

Perturbation Force, PF = 0.1 kip
Artifice spring stiffness, K_{spr} = 0.1 kip/in.

Fig. 1. Cable-stayed column showing applied load P *and SPM parameters* PF *and* K_{spr}.

Note that K_{spr} is always constant, while $K_{col}(P)$ decreases as P increases. At $P = 0$, the column takes a substantial portion of PF, while the artifice spring takes little. As P continues to increase, PF_{col} decreases while PF_{spr} increases. At $P = P_{cr}$, the column is devoid of any stiffness and cannot support any portion of PF, resulting in $PF_{col} = 0$ and $PF_{spr} = PF$. Thus, at buckling, the column is subjected exclusively to P and not at all to PF. Regardless of the value of PF used to trigger the column away from its initial vertical configuration, the resulting P_{cr} is not affected by PF. This is because at $P = P_{cr}$, the column is no longer subjected to PF; the latter is fully resisted by the elastic spring alone. Similarly, the value of K_{spr} does not affect the resulting value of P_{cr}. It only decides the limiting value of the transverse deflection for an equilibrium position of the augmented structure at $P = P_{cr}$. Therefore, any reasonable set of values for PF and K_{spr} (say, $PF = 0.1$ kips and $K_{spr} = 0.1$ kip/in., or $PF = 0.5$ kips and $K_{spr} = 0.2$ kip/in.) should render the same result for P_{cr}. We have verified that the equilibrium configurations at P_{cr} from the preceding two sets of PF and K_{spr} have the same shape, except that the target displacement is 0.1 kip/0.1 kip/in. = 1 in. for the former, and 0.5 kip/0.2 kip/in. = 2.5 in. for the latter set.

The purpose of using an artifice spring is thus clear. To wit, K_{spr} keeps the augmented structure stable even as the applied load approaches the column critical load. As a result, there is always computational control using SPM, and at the location of PF, the transverse deflection is always small and limited to the target value. An accurate calculation of P_{cr} is thus possible, with as many significant digits as desired. In the absence of an artifice spring, transverse deflections at P close to P_{cr} may increase nonsensically toward infinity, making an accurate calculation of P_{cr} difficult. We note again that at $P = P_{cr}$, all of the PF has been absorbed by the artifice spring, and none of it is acting on the column. As such, SPM differs substantially from the conventional way of triggering P-δ effects for which the initial perturbation force remains in the column and displacements grow uncontrollably as P approaches P_{cr}.

The artifice spring must be placed so that it acts together with the column as two springs in parallel, and not in series (Figure 2). For the configuration shown in Figure 2a, the column is between the PF and the artifice spring; both the column and the artifice spring are subjected to the same displacement, and both share PF according to their respective stiffness, $K_{col}(P)$ and K_{spr}. This is an acceptable configuration that we have used for the column shown in Figure 1. One could also achieve the same result by placing the PF between the column and the artifice spring (Figure 2b). What one cannot do is place the artifice spring between the column and the PF (Figure 2c). Such a location would make the artifice spring and the column act as two springs in series, rather than in parallel. As a result, the PF would not be shared because both the artifice spring and the column

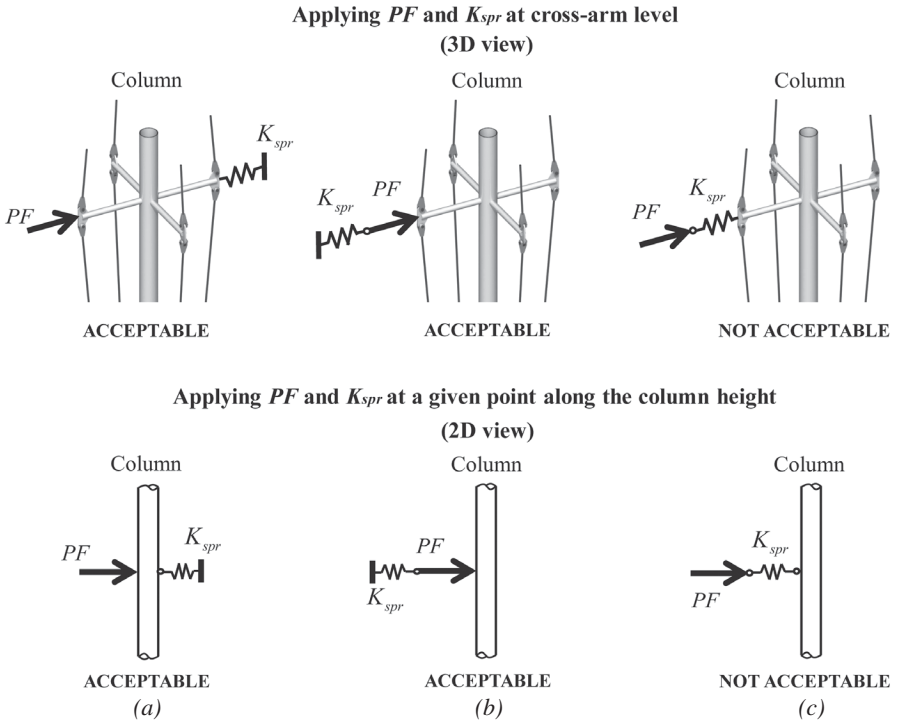

Fig. 2. Three possible ways for placing the PF *and* K_{spr} *with respect to the column.*

would take the whole *PF*, except at different displacements. To summarize, never place the artifice spring between the *PF* and the column.

For any given value of the load, *P*, we define the stiffness of the augmented structure, $K_{aug}(P)$, as the sum of the column stiffness, $K_{col}(P)$, and artifice spring stiffness, K_{spr}—that is, $K_{aug}(P) = K_{col}(P) + K_{spr}$. We calculate $K_{aug}(P)$ as the ratio $PF/\delta(P)$, where $\delta(P)$ is the transverse displacement of the column (in the presence of *P*) as measured at the location of *PF*. We may use any commercial program with a *P*-δ analysis option such as SAP 2000, to calculate $\delta(P)$. The quantities $K_{col}(P)$ and $K_{aug}(P)$ are functions of *P*, while K_{spr} is a constant. Once the quantity $K_{aug}(P)$ is calculated as before, we may find $K_{col}(P)$ as follows:

$$K_{col}(P) = K_{aug}(P) - K_{spr} \tag{3}$$

For an unloaded structure—that is, at $P = 0$—$K_{aug}(0)$ and $K_{col}(0)$ are maximum values. As *P* increases, both $K_{aug}(P)$ and $K_{col}(P)$ diminish in value. We probe the stiffness $K_{col}(P)$ as *P* increases. Instability ensues at $P = P_{cr}$ when the stiffness of the column $K_{col}(P_{cr})$ becomes zero. This leads to $K_{aug}(P_{cr}) - K_{spr} = 0$, or $K_{aug}(P_{cr}) = K_{spr}$. Note that although the column has buckled, the augmented structure remains stable at $P = P_{cr}$ because its remnant stiffness $K_{aug}(P_{cr}) = K_{spr}$ is greater than zero. Users of SPM may, alternatively, probe the transverse displacement $\delta(P)$, instead of $K_{col}(P)$, as an indicator to check the onset of instability. In which case, $\delta < \delta_{max}$ denotes $P < P_{cr}$, while $\delta = \delta_{max} = PF/K_{spr}$ is true only at $P = P_{cr}$. In addition, either the value of $PF_{col}(P)$ or $PF_{spr}(P)$ may also be probed as other possible indicators of instability. As such, instability may ensue when $PF_{col}(P) = 0$ or $PF_{spr}(P) = PF$.

The correctness and accuracy of SPM results have been verified using cases with closed-form solutions from Timoshenko and Gere (1961), Gurfinkel and Robinson (1965), Column Research Committee of Japan (1971), and others. SPM may be used to calculate structural instability caused not just by static compression loads, as discussed in the paper, but also by vibrations at their natural frequencies. The concept is the same whether instability ensues by either the application of a static load or by structural excitation to a natural frequency. They both would cause zero stiffness in any given structure. As such, the *P*-Δ effects caused by vibrating masses in reducing the natural frequency of a given structure may be readily calculated using SPM. That said, SPM is applicable to any problem for which the stiffness of a structure will go to zero, thereby leading to instability. Some other examples include lean-on columns, polygonal frames, arches, and domes. SPM has also been used in practice by the senior author in 2007 for stability calculations of a huge, steel-framed, paper storage structure that collapsed in Wisconsin. The method was used to calculate the critical load of cable-stayed struts on cable-dome structures by the co-author as part of his doctoral dissertation at the Department of Civil Engineering at the University of Illinois at Urbana-Champaign (Krishnan, 2015). SPM has been taught in class to graduate students by the senior author since 2010.

Numerical Example

We apply SPM to find the buckling modes for the stayed column shown in Figure 1 that are within the possible load range, $0 \le P \le P_{sl}$. Note that P_{sl} is the applied load that would be large enough to cause the stay cables to fully slacken. When this happens at $T(P) = 0$, the cables become ineffective thereby rendering the column into an unstayed tube. Let the steel cables be prestrained to $\varepsilon_{s_{spec}} = 0.002$, which results in an initial prestrain value $\varepsilon_{s_{ini}} = 0.00169$ after losses caused by compression of the tube. Also, let $PF = 0.1$ kips and $K_{spr} = 0.1$ kip/in.

Starting at $P = 0$, we increase the load, *P*, gradually for the sake of probing the variation of K_{col} with *P* in order to ascertain P_{cr}. The results are given in Figures 3 and 4.

For $P = 0$:

$$\delta(0) = 0.0289 \text{ in.}$$

$$\begin{aligned} K_{avg}(0) &= PF/\delta(0) \\ &= 0.100 \text{ kip}/0.0289 \text{ in.} \\ &= 3.46 \text{ kip/in.} \end{aligned}$$

$$\begin{aligned} K_{col}(0) &= K_{avg}(0) - K_{spr} \\ &= 3.46 \text{ kip/in.} - 0.100 \text{ kip/in.} \\ &= 3.36 \text{ kip/in.} \end{aligned}$$

Further increasing *P* results in $P_{cr} = 343$ kips at $K_{col} = 0$. At this point, we also find:

$$\begin{aligned} \delta &= \delta_{max} \\ &= PF/K_{spr} \\ &= 0.100 \text{ kip}/0.100 \text{ kip/in.} \\ &= 1.00 \text{ in.} \end{aligned}$$

Note that we have chosen not to plot $K_{aug}(P)$ because it is irrelevant for design and also for the sake of clarity. Had we done so, the plot of $K_{aug}(P)$ would have been exactly like $K_{col}(P)$ except separated above it by a vertical distance $K_{spr} = 0.1$ kip/in. As such, the value of *P* that would cause buckling of the entire augmented structure would always be larger than P_{cr} and lie to the right of it in Figure 3.

Finding $P_{cr} = 343$ kips is all a designer needs, and no further work would be necessary, as far as instability is concerned, because this is the load at which the given column would fail. Nevertheless, if we look at the column eigenvector (Figure 4b), we might be surprised to recognize it as a two-lobe, anti-symmetric configuration that is conventionally associated by designers with the second mode of buckling and not the first. Further loading of the column gives the actual second buckling mode as a one-lobe configuration at $P_{cr2} = 422$ kips > $P_{cr1} = 343$ kips (Figures 3 and 4d).

Table 1. Single Cross-Arm Column as Shown in Figure 1. Summary of SPM Results for the First Three Buckling Modes (results in bold characters are for the governing two-lobe buckling mode)

Buckling Lobes	Applied Load	Tension in Cables	Force in Tube	Transverse Display at *PF* location	Stiffness		Perturbation Force Components	
					Augmented Structure	Column	Artifice Spring	Column
No.	P kips	$\sum T\cos\alpha$ kips	N kips	$\delta(P)$[1] in.	$K_{aug}(P)$[2] kip/in.	$K_{col}(P)$[3] kip/in.	$PF_{spr}(P)$[4] kips	$PF_{col}(P)$[5] kips
—	0	162	162	0.0289	3.46	3.36	0.0029	0.0971
2	**343**	**109**	**452**	**1**	**0.1**	**0**	**0.1**	**0**
1	422	97	519	1	0.1	0	0.1	0
3	956	15	971	1	0.1	0	0.1	0

Notes
[1] Maximum value of δ at $P = P_{cr}$ is $\delta_{max} = PF/K_{spr}$. For the given case, $\delta_{max} = 1$ in.
[2] $K_{aug}(P) = PF/\delta(P)$; where $PF = 0.1$ kip.
[3] $K_{col}(P) = K_{aug}(P) - K_{spr}$; where $K_{spr} = 0.1$ kip/in.
[4] $PF_{spr}(P) = K_{spr}\,\delta(P)$.
[5] $PF_{col}(P) = PF - PF_{spr}(P)$.

This sequence of buckling configurations is definitively counterintuitive to conventional thinking. Finally, we find a third buckling mode (a three-lobe configuration) at P_{cr3} = 956 kips, which is still less than P_{sl} = 1,048 kips, although otherwise irrelevant (Figure 3). A summary of the results is shown in Table 1.

We emphasize in both Figures 3 and 4 that stable equilibrium for the given column under applied compression load, even ideally, would be only possible for $P < 343$ kips, and any applied load larger than that would not be realistic, but only a mathematical curiosity. In Figure 4, note that for all three buckling modes, the column is only subjected to the

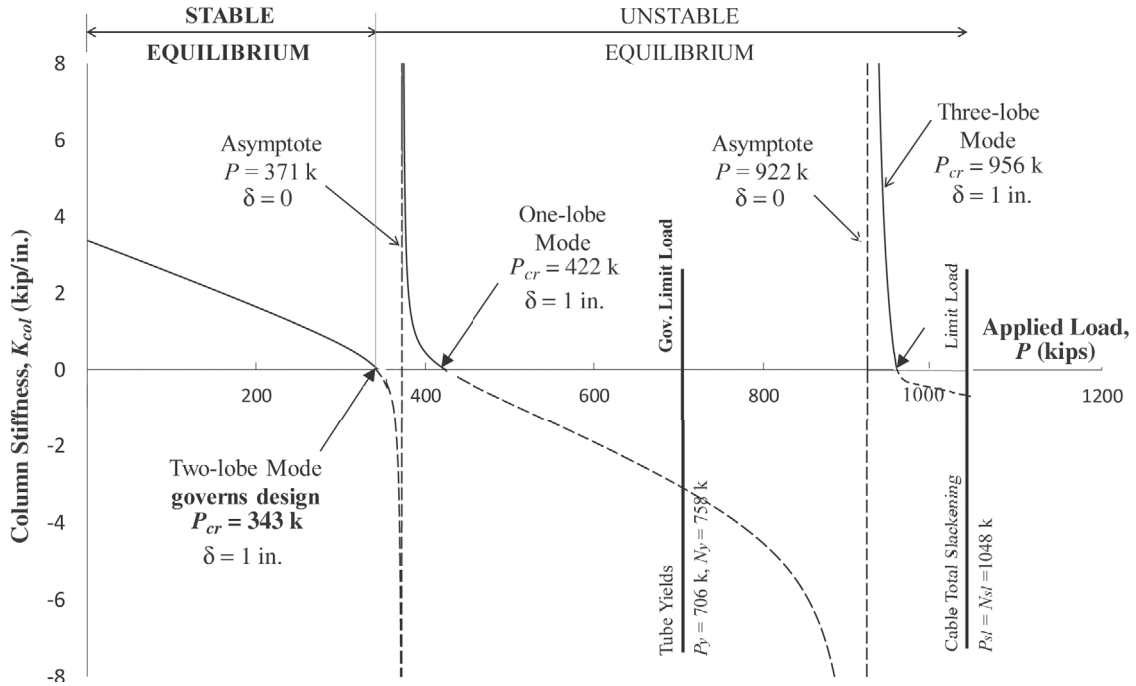

Fig. 3. Variation of column stiffness K_{col} *with applied load* P, *indicating* P_{cr} *for the first three modes of buckling and* P_{sl} *at the end of range. Note that the two-lobe buckling mode governs.*

corresponding P_{cr} and not to any transverse force or horizontal reactions at the column supports. This is true because using SPM guarantees that, at any $P = P_{cr}$, all of the PF is absorbed by the artifice spring—that is, $PF_{spr} = PF$. As such, no part of PF remains on the structure—that is, $PF_{col} = 0$.

Simplified SPM Models for Calculating P_{cr}

Let us try the following two simple models to ascertain which buckling mode governs. To find the one-lobe buckling mode, use the column in Figure 1 with the same perturbation set PF = 0.1 kips and K_{spr} = 0.1 kip/in., except located now at mid-height. Using SPM, again we obtain P_{cr} = 422 kips, at δ_{max} = 1 in. as before. Note that the two-lobe mode would not be captured by this model because it requires zero displacement at column mid-height, which is an obvious impossibility when the PF is located therein. To find the two-lobe buckling mode, use the column in Figure 1 again, except we apply instead a perturbation moment PM = 1 kip-in. and rotational artifice spring K_{rot} = 100 kip-in./rad at mid-height, which results in θ_{max} = 1/100 = 0.01 rad, at P_{cr}. Use SPM as before to obtain the two-lobe mode at P_{cr} = 343 kips as before. Neither the one-lobe nor the three-lobe modes may be captured using this model because they both require $\theta = 0$ at column mid-height, which is again an obvious impossibility when PM is located therein. Comparing the results from the two models, we find that the governing P_{cr} = 343 kips corresponds to the two-lobe configuration.

The calculation process for the preceding simplified models need not start at $P = 0$. We may use any reasonable value of $P_1 > 0$ for this purpose. If $K_{col}(P_1)$ were found to be

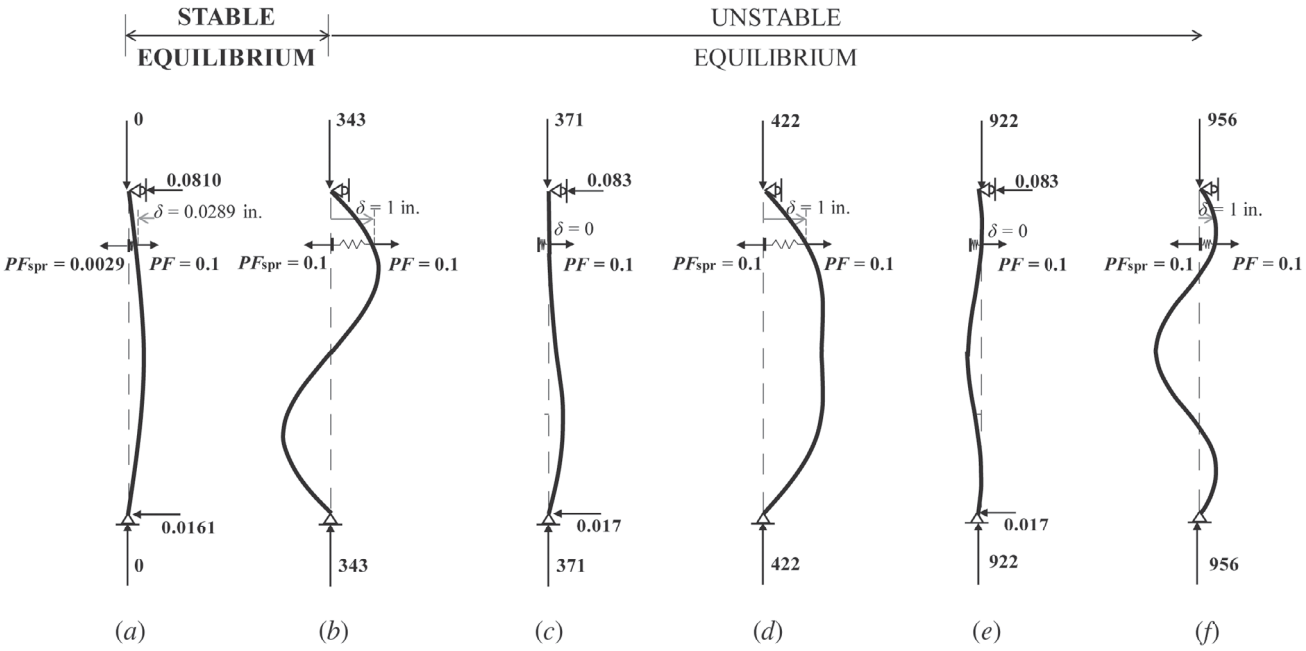

LOADING STAGES

Variables	Prestressed state	Two-lobe Mode	Asymptote	One-lobe Mode	Asymptote	Three-lobe Mode
P (kips)	0	**343**	371	422	922	956
δ (in.)	0.0289	**1**	0	1	0	1
PF_{spr} (kips)	0.0029	**0.1**	0	0.1	0	0.1
PF_{col} (kips)	0.0971	**0**	0.1	0	0.1	0
K_{col} (kip/in.)	3.36	**0**	—	0	—	0

Fig. 4. Column eigenvectors at various loading stages, including a tabulated list of variables; cable stays and cross-arms are not shown for clarity.

positive, this would mean $P_1 < P_{cr}$. We then try $P_2 > P_1$ and calculate $K_{col}(P_2)$. A negative value for $K_{col}(P_2)$ would mean $P_2 > P_{cr}$. Linear interpolation between $K_{col}(P_1)$ and $K_{col}(P_2)$ should provide an educated guess for the next trial $P = P_3$. The process should converge quickly to a value of $K_{col}(P_i)$ as close to zero as possible or to a value small enough to satisfy the designer's criterion for accuracy.

INTERNAL FORCES GENERATED IN CABLE-STAYED COLUMNS

Cable-stayed columns are usually hinged at both ends and braced there against lateral displacements. Actual bracing may take place either by direct attachment or through diaphragm action of the floor or roof against shear walls or X-braced frames available elsewhere in the structure. For design purposes, we emphasize two distinct stages of loading: at initial cable stressing and at ultimate cable stressing. Vertical equilibrium calls for the following equation:

$$N = P + \sum T(P)\cos\alpha \tag{4}$$

to be true at all times, where $\sum T(P)$ is the sum of the tension of all four individual cables at any given load P and α is the angle between each cable and the axis of the tube. We also consider the small variation of the angle α between the initial stage and any given value of P that is caused by column shortening. Although practically this variation is negligible, we have accounted for it by automatically updating the angle α as the load increases. We recognize that $N(P) > P$ at all times. The difference $N(P) - P$ is largest at cable prestressing ($P = 0$), and smallest at buckling ($P = P_{cr}$) when the cables are subjected to a residual tension, $T_{res} > 0$. Only for the unacceptable case when cables slacken totally as P increases (usually because of small initial prestressing) would $\sum T = 0$ and $N(P) = P$. The quantity T_{res} depends mostly on the amount of initial cable prestressing T_o, which is gradually reduced as the column shortens by a strain $\Delta\varepsilon$, while inclined cables shorten simultaneously, except by a smaller strain equal to $\Delta\varepsilon\cos^2\alpha$.

Consider now a stayed column with two tiers of crossarms. Force equilibrium at the two end segments of this column is also given by Equation 4. For the central segment, the same equation holds true, except for $\alpha = 0$. Our previous discussion on the difference between forces N and P is applicable here as well. However, we note that the change in strain imposed on the central segment by a change in applied load, is identical to that in the corresponding steel cables. This is because being parallel to each other makes the cables and the central segment of the tube of the same length. Also for $\alpha = 0$, $\Delta\varepsilon\cos^2\alpha = \Delta\varepsilon$, which results in the tube internal force N being always somewhat larger in the central rather than in the end segments. Regardless of the number of tiers of crossarms, it is the maximum force in the tube $N(P_{cr})$, and not the applied P_{cr}, that governs the design of the tube.

PRESTRAINING THE STAYED CABLES

The amount of cable prestraining influences the behavior of a stayed column under axial load. For any given cable-stayed column, the amount of initial straining that is imposed on the stays determines the axial strength of the column. Consider the stayed column shown in Figure 1. We may specify the amount of cable prestrain by requiring that either the cables be stretched by a certain amount (as measured by cable elongation or recovery) or, at the end of the stretching operation, they be prestrained to a given level (as measured by a strain gauge or transverse vibration device). Let us specify a prestrain $\varepsilon_{s_{spec}} = 0.002$ for the inclined cable segment measuring 468 in. We calculate the cable elongation at 0.002(468 in.) = 0.936 in. but recognize that, at the end of the cable-stretching operation, the actual prestrain in the cable would be less than 0.002 because of tube shortening from cable-induced compression. We may calculate the prestrain in the cable using the following approximate formula:

$$\varepsilon_{s_{ini}} = \frac{\varepsilon_{s_{spec}}}{\left[1 + \left(\frac{\sum A_s}{A}\right)\left(\frac{E_s \cos^2\alpha}{E}\right)\right]} \tag{5}$$

where

$\varepsilon_{s_{ini}}$ = actual initial strain in the stays at $P = 0$
$\varepsilon_{s_{spec}}$ = specified prestrain
$\sum A_s$ = total area of the cables, in.^{2}
A = area of the tube, in.^{2}
E_s and E = respective moduli of elasticity of the cable-stays and the tube, ksi
α = initial value of the angle between the cables and the axis of the tube

Substituting $\varepsilon_{s_{spec}} = 0.002$ and the values of other variables shown in Figure 1 into Equation 5, we obtain $\varepsilon_{s_{ini}} = 0.001693 < 0.002$, as expected. Compare this value to $\varepsilon_{s_{ini}} = 0.001695$ obtained using SAP 2000 or an equivalent program, which accounts not just for the shortening of the column as in Equation 5, but also for the resulting small increase in angle α, which Equation 5 would not do. The two results are practically identical.

The second option considers the specified prestrain as that required in the cable at the end of the prestretching operation—say, $\varepsilon_{s_{ini}} = 0.002$. This is the strain to be read in a strain gauge attached to the stay when we stop stretching the cable. Using Equation 5, we calculate an equivalent $\varepsilon_{s_{spec}} = 0.002363$ and a corresponding cable elongation of 1.105 in. As expected, both values for the second option are larger than those corresponding to the first option. For computational purposes, we recommend $\varepsilon_{s_{spec}}$, while for implementation in the field, the anticipated value of $\varepsilon_{s_{ini}}$ would be easier to verify for consistency. Whichever option is used must be clearly specified by the designer for proper implementation

in the field. As far as our study is concerned, we shall show both corresponding values in our results. Further, we expect that a designer would specify low-relaxation cables. As such, any consideration of time-induced prestrain loss in the cables can be safely ignored.

LIMIT LOADS

We now discuss the following two limit loads, namely, 1. Load at which stay cables fully slacken; and 2. Load at which the steel tube yields. We calculate these loads to verify if any of the two might be lower than the column critical load.

1. Load at Which Stay Cables Fully Slacken

Design of a cable-stayed column is not adequate unless the stays remain taut as the load varies from zero to ultimate. We must guarantee that $P_{sl} > P_{cr}$ is satisfied by a reasonable margin, where P_{sl} is the load at which full slackening may occur and P_{cr} is the column buckling strength. Let us calculate P_{sl} now.

We first recognize that the initial tensile strain in the stay cables, $\varepsilon_{s_{ini}}$, is reduced by the load P. Also, the actual strain in the cables, $\varepsilon_s(P)$, is given as the difference between $\varepsilon_{s_{ini}}$ and the strain caused by the shortening of the tube under the load, P. Using elastic analysis, we find:

$$\varepsilon_s(P) = \varepsilon_{s_{ini}} - \frac{(P/AE)}{\left[1+\left(\frac{\sum A_s}{A}\right)\left(\frac{E_s \cos^2\alpha}{E}\right)\right]} \tag{6}$$

where all terms have been previously identified. Consider the column example in Figure 1. Let us calculate if the stay cables are still taut for $P = P_{cr} = 343$ kips (Figure 3). We have already found $\varepsilon_{s_{ini}} = 0.001693$ after specifying $\varepsilon_{s_{spec}} = 0.002$. Substituting $P = 343$ kips and the values of all other variables in Equation 6, we find $\varepsilon_s(P) = 0.001693 - 0.000554 = 0.00114 > 0$. Thus, at $P = 343$ kips, there is residual tension in the cables at $T_r = 0.00114\ (24{,}000\ \text{ksi})(1\ \text{in.}^2) = 27.36$ kip/cable. As such, full cable slackening will not occur at a load smaller than the critical load. To calculate the actual value of the load $P = P_{sl}$ at which full slackening occurs, we substitute $\varepsilon_s(P_{sl}) = 0$ into Equation 6 and obtain:

$$P_{sl} = \varepsilon_{s_{ini}} EA\left[1+\left(\frac{\sum A_s}{A}\right)\left(\frac{E_s \cos^2\alpha}{E}\right)\right] \tag{7}$$

Using Equation 7 or SAP 2000, we find $P_{sl} = 1{,}048$ kips after substituting all previous values from Figure 1 for the given column. Note this limit load is indicated by a thick vertical line in Figure 3. Because $P_{cr} = 343$ kips $< P_{sl}$, the stay cables will not fully slacken before failure. For the unacceptable case where $P_{sl} < P_{cr}$, the designer must increase the specified cable prestrain to a value large enough to guarantee compliance.

Note that for the case of a column with two cross-arms, where cable slackening may first occur at the central segment of the tube, use $\alpha = 0$ in Equations 6 and 7.

2. Load at Which Steel Tube Yields

We now consider the possibility that the steel tube for the column in Figure 1 may yield under a force, N_y, caused by a load $P_y < P_{cr}$. If such were the case, total slackening of the stay cables might occur abruptly following inelastic deformations in the steel tube. Failure would result from the column reverting to an unstayed-tube condition.

Hand calculation of P_y is possible using the following linearized relation between P_y and P_{sl}:

$$P_y = P_{sl}(N_y - N_o)/(N_{sl} - N_o) \tag{8}$$

which assumes that the cable inclination angle α remains constant. Substituting data already available to us in Equation 8, such as $N_o = 162$ kips from Table 1, $P_{sl} = N_{sl} = 1{,}048$ kips, and $N_y = 758$ kips from Figure 3, we obtain $P_y = 706$ kips. This value is also indicated by a thick vertical line in Figure 3. Because $P_y > P_{cr} = 343$ kips, the latter value remains the governing critical load.

DECIDING COLUMN CRITICAL AXIS

The core of cable-stayed columns is conventionally made of a steel tube, although we note that a solid wood core has been used in Germany (Keil, 2000). Whether hollow or solid, the core is axisymmetric and may buckle about any transverse plane that contains its axis. However, once four stay cables are attached in cruciform fashion to the core, two distinct transverse planes are created about which the column may buckle. These we have labeled *a-a* (case A) and *b-b* (case B) in Figure 1. Plane *a-a* passes through the center of the core and two of the stays. Plane *b-b* makes a 45° angle with plane *a-a*, and does not contain any of the cable stays. Both planes create corresponding axes of bending about the column cross-section.

We calculate P_{cr} for both such axes of the one cross-arm column shown in Figure 1 using SPM. Various cable prestrains are considered. The relative difference between any pair of results for cases A and B for any given prestrain is small and well within 2% of each other. Similar results are found for a stayed column with two cross-arms. For practical design purposes, the buckling strength of a stayed column may be considered the same about either of its principal axes. These findings stem from our selected numerical examples and are not the result of a parametric study.

Tacitly, however, the transverse axis about which the column section buckles is within the prerogative of the column designers, who ultimately decide the position of both pin

ends and their corresponding axis of rotation. The latter are conventionally contained in the same vertical plane, one at the top and one at the bottom of the column. As such, column buckling may take place only in a vertical plane normal to the axis of rotation of both hinges. Usually, designers provide hinges made of opposing vertical steel plates that transfer the load through a steel pin placed across them. This hinge is not perfect in that it may provide a small rotational restraint, mostly generated by friction of the transverse pin against its supporting plates. This may cause the actual ultimate load to exceed P_{cr} by a margin. Thus, calculating P_{cr} as if the column were ideally double hinged is conservative.

The axis of buckling, whether it is case A or B, is determined by the designer's selection of the position of the end hinges. As a result, only P_{cr} about the actual axis of buckling need be calculated. Buckling about the other axis would call for larger values of P_{cr} because of the resulting rotational restraint at the ends. For the same reason, if the two end hinges were placed in planes normal, rather than parallel, to each other, one could expect higher values of P_{cr}. In the extreme case where fixed ends were provided, using either bolted or welded end-plate connections instead of hinges will result in even higher values of P_{cr}. Using fixed-ends to enhance P_{cr} may become more cost-effective for large slenderness of the tube. The subject of cable-stayed columns on end supports other than hinges is outside the scope of this paper.

CRITICAL LOAD

Previously we showed that cable-stayed columns may fail by cable total slackening at an axial load that causes stayed-cable action to cease and the column to revert to a slender unstayed tube. However, the most prevalent cause for failure of these naturally slender columns is at an applied load equal to P_{cr}. Even after P_{cr} is calculated, we must design the tube to resist the force $N(P_{cr})$. This, because $N_{cr} > P_{cr}$ due to the additional compression imposed by the residual tension in the cables (see Equation 4). Once $N(P_{cr})$ is calculated, the design procedure for a cable-stayed column need not be different from that provided by the AISC *Specification* (2010) for a conventional steel column.

For any given column, P_{cr} is calculated using SPM to find the lowest value, which is given by either the one-lobe symmetric or the two-lobe anti-symmetric modes of buckling. As shown in Figures 3 and 4, this example confirmed that the anti-symmetric mode gives the lowest P_{cr} and may thus prevail as the governing condition. In the following section, we check the design validity of the tube selected for Figure 1.

First, however, we study the effects of cable size and number of cross-arms on the axial strength of cable-stayed columns. We run a series of numerical evaluations for the governing buckling load for two types of columns, one with a single mid-height cross-arm and the other with two cross-arms at mid-third points. For either case, we consider four cable stays, placed orthogonally to each other, and use three specific areas of steel cable, namely, $A_s = 0.5$ in.^{2}, $2A_s = 1.0$ in.^{2} and $4A_s = 2.0$ in.^{2} per cable. Various levels of cable prestrain ranging between zero and 0.004 are used.

The results are shown in two sets of three plots each (see Figure 5). All plots show the two respective variations of P_{cr} (but N_{cr} only for governing P_{cr}) with cable prestrains $\varepsilon_{s_{spec}}$ and $\varepsilon_{s_{ini}}$. Specifically shown is the following information: (1) column buckling load, P_{cr}, for the two buckling modes, including the governing P_{cr} shown in bold; (2) compression force in the tube, N_c, for the governing mode only; and (3) two indicators of tube compressive strength—namely, Euler buckling load of the unstayed tube, $N_E = (\pi/L)^2\ EI = 98.86$ kips as the lower limit, and yield load, $N_y = AF_y = 758$ kips of a robust short tube as the upper limit. Each point indicates the results for either the one or two cross-arm column at a given cable prestrain. It is always true that (1) $N_{cr} > P_{cr}$ and (2) the quantity $T_{res} = N_{cr} - P_{cr}$ measures the residual tension in the stay cables. Theoretically, for a given solution to be acceptable, N_{cr} must not exceed the upper limit, N_y. However, to account for potential nonlinear behavior and uncertainties predicting column strength, we conservatively recommend that this limit be taken instead as $0.85N_y$. If the latter value were exceeded by N_{cr}, a designer should consider specifying a higher yield strength for the steel.

Engineers interested in drawing the most value from their designs may wish to use the optimum cable prestrain for that purpose. We define this prestrain as that which generates the largest P_{cr} of the governing set; see the bold variations in each plot of Figure 5. For the four plots in Figures 5b and 5c, the optimum prestrain is found at the intersection of the P_{cr} (symmetric) and the P_{cr} (anti-symmetric) buckling modes. As such, it is the prestrain at which both modes give the same value of P_{cr}. For the two plots in Figure 5a, the variations of P_{cr} do not intersect; the optimum prestrain for both plots is given by the largest value of the P_{cr} (symmetric) variations. Clearly, for the latter case, the anti-symmetric buckling mode never governs. This makes the resulting stayed columns behave as conventional columns if ever loaded to buckling. Optimum prestrain points are identified by large solid circles in Figure 5.

We recognize both quantities N_y and N_E as approximate bounds to the corresponding actual values for the lower and upper strengths, respectively, of the cable-stayed column. As such, it may not be unreasonable to take the vertical distance between N_y and N_E in Figure 5 as an approximate indicator of the maximum amount of strength enhancement caused by the transformation of a steel tube into a cable-stayed column. Justification for this transformation increases with the quantity $N_y - N_E$, as in the case of slender columns. From a strength point of view, tubes need not be transformed when

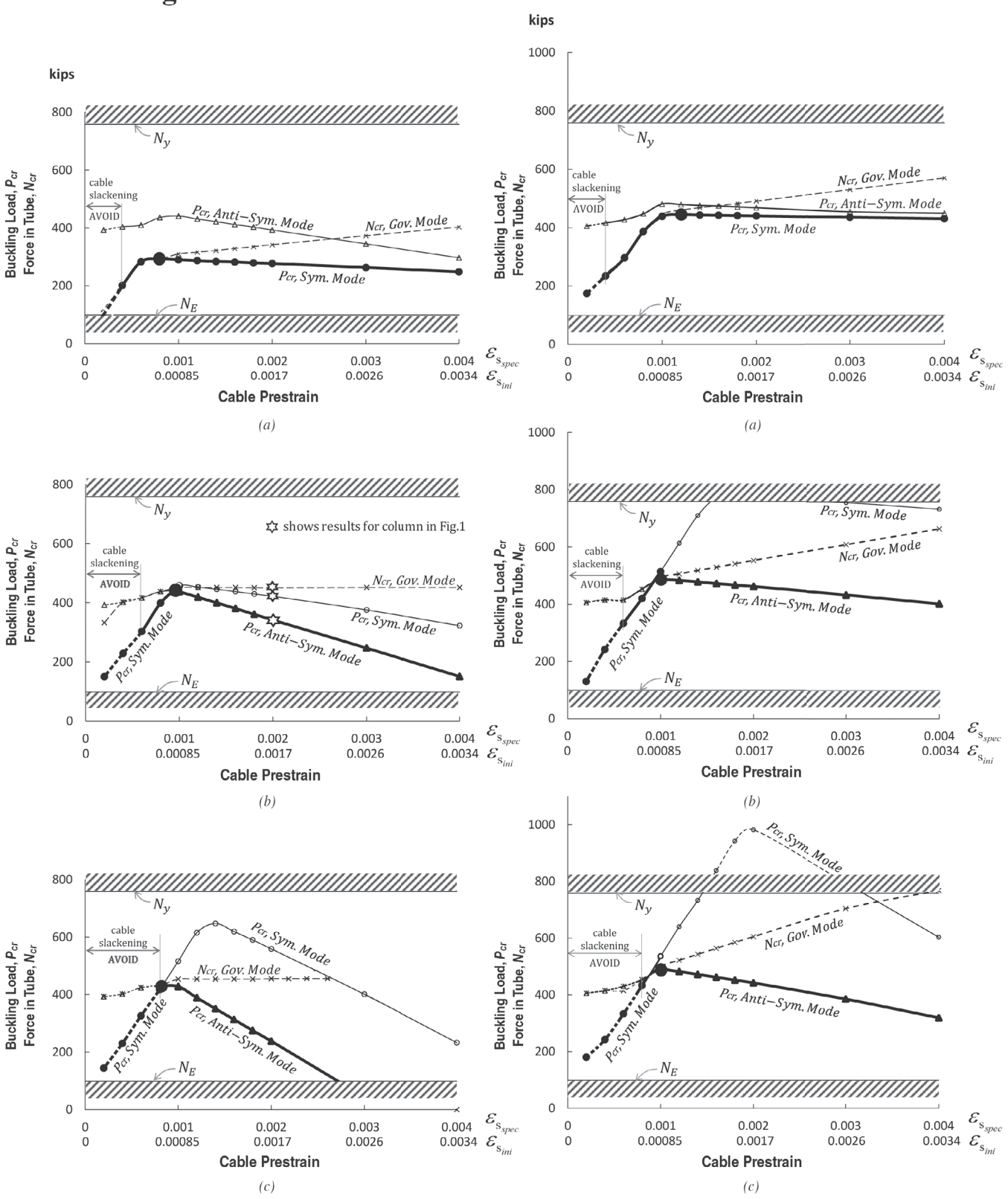

Fig. 5. Variation of P_{cr} *and* N_{cr} *with* ε_{Sspec} *and* ε_{Sini} *for single and double cross-arm columns with four cables each at (a) 0.5 in.*^{2}*, (b) 1.0 in.*^{2} *and (c) 2.0 in.*^{2}*.* P_{cr} *is given for both symmetrical and anti-symmetrical modes. The governing* P_{cr} *variation is shown in bold.* N_{cr} *is only shown for the governing* P_{cr}*. Optimum cable prestrain for maximum* P_{cr} *is shown by large solid circles.*

the quantity $N_E \geq N_y$ as in the case of robust tubes. On the other hand, if $N_y > N_E$ were true for a given tube, a simple indicator (of the minimum value of slenderness for a double-hinged tube) that might justify transforming it into a cable-stayed column would be obtained as follows:

$$(L/r)_{min} = \pi\sqrt{E/F_y} \tag{9}$$

Note, however, that the additional costs in materials and labor that are associated with cable-stayed columns may make the preceding limit on slenderness substantially smaller than the actual practical value.

For the steel tube used in this study (Figure 1), we substitute $E = 29{,}000$ ksi, $F_y = 42$ ksi, in Equation 9 and obtain $(L/r)_{min} = 82.55$ and $L_{min} = 82.55(4.07 \text{ in.}) = 336$ in. Compare this to the actual L/r of the tube at 930.71 in./4.07 in. = 229 > 82.55. This difference may be enough to justify converting the given steel tube into a cable-stayed column to seek additional compressive strength. An alternative solution for using instead a larger and heavier conventional steel tube may be less attractive.

All six plots in Figure 5 show two distinct variations for P_{cr} as cable prestrain increases. There is first a steep increase to a maximum value of P_{cr} at a certain optimum cable prestrain. This is followed by a gradual decline for P_{cr} as cable prestrain increases beyond the optimum. For the initial segment, we find the quantity $T_{res} = N_{cr} - P_{cr}$ is rather small. It is only past the optimum value for P_{cr} that T_{res} increases gradually as cable prestrain increases. We have no structural concern with the latter effect unless it causes the compression force in the tube, N, to reach an unacceptable stress level under service conditions that would require using a heavier tube. There is no good reason to seek a larger prestrain for the stay cables than that necessary to obtain the optimum value for P_{cr} (Figure 5).

At the low end of cable prestrains, total slackening may result from the loss of cable tension as the applied axial load increases, thereby negating cable-stayed action for the column. Thus, all six plots in Figure 5 indicate an AVOID range for prestrain that leads to total cable slackening under the applied load. Designers should heed this advice by making sure that enough prestraining is specified to prevent premature failure.

We now examine Figure 5 again to compare the strength of stayed-columns with either one or two cross-arms for the same given cable areas and prestrain. All columns with one cross-arm provide a smaller buckling strength, case by case, than corresponding columns equipped with two cross-arms. We conclude that cable-stayed columns with two cross-arms are more efficient than those with one cross-arm because they require a smaller amount of cable area to achieve the same strength. Whether they are also more cost efficient would require a comparison accounting for the cost of additional cross-arms, connections and labor.

DESIGN AXIAL LOAD

Calculation of the critical load of a stayed column, P_{cr}, is followed by determination of its nominal compressive strength, $P_n = F_{cr}A_g$, where F_{cr} is the nominal critical stress and A_g is the gross area of the tube. We use the provisions of AISC *Specification* Chapter E, Section E3 (AISC, 2010) to calculate P_n for the one cross-arm stayed-column shown in Figure 1. Our previous calculations using SPM (see Figure 3 and Table 1) indicate that the two-lobe rather than the one-lobe buckling configuration governs the strength of the column. We obtain $P_{cr} = 343$ kips from Table 1. This corresponds to a compression force in the tube, $N_{cr} = 452$ kips, for which the compressive stress, given by $N_{cr}/\text{A} = 452 \text{ kips}/18.06 \text{ in.}^2 = 25$ ksi. This is well within the elastic range for steel specified at 42 ksi yield strength and our recommended 0.85(42 ksi) = 37.5 ksi maximum compressive stress. There is also a residual vertical tension force in the stay cables, $\sum T\cos\alpha = 109$ kips. These results verify $N_{cr} = P_{cr} + \sum T\cos\alpha$. We recognize that it is the force in the tube, N_{cr}, and not the applied load, P_{cr}, that controls the nominal compressive strength of the stayed column. As such, the value of AISC's design strength, F_{cr}, depends exclusively on the tube.

We may find the equivalent slenderness ratio of the cable-stayed tube, kL/r, using:

$$N_{cr} = \frac{\pi^2 EA}{\left(\frac{kL}{r}\right)^2}$$

Solving for kL/r:

$$\frac{kL}{r} = \sqrt{\frac{\pi^2 EA}{N_{cr}}}$$

$$= \sqrt{\frac{\pi^2 (29{,}000 \text{ ksi})(18.06 \text{ in.}^2)}{452 \text{ kips}}}$$

$$= 107 < 200$$

Because AISC's control quantity $\lambda = 4.71\sqrt{E/F_y} = 4.71\sqrt{29{,}000 \text{ ksi}/42 \text{ ksi}} = 123.8 > 107$, we calculate F_{cr} using AISC *Specification* Equation E3-2:

$$F_{cr} = \left[0.658^{\frac{F_y}{F_e}}\right] F_y \qquad (\textit{Spec.} \text{ Eq. E3-2})$$

where

$$F_e = \frac{\pi^2 E}{\left(\frac{kL}{r}\right)^2} \qquad (\textit{Spec.} \text{ Eq. E3-4})$$

$$F_e = \frac{\pi^2 (29{,}000 \text{ ksi})}{(107)^2}$$

$$= 25 \text{ ksi}$$

and then,

$$F_{cr} = \left[0.658^{\frac{42 \text{ ksi}}{25 \text{ ksi}}}\right](42 \text{ ksi})$$
$$= 20.8 \text{ ksi}$$

With this value of F_{cr}, the nominal compressive strength of the tube is:

$$N_a = F_{cr} A_g$$
$$= (20.8 \text{ ksi})(18.06 \text{ in.}^2)$$
$$= 375 \text{ kips}$$

Let us now calculate the value of P_n on the column that would correspond to the preceding value of N_n. Hand calculation is possible using the following linearized relation between P_n and N_n, which is similar to Equation 8, except adapted to AISC design notations:

$$P_n = P_{cr}(N_n - N_o)/(N_{cr} - N_o) \quad (10)$$

Equation 10 also assumes that the cable inclination angle α remains constant. Using Table 1, we find N_o = 162 kips, N_{cr} = 452 kips, and P_{cr} = 343 kips. Substituting these values and the preceding N_n = 375 kips into Equation 10, we find P_n = 252 kips. This value is slightly larger than the more accurate value 251.6 kips provided by computer analysis that accounts for the slight increase in the angle α due to tube shortening under load.

Designers using LRFD or ASD may now take the design compressive strength at ϕP_n = 0.90(252 kips) = 226 kips or the allowable compressive strength at P_n/Ω = 252 kips/1.67 = 151 kips, respectively. Let us compare P_n = 252 kips for the given cable-stayed column to that of the tube alone. We find kL/r = 1.0(931 in.)/(4.07 in.) = 229 > 200. While this exceeds the recommended limit of 200 for non-stayed columns as mentioned in AISC *Specification* Section E2 (AISC, 2010), it is viewed as acceptable for the purpose of strength comparison. We now calculate P_n:

$$P_n = AF_{cr}$$

Because $\lambda = 123.8 < kL/r = 229$, use AISC *Specification* Equation E3-3:

$$F_{cr} = 0.877F_e \quad (\textit{Spec.} \text{ Eq. E3-3})$$

where,

$$F_e = \frac{\pi^2 E}{\left(\frac{kL}{r}\right)^2} \quad (\textit{Spec.} \text{ Eq. E3-4})$$
$$= \frac{\pi^2 (29{,}000 \text{ ksi})}{(229)^2}$$
$$= 5.46 \text{ ksi}$$

and then,

$$F_{cr} = 0.877(5.46 \text{ ksi})$$
$$= 4.79 \text{ ksi}$$

Using this value of F_{cr}, $P_{n,tube}$ is calculated as:

$$P_{n,tube} = (18.06 \text{ in.}^2)(4.79 \text{ ksi})$$
$$= 86.5 \text{ kips} << 252 \text{ kips}$$

The nominal strength enhancement of the cable-stayed column over that of the tube alone is measured by the difference of the corresponding nominal strengths, which is substantial:

$$P_n - P_{n,tube} = 252 \text{ kips} - 86.5 \text{ kips}$$
$$= 165.5 \text{kips}$$

The nominal strength enhancement ratio (*SER*) may be defined as the ratio $(P_n - P_{n,tube})/P_{n,tube}$. For the given column, we find *SER* = 165.5 kips/86.5 kips = 1.91. In other words, the relative nominal strength of the cable-stayed tube will be 2.91 times as large as that of the unstayed-tube.

At this point, a designer may question whether higher column strength could have been attained had a cable prestrain other than $\varepsilon_{s_{spec}} = 0.002$ been chosen. It behooves the designer to do so as our previous work clearly indicates (see Figure 5, plot 1b). Thus, had the optimum prestrain at $\varepsilon_{s_{spec}} = 0.000888$ been found first and selected for use, this new design would have provided N_o = 71.4 kips at P = 0, P_{cr} = 446 kips and N_{cr} = 449 kips from SPM. Now using the AISC *Specification* obtain F_e = 24.9 ksi, F_{cr} = 20.7 ksi, N_n = 374 kips, and finally, P_n = 357 kips. The latter value exceeds that of the previous design, P_n = 253 kips, by a substantial margin. This is due to the much smaller cable residual tension 39.2 kips at optimum prestrain $\varepsilon_{s_{spec}} = 0.000888$ versus 139 kips at $\varepsilon_{s_{spec}} = 0.002$. Even when a designer would likely not know the optimum cable prestrain at the outset, evaluating a few values of cable prestrain may help enhance P_n as desired.

SUMMARY AND CONCLUSIONS

1. Adding cross-arms and cables to a slender steel tube transforms it into a cable-stayed column with a substantially larger axial compressive strength. A simple approximate formula is given that evaluates the minimum tube slenderness for which this transformation may be justified. Because the formula is based only on strength considerations, and does not account for additional costs involved in the transformation, the result should be considered a low estimate.
2. A cable-stayed column with two cross-arms at the mid-third points of its height may resist a larger applied compression load for the same size cables and prestraining than an identical column with only one set of cross-arms at mid-height.

3. The amount of cable prestraining is important. Too little prestrain must be avoided to prevent total cable slackening and premature column failure under applied load. Too much prestrain may cause overstressing of the steel tube and a subsequent reduction in column strength. An optimum value for cable prestraining that provides the highest column strength for a given set of cables can be calculated.

4. Once the stay cables are pretensioned, they impose an initial compression force on the tube. The applied load increases the tube compression force but reduces the cable initial tension. The axial compression force in the tube is always larger than the applied load by the amount of residual tension in the cables. It is the axial force in the tube, and not the applied load causing column buckling, that must be used to verify the nominal strength of the cable-stayed column.

5. Premature failure caused by total cable slackening due to low prestraining can and must be avoided. Failure of cable-stayed tubed caused by buckling under increasing axial load may occur in both the symmetric (one-lobe) and anti-symmetric (two-lobe) modes. The critical load for both modes must be calculated to ascertain which one governs. Although counterintuitive to conventional column design, it is a fact that the anti-symmetric mode may govern design.

6. Buckling calculations for cable-stayed columns are easily accomplished using the stiffness probe method (SPM), which is presented here for the first time. SPM is conceptually based on the fact that the local structural stiffness at the point of application of a perturbation force (or moment) in the presence of an artifice spring (translational for a perturbation force and rotational for a perturbation moment) degrades from a maximum for the unloaded column to zero at the buckling load. This measurement of the stiffness under controlled deformations as the structure approaches instability allows for a very accurate calculation of the buckling load. SPM has been successfully used in various structures to predict elastic instability generated not just by compression loads as shown herein, but also by masses forced to vibrate at their natural frequencies.

ACKNOWLEDGMENTS

The authors are grateful to the Department of Civil and Environmental Engineering at the University of Illinois for making their resources available for this research. We are also grateful to all reviewers of this paper for their constructive remarks and suggestions.

SYMBOLS

A	Cross-sectional area of core (tube), in.^{2}
A_{ca}	Cross-sectional area of cross-arm, in.^{2}
A_g	Gross cross-sectional area of core (tube), in.^{2}
A_s	Cross-sectional area of each stay cable, in.^{2}
E	Modulus of elasticity of core (tube), ksi
E_{ca}	Modulus of elasticity of cross-arm, ksi
E_s	Modulus of elasticity of cable, ksi
F_{cr}	Critical compressive stress used to calculate nominal strength, ksi
F_e	Critical elastic buckling stress of core (tube), ksi
F_u	Specified minimum tensile strength of the type of steel used, ksi
F_y	Specified minimum yield stress of the type of steel used, ksi
I	Moment of inertia of core (tube), in.^{4}
K_{aug}	Stiffness of augmented column, kip/in.
K_{col}	Column stiffness, kip/in.
K_{rot}	Rotational spring stiffness, kip-in./rad.
K_{spr}	Translational spring stiffness, kip/in.
L	Length of core (tube), in.
N	Compression force in tube due to applied load, kips
N_{cr}	Compression force in tube at buckling, kips
N_E	Euler buckling force for core (tube) alone, kips
N_n	Nominal design force for core (tube), kips
N_o	Axial force in core (tube) at $P = 0$, kips
N_y	Yield force for core (tube) cross-section, kips
P	Applied axial load at column ends, kips
PF	Perturbation force, kips
PM	Perturbation moment, kip-in.
P_{cr1}	Governing critical buckling load for cable-stayed column, kips
P_{cr2}, P_{cr3}	Buckling loads for unattainable modes 2 and 3, respectively, kips
P_n	Nominal compressive strength, kips
$P_{n,\,tube}$	Nominal compressive strength of unstayed-tube, kips
P_{sl}	Axial load causing cables to fully slacken ($T = 0$), kips

P_u Ultimate strength of cable-stayed column, kips

SER Strength enhancement ratio

$T(P)$ Tension force in stay cable at a given load P, kips

T_o Initial tension in stay cables, kips

T_{res} Residual tension in stay cables, kips

b_{ca} Horizontal length of cross-arm between cable attachments, in.

k Effective length factor for compression members

kL/r Equivalent slenderness ratio of cable-stayed core (tube)

r Radius of gyration of the tube, in.

Ω Safety factor

α Angle between the core (tube) and stay cables, deg. or rad.

δ Transverse displacement of the artifice translational spring, in.

ε_s Strain in cable

$\varepsilon_{s_{ini}}$ Initial strain in cable

$\varepsilon_{s_{spec}}$ Specified strain in cable

λ Control quantity used for steel column design

θ Nodal rotation of the artifice rotational spring, rad.

ϕ Strength reduction factor

REFERENCES

AISC (2010), *Specification for Structural Steel Buildings,* ANSI/AISC 360-10, American Institute of Steel Construction, Chicago, IL.

Bleich, F., Ramsey, L.B. and Bleich, H.H. (1952), *Buckling Strength of Metal Structures* (Engineering Societies Monographs), McGraw-Hill, New York, NY.

Blumenthal, O. (1937), "Ueber die Knickung eines Balkens durch Laengskraefte," *Zeitschrift fuer Angewaendte Matemathik und Mechanik,* Vol. 17.

Column Research Committee of Japan (1971), *Handbook of Structural Stability*, Corona Publishing Co., Tokyo.

Gurfinkel, G.R. and Robinson, A.R. (1965), "Buckling of Elastically Restrained Columns," *Journal of the Structural Division*, ASCE, Vol. 91, No. ST6, Proc. Paper 4574, pp. 159–183.

Hafez H.H., Temple M.C. and Ellis J.S. (1979), "Pretensioning of Single-Crossarm Stayed Columns," *Journal of the Structural Division*, ASCE, Vol. 105, pp. 359–375.

Hathout I.A., Temple M.C. and Ellis J.S. (1979), "Buckling of Space-Stayed Columns," *Journal of the Structural Division*, ASCE, Vol. 105, pp. 1,805–1,823.

Hoff, N.J. (1941), "Stable and Unstable Equilibrium of Plane Frameworks," *Journal of the Aeronautical Science*s, Vol. 8, No. 3, pp. 115–119.

Hoff, N.J. (1956), *The Analysis of Structures, Based on the Minimal Principles and the Principle of Virtual Displacements,* Wiley, New York, NY.

Keil A. (2000), "Mont-Cenis Academy in Herne, Germany," *Structural Engineering International*, Vol. 10, No. 3, pp. 172–174.

Krishnan S. (2015), *Prestressed Cable Domes: Structural Behavior and Design*, Doctoral Dissertation, Department of Civil Engineering, University of Illinois at Urbana-Champaign, Urbana, IL.

Newmark, N.M. (1943), "Numerical Procedure for Computing Deflections, Moments and Buckling Loads," *Transactions ASCE*, Vol. 108, pp. 1,161–1,234.

Saito D. and Wadee M.A. (2009), "Buckling Behavior of Prestressed Steel Stayed Columns with Imperfections and Stress Limitation," *Engineering Structures*, Vol. 31, No. 1, pp. 1–15.

Smith E.A. (1985), "Behavior of Columns with Pretensioned Stays," *Journal of Structural Engineering*, ASCE, Vol. 115, pp. 961–972.

Smith R.J., McCaffrey G.T. and Ellis J.S. (1975), "Buckling of a Single-Crossarm Stayed Column," *Journal of the Structural Division*, ASCE, Vol. 101, pp. 249–268.

Temple M.C. (1977), "Buckling of Stayed Columns," *Journal of the Structural Division*, ASCE, Vol. 103, pp. 839–851.

Temple M.C., Prakash M.V. and Ellis J.S. (1984), "Failure Criteria of Stayed Columns," *Journal of Structural Engineering*, ASCE, Vol. 110, pp. 2677–2689.

Timoshenko, S.P. and Gere, J.M. (1961), *Theory of Elastic Stability*, McGraw Hill, New York, NY.

Guide for Authors

Scope

Engineering Journal is dedicated to the improvement and advancement of structural steel construction. Its pages are open to all who wish to report on new developments or techniques in structural steel design, research, construction, steel fabrication methods, or new products of significance to the use of structural steel in construction. Only original papers may be submitted. Determining the appropriateness of submissions for the review process is the purview of the editors.

General

Papers intended for publication should be submitted by email Margaret Matthew, Editor, at matthew@aisc.org.

The articles published in the *Engineering Journal* undergo peer review before publication for (1) originality of contribution; (2) technical value to the steel construction community; (3) proper credit to others working in the same area; (4) prior publication of the material; and (5) justification of the conclusion based on the report.

All papers within the scope outlined above will be reviewed by engineers selected from among AISC staff, industry, design firms, and universities. The standard review process includes outside review by an average of three reviewers, who are experts in their respective technical area, and volunteers in the program. Papers not accepted will not be returned to the author. Published papers become the property of the American Institute of Steel Construction and are protected by appropriate copyrights. No proofs will be sent to authors. Each author receives three complimentary copies of the issue in which his contribution appears.

Manuscripts

Manuscripts must be provided in Microsoft Word format. Include a PDF version of your submission so we may verify fonts, equations and figures. View our complete author guidelines at **www.aisc.org/ej**.

There's always a solution in steel.

Engineering Journal
American Institute of Steel Construction
130 E. Randolph Street, Suite 2000
Chicago, IL 60601

312.670.2400 www.aisc.org